CHARACTERIZING TRANSITION METAL HOMEOSTASIS AT THE HOST-PATHOGEN INTERFACE

By

Edward McLouth Culbertson

A dissertation submitted to Johns Hopkins University in conformity with the requirements for the degree of Doctor of Philosophy

Baltimore, Maryland

September 2020

Abstract

Transition metals such as Mn, Zn, Fe and Cu are essential micronutrients to living organisms but have the potential to become toxic. Due to this dual nature, transition metal homeostasis is tightly controlled. During infection, the pathogen and host fight over control of these micronutrients, a process that is termed “nutritional immunity”. The best characterized examples of nutritional immunity involve the metal binding protein calprotectin and the anemia of inflammation response with Fe. Recent work from the Culotta lab and others have shown there is also a nutritional immunity response for Cu.

One mechanism by which hosts limit pathogens of transition metals is the metal binding protein calprotectin. Calprotectin binds to transition metals around pathogenic lesions to withhold these metals from the invaders. In Chapter 2 we focus on the role of calprotectin during infection with the Lyme disease pathogen *Borrelia burgdorferi*. This work establishes and quantifies the presence of calprotectin at sites of *B. burgdorferi* infection in humans. Furthermore, unlike other for pathogens, calprotectin inhibits *Borrelia* growth without metal binding through a mechanism that requires physical interaction with *B. burgdorferi.*

Perhaps the best characterized example of nutritional immunity is anemia of inflammation. During this response, the circulating Fe pool carried by serum transferrin precipitously drops. We find in Chapter 3 that anemia of inflammation is transient and that circulating Fe pools can be restored at later stages of infection by a multicopper oxidase ceruloplasmin, that promotes Fe-transferrin binding.

Is there a nutritional immunity response with Cu? We previously showed that kidney Cu levels drop during infection by the opportunistic fungal pathogen *Candida albicans,* and in Chapter 3 we demonstrate this is a global response to infection also

seen with the malaria parasite *Plasmodium berghei*. In Chapter 4 we focus on the fungal response to host withholding of Cu. We find that the Cu-sensing transcription factor Mac1p, which functions to activate Cu acquisition mechanisms during Cu starvation, is an important virulence factor for *C. albicans*. Beyond Cu acquisition, we find that *C. albicans* Mac1p is important for maintaining cellular respiration and Fe uptake processes that are dependent on Cu, thereby promoting survival in the low Cu environment of the host.

Advisor: Valeria Culotta

Primary Readers: Fengyi Wan, David Sullivan, Brendan Cormack

Secondary Readers: Svetlana Lutsenko, Scott Bailey

Acknowledgements

First and foremost, I would like to thank my advisor Dr. Val Culotta. How she has put up with me for the last six years, I will never know! Val has taught me what it takes to be a successful scientist. I truly believe that I would not have had such a successful and fun PhD without Val and I really cannot thank her enough.

I would be remiss if I didn't thank all of the wonderful people in the Culotta lab. I still can't believe how blessed I have been to work with these incredible people. I cannot praise Angelique enough for helpful science discussions, help with mouse experiments, help with math when my brain died, and just being one of the best people I know. I would also like to thank Natalie for being a great friend and also being available to help me with things. I want to thank the other post-docs in the Culotta lab who have taught me so much about science from a practical standpoint. Specifically, I want to thank Courtney for helpful discussions, Julie for helping me early in my PhD, and Ryan for the science help and also being a great friend outside of lab. I also want to thank the amazing PhD students that I have had the honor to call my colleagues along the way; Cissy for helping me get my project on its feet; Chynna for being a scientific mentor and a great friend; and Sabrina for being my partner in crime/embarrassing mistakes. I would also like to thank honorary Culotta lab member Danielle for all the helpful discussions about science, grad school, and life.

None of this would have been possible without the mentorship of a number of Johns Hopkins faculty members. I would like to thank my committee for many helpful discussions and guidance. Specifically, I would like to thank Dr. Brendan Cormack for all his help during mouse infection experiments; without him this work would not have been possible. I want to thank Dr. Svetlana Lutsenko for all the material and intellectual help

she has given me over the years. I also want to thank Svetlana for her undying enthusiasm for my results even when I was disappointed or frustrated. I also want to thank Dr. David Sullivan for helpful discussions during committee meetings and also for allowing me into his lab to work with *Plasmodium berghei*. That experiment turned out to be critical to the thesis and I am so grateful that I was able to work with you. Finally, I need to thank Dr. Fengyi Wan for his helpful thoughts and discussions.

I want to thank my Kevin L. Culbertson and Elizabeth M. Culbertson, my dad and mom. They are the best people in the world and I countlessly rely on their wisdom and guidance. I also need to thank my two brothers, Charles and Max. They have always been around as a constant source of support and encouragement.

Table of Contents

Contents

List of Tables

List of Figures

CHAPTER 4: CHANGES IN MAMMALIAN COPPER HOMEOSTASIS DURING MICROBIAL INFECTION

Chapter 1

Background and significance

Introduction to nutritional immunity

Transition metals such as Mn, Zn, Fe, and Cu are essential micronutrients for living organisms, yet have the potential to become toxic. Due to this dual nature, transition metal homeostasis is tightly controlled. During infection, pathogens must acquire micronutrients from the host. In a process termed “nutritional immunity” the host withholds micronutrients from pathogens (1-3).

Nutritional immunity involving circulating Fe

Nutritional immunity was first described for Fe (4). The labile Fe pool in the serum is comprised of Fe bound to transferrin (5). Fe efflux from cells is executed by the Fe-transporter ferroportin and subsequent oxidation by the multicopper oxidase (MCO) ceruloplasmin, promotes Fe-transferrin binding (6-11) (Fig. 1-1). During infection, the small peptide hormone hepcidin is secreted from the liver (12-14). It binds to ferroportin which mediates its internalization and subsequent degradation (15) (Fig. 1-1). As a result, Fe-transferrin levels drastically plummet in the serum (16). This creates a condition known as anemia of inflammation (17). Successful pathogens have evolved with methods of acquiring Fe in spite of this host-imposed anemia and a fierce battle for Fe nutrients at the host-pathogen interface ensures (18).

Curiously the MCO ceruloplasmin that loads Fe onto transferrin is an acute phase protein, meaning it is induced during conditions of infection and inflammation (19). This would seem at odds with the host response to prevent Fe-transferrin binding. In this thesis we investigate this apparent paradox in Chapter 3.

Nutritional immunity involving Calprotectin

A second type of nutritional immunity has been characterized involving the metal binding heterodimer of the S100A8 and S100A9 proteins, named calprotectin (20,21). Calprotectin is produced by epithelial cells, keratinocytes, macrophages, monocytes, and neutrophils (22-24). In neutrophils it can comprise as much as 40% of the total proteins in the cytosol (25). It has been demonstrated that calprotectin can bind Fe, Mn, and Zn (2,26,27). Calprotectin binds to these metals with high affinity to withhold them from pathogens and can be present in the extracellular space surrounding pathogenic lesions at concentrations as high as 1 mg/mL (28,29). The Culotta lab has also shown that calprotectin can bind Cu and withhold Cu from a fungal pathogen in culture (30). In this thesis we show there is more to calprotectin than just metal withholding. In studies with the Lyme disease pathogen *Borrelia burgdorferi* we show that calprotectin has additional anti-microbial functions that are independent of metal withholding (Chapter 2).

Nutritional Immunity involving Cu

Up until 2015, it was believed that Cu was not involved in nutritional immunity, rather the opposite that the host exploits Cu toxicity to thwart growth of microbial pathogens. Cu is not only a nutrient, but is highly reactive in biological systems and can cause production of deleterious reactive oxygen species (ROS) through so-called Fenton chemistry, and can displace other metal co-factors from their sites in metalloenzymes, including Fe-S clusters (31). The belief that Cu is mainly used by the host as a toxin comes from a number of observations in macrophages. These studies have shown that Cu is elevated in the phagolysosome compartment of the macrophage following engulfment of the pathogen. Bacterial and fungal pathogens with impaired Cu-toxicity tolerance pathways are more susceptible to killing by activated macrophages

(32-38). Much of this earlier work on Cu in infection focused on bacterial pathogens that are highly vulnerable to Cu toxicity, but do not require Cu as a nutrient for intracellular cuproenzymes. Due to the highly toxic nature of Cu, bacteria eliminate all Cu from the cytosol and all bacterial cuproproteins are extracellular or periplasmic (39-42). However, unlike bacteria, eukaryotes including fungal pathogens have evolved with numerous intracellular cuproenzymes in the cytosol, the mitochondria, chloroplasts and secretory pathway. In theory, eukaryotic pathogens should be vulnerable to the effects of Cu starvation.

Studies since 2015 have shown that eukaryotic pathogens can indeed be subject to nutritional immunity for Cu (30,43-50). To-date, these studies have only shown Cu withholding with fungi, but similar principles should apply to parasitic pathogens as well. The major focus of this thesis is on Cu in fungal pathogens and how Cu is managed at the host-fungal pathogen interface.

Cu homeostasis of the Host

Cu homeostasis in mammals is tightly controlled as defects in Cu homeostasis are debilitating and often lethal. The major Cu-transporting proteins in mammals are the high affinity Cu uptake transporter CTR1, and Cu efflux is executed by two P-type ATPases, ATP7A and ATP7B. CTR1 is the major Cu permease in all eukaryotes from yeast to mammals and accounts for 70% of the Cu import into mammalian cells (51). ATP7A transports Cu from the cytosol to the trans-Golgi network, intracellular vesicles, and to secretory granules (52). In the trans-Golgi network, the Cu from ATP7A is used to activate cell surface or secreted cuproproteins as they transit the secretory pathway. ATP7A can also localize to the basolateral membrane of polarized epithelial cells to export Cu from the cell (53). ATP7A is expressed in the majority of tissues with the

exception of the liver (54) and is responsible for the aforementioned elevated Cu in the phagolysosome of macrophages during the Cu burst of infection. The second Cu-transporting ATPase, ATP7B is known to function in the liver, kidney, mammary gland and brain (53,55-58). It is perhaps best known for its roles in the liver; transporting Cu to the bile and shuttling Cu into the secretory pathway for the synthesis of the MCO ceruloplasmin (59,60). As described above, ceruloplasmin functions in Fe loading of transferrin, establishing an important requirement for Cu in Fe homeostasis.

Essential fungal cuproproteins

Fungi use Cu for a number of vital cellular processes and this thesis specifically highlights the role of Cu in antioxidant defense via superoxide dismutase (SOD), in cellular respiration via cytochrome C oxidase, and in reductive Fe uptake mediated by the fungal FET family of MCOs.

For clarity, this discussion will focus on the intracellular Cu/Zn-Sod1p, although there are other fungal Cu containing SOD enzymes, such as the Cu-only SODs of *Candida albicans* (61). Fungal Cu/Zn-Sod1p is mainly found in the cytosol, although it also localizes to the intermembrane space of mitochondria (62) and other locations including the nucleus. Cu/Zn-Sod1p enzymes in fungi are used for antioxidant defense, cellular signaling, and in the nucleus, Sod1p can operate in transcriptional regulation (63-68). Superoxide anion radical is a dangerous free radical that can be generated largely from the mitochondrial electron transport chain, but also other locations including the cytosol (69-71). SOD enzymes disproportionate superoxide anion in a two-step reaction forming hydrogen peroxide and molecular oxygen (72):

$$Cu(II) + O_2^{\bullet -} \rightarrow Cu(I) + O_2$$

$$Cu(I) + O_2^{\bullet -} + 2H^+ \rightarrow Cu(II) + H_2O_2$$

In the mitochondria, Cu/Zn-Sod1p is important in detoxification of superoxide (62,73-75) while in the cytosol, fungal Cu/Zn-Sod enzymes also participate in cellular signaling (67,68). One of the best studied examples of cytosolic signaling via SOD enzyme involves glucose signaling, where Sod1p catalysis functions in glucose control of mitochondrial respiration versus fermentation in yeast cells (68,76). In transcriptional regulation, Sod1p of *S. cerevisiae* can control the responses to DNA damage (66) and regulation of Cu uptake genes (77).

In addition to *SOD1*, another Cu-dependent process in the cell involves oxygen consumption through mitochondria respiration. Complex IV of the electron transport chain (ETC), cytochrome C oxidase, is a heme and Cu-containing oxidase protein consisting of 11 subunits (78). Complex IV driven oxidative phosphorylation is the mechanism by which cells produce the majority of their ATP (79). A number of pathogenic fungi require ETC function for full virulence, including *C. albicans* and *Aspergillus fumigatus* (80,81).

Fungi also make use of MCOs for a number of biochemical processes. As is the case with the mammalian MCO ceruloplasmin, all fungal MCOs acquire their Cu co-factor as they transit the secretory pathway. One example of a fungal MCO is laccase of the fungal pathogen *Cryptococcus neoformans* that is used to produce melanin for its protective capsule (described in more detail below). The best studied MCO among fungi are the large family of FETs, that are used for reductive Fe transport. Ionic Fe transport in fungi is driven by the Fe permease Ftr1p as part of the reductive Fe pathway. This pathway involves three key proteins membrane-bound proteins: a ferric reductase, a FET ferrous oxidase, and an ionic Fe permease. Fe is first reduced from Fe(III) to Fe(II) by a ferric reductase of the FRE family (82). Next, Fe is oxidized by the FET enzyme, analogous to the MCO ceruloplasmin in mammals (83,84). The reason for the FET oxidation step in Fe transport is not entirely clear, although it is thought that Fe is

oxidized to prevent the spontaneous generation of free radicals by Fe(II) (85,86). This Fe(III) generated by FET is transported by the Fe permease Ftr1p into the cytosol (87).

Fungal Cu sensing Transcription factors

Due to their heavy reliance on cuproenzymes as well as the potentially toxic nature of Cu, fungi must be able to sense and adapt to changes in their surrounding environmental Cu status. Fungi use Cu-sensing transcription factors to modulate Cu homeostasis and the mechanisms of fungal Cu-sensing can be best understood with the baker's yeast *Saccharomyces cerevisiae. S. cerevisiae* has two Cu-binding transcription factors that control Cu homeostasis: Ace1p and Mac1p (88). Ace1p senses elevated Cu concentrations and upregulates Cu detoxification machinery, namely Cu-binding metallothioneins (89,90). Low Cu is sensed by the Cu-binding transcription factor Mac1p (91). Mac1p is a nuclear protein that can bind DNA with an N-terminal DNA binding domain. Mac1p has two main metal binding regions: two Zn sites within the DNA binding N-terminal 159 residues, and Cu-binding regions at two cystine rich regions of the C terminus (residues 252-341) (92,93). The Cu-binding regions of *S. cerevisiae* Mac1p are composed of two repeats of Cys-X-Cys-X4-Cys-X-Cys-X2-Cys-X2-His (the downstream repeat contains an additional Cys-X-Cys motif) (93). Cu(I) binds to Mac1p with an 8 to 1 stoichiometry, which triggers an intramolecular interaction between the C-terminus and the N-terminal DNA binding domain (93). This interaction inhibits the Mac1p transactivation domain located within the Cu-binding sequences (88,94) and also results in Mac1p dissociation from DNA (88). Under Cu deplete conditions when Mac1p does not bind Cu, Mac1p binds its consensus sequences and upregulates transcription of the high affinity Cu-transporters *CTR1* and *CTR3* as well as the cupric reductases *FRE1* and *FRE7* (95,96). Like in mammalian cells, the Ctr1p Cu permeases in yeast cells only

transport the reduced Cu(I) form of Cu and the cupric reductase facilitates Cu uptake by Ctr1p by converting extracellular Cu(II) to Cu(I). The cupric reductases for fungi are members of the same family of FRE oxidoreductases that reduce ferric Fe for Fe transport as described above. Other than *CTR1* and *FRE* cupric reductases, no other targets of Mac1p control have been identified for the simple bakers' yeast. Overall, Mac1p in the non-pathogenic yeast *S. cerevisiae* appears to have evolved for the sole purpose of increasing Cu uptake when extracellular Cu is low.

Cu homeostasis in fungal pathogens: Cryptococcus neoformans and Aspergillus fumigatus

Compared to *S. cerevisiae*, transcriptional regulation of Cu homeostasis in fungal pathogens seems to have diverged in two directions. Some pathogenic fungi use a single Cu-responsive transcription factor, Cuf1p, which bears homology to both *S. cerevisiae* Ace1p and Mac1 while others are more like *S. cerevisiae* and have two distinct transcription factors.

Cryptococcus neoformans is a major fungal pathogen that infects an estimated 220,000 people a year (97). It is an environmental fungus that can infect through inhalation. *Cryptococcus* initially infects the lung but can disseminate to other areas of the body (98). While cases of infection are rare in healthy people, *C. neoformans* has a high mortality rate in individuals with compromised immune systems (99,100). *C. neoformans* is famous for its capsule which is a polysaccharide barrier and melanin, a compound that is synthesized by the MCO laccase as mentioned above (101,102).

C. *neoformans* senses Cu via the Cuf1p transcription factor (103). As the sole Cu-responsive transcription factor in *C. neoformans,* it manages both Cu toxicity and Cu starvation. During times of Cu toxicity, Cuf1p upregulates two metallothioneins

CMT1/*CMT2*, while under Cu starvation it induces Cu-uptake transporters *CTR1*/*CTR4* (104,105). Similar to *S. cerevisiae* Mac1p, Cuf1 induces transcription of the *CTR* family of genes of *C. neoformans* as well as the cupric reductase *FRE7* (105). Because Cuf1p is governing Cu homeostasis during conditions of Cu toxicity and Cu starvation, *cuf1Δ/Δ* mutants are very sensitive to fluctuations in Cu (104). These dual roles of Cuf1p in both protecting against Cu toxicity and in the adaptation to low Cu are born out during pathogenesis of the fungus as it infects the animal host.

C. neoformans initially infects the lungs, where host Cu levels are high and Cu detoxification machinery like the metallothioneins *CMT1*/*CMT2* are vital for virulence (106). Here in the lung, Cuf1p plays a critical role in *C. neoformans* protection against the Cu-burst of pulmonary macrophages by inducing these metallothionein genes. At later stages of infection, *C. neoformans* disseminates to the brain to cause meningoencephalitis (107). In the brain *C. neoformans* experiences a Cu limiting environment and *C. neoformans* using Cuf1p to upregulate the Cu-transporter *CTR4* (47,48,50). In patients, *CTR4* induction has been observed during neurologic infection and high *CTR4* expression levels are associated with dissemination to the CNS by *C. neoformans* (47).

Aspergillus species are a major public health concern. In 2014 alone, there were 15,000 aspergillosis-associated hospitalization in the United States (108). *Aspergillus. fumigatus* accounts for ~90% of infections by Aspergillus species in humans (109). *A. fumigatus* is an environmental fungus that can become an opportunistic pathogen under certain circumstances, namely immunosuppression (109). Like *C. neoformans*, *A. fumigatus* can be inhaled into the lungs, which are the primary site of infection. *A. fumigatus* has retained the Ace1/Mac1 system as two separate proteins. Ace1p induces transcription of metallothioneins when Cu is high and when Cu is low, Mac1p induces the core Cu regulon: the *CTR* family of high affinity Cu transporters, and the cupric

reductase FetDp (110-112). Unlike *S. cerevisiae*, *A. fumigatus* Mac1p also regulates Fe uptake independently of Cu and binds a unique consensus site found in the promoters of Fe uptake genes such as the siderophore genes *SIDA,* and *SIDD* (113). *A. fumigatus afmac1* mutants have a large virulence defect in mice in an intranasal injection model and are more susceptible to killing by both neutrophils and macrophages (45). It is not clear whether the role of AfMac1 in virulence here is due to host-impose Cu or Fe starvation in that AfMac1 regulates the uptake of both metals (113).

Cu homeostasis in Candida albicans

Candida species are a major public health concern and this thesis focuses on specifically on *Candida albicans* (Chapters 3 and 4). *C. albicans* is a polymorphic yeast which is normally found as a harmless commensal species of the human flora. *C. albicans* can typically be found in the gastrointestinal tract, oral cavity, and vagina. Disruption of the local flora or immune system can allow *C. albicans* to disseminate to internal tissues. *C. albicans* causes infections such as thrush in the mouth and throat, and vaginal yeast infection. Typically, these conditions are not life threatening. However, if the epithelial integrity is compromised or when the immune system is suppressed, *C. albicans* can enter the blood stream and disseminate to other organs including the lung, gastrointestinal tract, kidney, liver and spleen (114,115). The CDC estimates that ~25,000 cases of invasive candidiasis occur each year in the USA and of these, infection with *C. albicans* accounts for ~1/3 the cases (116-118). These infections are very dangerous and have an associated mortality rate of ~20% (119).

Like other fungi including *S. cerevisiae* and *A. fumigatus, C. albicans* has separate Ace1p and Mac1p regulators for adapting to high and low Cu, respectively. Ace1p activates metallothioneins as well as a Cu-exporting ATPase *CRP1*. When Cu is

low, Cu is sensed in *C. albicans* by Mac1p that upregulates *CTR1* and *FRE7* (120,121) (Fig. 1-2). *C. albicans* Mac1p has evolved to also self-regulate *MAC1,* as well as *AOX2* encoding an anti-oxidant enzyme in the mitochondria that prevents superoxide formation by the electron transport chain (121,122)(Fig. 1-2). Induction of all four genes involves Mac1p binding consensus sequences in the upstream promoter regions under Cu starvation conditions. In addition to these four targets, the Culotta laboratory discovered in 2015 that *C. albicans* Mac1p regulates superoxide dismutases, including the above mentioned Cu/Zn-Sod1p and a novel cytosolic version of a Mn containing *SOD3* (43). In *Candida,* Cu/Zn-Sod1p is found in the cytosol and in the intermembrane space (IMS) of mitochondria (123,124). Mac1p down regulates Cu/Zn-Sod1p during Cu limitation and this involves a Mac1p binding sequence in an intron downstream of the transcriptional start site (43). This was the first evidence that Mac1p could act as a transcriptional repressor. Subsequently, *SOD1* was also found to be a target of repression by *C. neoformans* Cuf1p, indicating that the repression of Cu/Zn-Sod1p during Cu starvation may be widespread in fungi (105). The second SOD encoding target of Mac1p in *C. albicans* is a highly unusual Mn-containing cytosolic *SOD3*. In all other eukaryotes Mn-containing SODs are typically restricted to the mitochondrial matrix, not cytosolic (125). *C. albicans* has both types of Mn-SOD, and only the cytosolic *SOD3*, but not the mitochondrial *SOD2*, is induced by Mac1p (43,126). Like *CTR1, FRE7, AOX2* and *MAC1, SOD3* is induced by Mac1p under Cu starvation conditions using consensus binding sequences in the upstream promoter (43). Together, the regulation of anti-oxidants *AOX2, SOD1* and *SOD3* by Mac1p serve to maintain ROS homeostasis during Cu starvation. Mn-Sod3p is a bona fide SOD enzyme that substitutes for Cu/Zn-Sod1p in cytosolic signaling involving ROS, but Sod3p is not present in the mitochondria (126). The Mac1p induction of the alternative oxidase *AOX2* serves to protect the cell from mitochondria ROS when *SOD1* is repressed during Cu starvation (123). While *C.*

albicans Mac1p clearly participates in activating Cu uptake and maintaining ROS homeostasis during Cu limitation, is there another function? In Chapter 4 of this thesis, I investigate the expanded roles of *C. albicans* Mac1p in metal homeostasis.

C. albicans initially faces Cu toxicity and then Cu starvation in the murine kidney

One of the best studied models for *C. albicans* infection involves the murine model of disseminated candidasis where the kidney is the organ with the highest fungal burden. In this tissue, it has been observed that Cu levels change dynamically (30,43,46,127). Initially kidney Cu is elevated and *C. albicans* activates its Cu detoxification machinery involving Ace1p (43,46). X-ray fluorescence microscopy data show elevation of Cu in the renal cortex after 24 hours of infection and the same has been shown for total Cu measurements by atomic absorption spectroscopy (30,43,46). The changes in kidney Cu coincide with elevated *SOD1* and the Cu exporter *CRP1* expression, showing that the yeast is responding to the high Cu levels (30,43,46). Later in infection, however, kidney Cu levels decline and the yeast responds by activating its Cu starvation response: namely transcription of *CTR1* and *SOD3,* and down regulation of *SOD1* (30,43,46).

The mechanism by which kidney responds to infection through such dynamics in Cu levels was unknown. Possibilities include the Cu exporter ATP7B and ceruloplasmin were both shown to be upregulated in infected kidneys, either of which could explain kidney Cu loss (46). Furthermore, a dramatic increase in serum Cu coincided with kidney Cu loss (43). Could the loss in kidney Cu be related to this rise in kidney Cu and what was the mechanism for the elevated Cu in serum? Prior to this work, the role of ATP7B and ceruloplasmin in the kidney was unclear and it was also unclear if the rise in serum Cu had a connection to kidney Cu loss. The connection and relevance of these data are investigated in Chapter 3.

Regardless of how the host is modulating the kidney, it is clear that *C. albicans* is able to sense and adapt to the changing Cu environment. The ability of *C. albicans* to respond to both the initial high Cu state and the subsequent low Cu state of the kidney are important for fungal fitness, since mutations in genes encoding the Cu exporter Crp1p and Cu importer Ctr1p lead to decreased CFUs in the kidney during this mouse model for disseminated candidiasis (46). Prior to this thesis, the role of Cu sensing via Mac1p during fungal infection was unknown. In Chapter 4 of this thesis we investigate the importance of *C. albicans* Mac1p during fungal invasion of the kidney during disseminated candidiasis.

Overview of thesis work

The work described in this thesis centers on the role of transition metals at the host-pathogen interface. Chapter 2 focuses on the role of the metal binding host immune protein calprotectin during infection with the Lyme disease pathogen *Borrelia burgorferi.* We characterized the presence of calprotectin positive cells around the sites of *B. burgdorferi* infection in skin biopsies of Lyme disease patients. We found that the majority of calprotectin is found in the keratinocytes of the epidermis. In the dermis, a significant fraction of CD68+ macrophages were also positive for calprotectin. Our data highlight the prevalence of non-neutrophil sources of calprotectin during *B. burgdorferi* infection. We further go on to show using *in vitro* cultures that unlike with other microbial pathogens from bacteria to fungi, calprotectin mediated toxicity to *B. burgdorferi* is independent of metal withholding and involves a direct physical interaction.

Chapter 3 investigates host changes in Cu homeostasis during infection with *C. albicans*. We determined that the rise of serum Cu during *C. albicans* infection is attributable to liver produced ceruloplasmin. Furthermore, we show that the transporter ATP7B is dispensable for kidney Cu loss during *Candida* infection. It was previously

unknown whether the kidney Cu loss phenomenon was due to local invasion of the tissue by the fungus. We found instead that this Cu loss in the kidney is a global response to infection and also occurs with the intravascular malaria parasite *Plasmodium berghei.*

In the final research chapter (Chapter 4) of this thesis we switch from the host to the fungal pathogen and investigate the role of Cu-sensing transcription factor Mac1p in *C. albicans.* We found that Mac1p is an important virulence factor in this disseminated model of candidiasis. We show that *mac1*Δ/Δ mutants of *C. albicans* are deficient in both mitochondrial respiration and in Fe accumulation and that these deficiencies are not due to impaired Cu uptake alone, but rather defects in Cu allocation. This work highlights the need of *C. albicans* to maintain high cellular respiration and shows the great lengths *Candida* will go to spare Cu for it. Taken together, this work highlights the defense mechanisms of the host and the clever adaptations that *C. albicans* uses to thwart host-imposed Cu starvation.

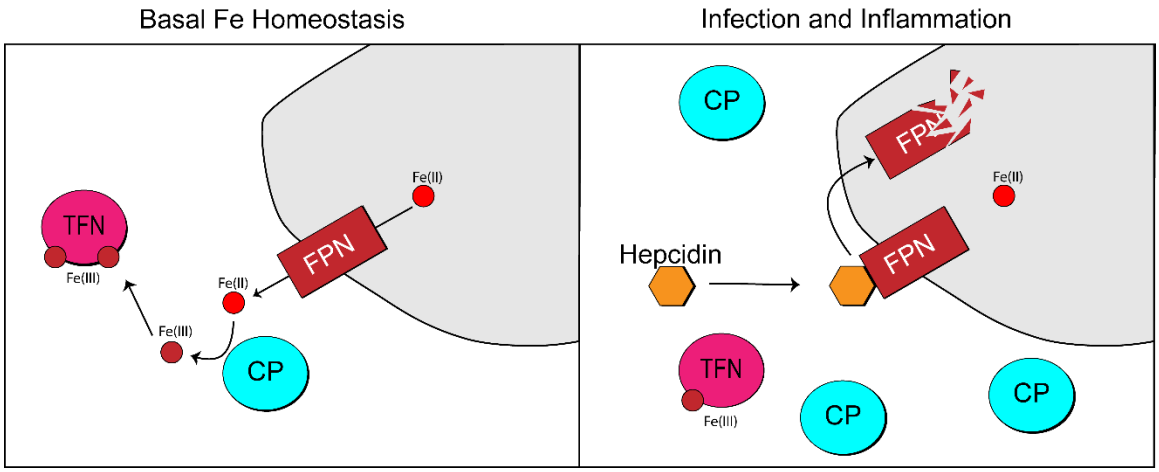

Figure 1-1 Mammalian Fe homeostasis during infection and inflammation. Under basal conditions, ferroportin (FPN) exports Fe(II) from a number of different cell types including macrophages, Kupffer cells, and enterocytes (128). This Fe is oxidized by ceruloplasmin (CP) to promote loading onto transferrin (TFN) (8,129,130). When the acute phase response is triggered, the small peptide hormone hepcidin is secreted from the liver (12,13). It binds to FPN leading to its internalization and subsequent degradation (15). Paradoxically, CP is also highly upregulated during this condition (19).

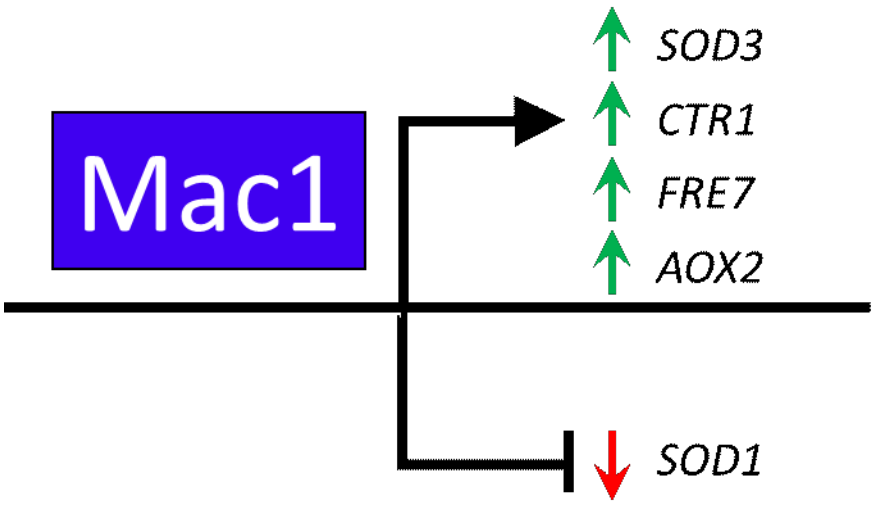

Figure 1-2 *Candida albicans* Mac1p Cu regulon. During Cu limitation, Mac1p upregulates *SOD3, CTR1, FRE7,* and *AOX2* and down regulates *SOD1* (43,121).

Chapter 2

Antimicrobial action of calprotectin that does not involve metal withholding

This chapter was published in *Metallomics* (2018, Dec 12;10(12): 1728-1742) and is reproduced here with copyright permission from the Royal Society of Chemistry. Ed Culbertson and Angelique Besold are co-first authors on this work. Ed Culbertson contributed Table 2-1, 2-2, S2-1, and S2-1 and Figures 2-1, -2, -3, -4.

Abstract

Calprotectin is a potent antimicrobial that inhibits the growth of pathogens by tightly binding transition metals such as Mn and Zn, thereby preventing their uptake and utilization by invading microbes. At sites of infection, calprotectin is abundantly released from neutrophils, but calprotectin is also present in non-neutrophil cell types that may be relevant to infections. We show here that in patients infected with the Lyme disease pathogen *Borreliella (Borrelia) burgdorferi*, calprotectin is produced in neutrophil-free regions of the skin, in both epidermal keratinocytes and in immune cells infiltrating the dermis, including CD68 positive macrophages. In culture, *B. burgdorferi*'s growth is inhibited by calprotectin, but surprisingly, the mechanism does not involve the classical withholding of metal nutrients. *B. burgdorferi* cells exposed to calprotectin cease growth with no reduction in intracellular Mn and no loss in activity of Mn enzymes including the SodA superoxide dismutase. Additionally, there is no obvious loss in intracellular Zn. Rather than metal depletion, we find that calprotectin inhibits *B. burgdorferi* growth through a mechanism that requires physical association of calprotectin with the bacteria. By comparison, calprotectin inhibited *E. coli* growth without physically interacting with the microbe, and calprotectin effectively depleted *E. coli* of intracellular Mn and Zn. Our studies with *B. burgdorferi* demonstrate that the antimicrobial capacity of calprotectin is complex and extends well beyond simple withholding of metal micronutrients.

Introduction

Transition metals such as Mn, Zn, Cu and Fe are essential micronutrients for virtually all living organisms, yet these same elements are potentially toxic. During infection, the host exploits this double-edged sword as part of the immune response against invading pathogens. The host may either attack pathogens with high/toxic levels of metals or starve the invading microbe of metal micronutrients through a process called nutritional immunity (1,2,131). One of the best studied examples of nutritional immunity involves calprotectin, a member of the S100 family of proteins (2). Calprotectin consists of a heterodimer of S100A8 and S100A9 proteins and has been shown to form higher order oligomers in the presence of Zn or excess calcium (132-135). Each heterodimer binds transition metals with high affinity through two distinct metal coordinating sites at the dimer interface (1,2,136,137). Site 1 consists of six histidine residues (two from S100A8 and four from S100A9), while site 2 consists of two histidine residues from S100A8 and a histidine and aspartate from S100A9. Both sites have been shown to tightly bind Zn with affinities ranging from low nanomolar to sub-picomolar (26,138-140). Unlike Zn, Mn only binds site 1 with high affinity (sub-nanomolar to low nanomolar range) (138,139,141,142); the relatively poor binding of Mn to site 2 (micromolar range) is not likely to contribute to Mn sequestration (138,141). Both sites are reported to bind other transition metals including Cu, Fe and Ni (30,143,144). Calprotectin is an abundant component of neutrophils that is released at sites of infection in concentrations reaching 1 mg/mL (145). With its

high affinity for transition metals, calprotectin can effectively deplete the extracellular environment of metals such as Mn and Zn, thereby starving neighboring microbes of these metal nutrients (1,2). Calprotectin has been reported to act as an antimicrobial for numerous bacteria (26,29,131,139,143,146-150) and the mechanism has been widely ascribed to the withholding of metal nutrients (26,27,29,131,138,139,143,147,148,151-155).

As with many bacterial microbes, the Lyme disease (LD) pathogen *Borrelia burgdorferi* (*Bb*) is susceptible to growth inhibition by calprotectin *in vitro* (146,156). *Bb* represents a particularly interesting case of metals in biology in that the organism has uniquely evolved with no known requirement for Fe (157,158). Additionally, there is no known nutritional requirement for Cu, although the spirochete has evolved methods to detoxify the metal (159). *Bb* can accumulate high levels of Mn through at least two Mn uptake systems(160,161), and Mn acquisition is essential for pathogenesis (161). This high Mn is required to activate a Mn containing SodA superoxide dismutase (158,162,163) essential for virulence (164). Aside from Mn, *Bb* requires Zn to activate numerous Zn metalloenzymes (165-168) and the spirochete is capable of maintaining constant Zn levels despite fluctuations in environmental Zn (169). Based on *Bb*'s dependence on Mn and Zn micronutrients, it is possible that withholding of one or both metals accounts for this anti-*Borrelia* activity of calprotectin, although this has never been directly tested.

As mentioned above, neutrophils are believed to be the primary source of anti-microbial calprotectin for diverse microbial pathogens. In LD, neutrophils can

play a significant role in the inflammatory response of persistent infections, particularly in joints and synovial fluid (146,156). However, the predominant target of *Bb* infections in both early and early disseminated stages of disease is the skin, classically presenting as the erythema migrans (EM) rash at the site of the tick bite, as well as multiple EM as a result of hematogenous dissemination of the spirochete. These rashes show little or no infiltration with neutrophils (170,171). However, in a transcriptome study, S100A8 and S100A9 were significantly upregulated in EM lesions (172). Moreover, the skin is known to produce many S100 family members including S100A7, S100A12, S100A8 and S100A9, and calprotectin is known to be secreted by keratinocytes (22,173-178).

Herein, we use a combination of human tissue analyses and microbiology to explore the connection between calprotectin and *Bb*. We provide evidence for a non-neutrophil origin of calprotectin relevant to LD. Specifically, calprotectin is widely apparent in the EM rashes of LD patients in both the epidermal and dermal layers of the skin. In our *in vitro* studies, calprotectin exhibits potent anti-*Borrelia* activity in laboratory cultures, but growth inhibition occurs in the absence of any detectable metal withholding. Calprotectin inhibits *Bb* growth at relatively low doses that are ineffective in withholding either Mn or Zn micronutrients from the spirochete. Our findings support a model in which toxicity results from physical interactions between calprotectin and the spirochete, associated with an increased susceptibility to hypotonic stress.

Results

Non-neutrophil origins of calprotectin at sites of Bb infection

In cases where calprotectin is reported to withhold metals from microbes, the host cell source is largely believed to be neutrophils (29,138,147,179). However, the primary site of infection with *Bb*, namely the EM rash in the skin, appears devoid of these immune cells (170,171). To determine if *Bb* may be exposed to non-neutrophil sources of calprotectin in the skin, we analyzed sections of skin biopsies taken from the site of EM rashes from Lyme disease (LD) patients in comparison to the skin of control patients (non-LD surgical controls). As seen in the immunofluorescent microscopy images of skin in Fig. S2-1 (ESI†) and in the enlarged images of Fig. 2-1, variable staining with a S100A8 antibody was seen in individual cells of the epidermis (defined by DAPI staining), where one LD patient (patient C) had particularly high epidermal S100A8. Upon quantification of multiple images, there was no major difference between S100A8 positive epidermal cells in the EM rash of LD patients versus the skin of controls (Fig. 2-2A). *Bb* is known to colonize the dermal layer of skin (180), and we observed punctate staining of S100A8 in specific dermal cells of all three patients (Fig. 2-1). This precise pattern of punctate dermal staining for CP has been previously noted in cases of skin inflammation and wound healing (175,181-183). Upon quantification, the total number of S100A8 positive cells in the dermal layer varied among the individuals (Fig. 2-2B), although there was a trend towards increased S100A8 positive cells in the skin of LD patients compared to controls (see legend to Fig. 2-2B).

The epidermal staining of S100A8 is likely keratinocytes, which comprise approximately 95% of cells within the epidermis (184), and these cells are well known to produce and secrete calprotectin(173,174,185). By contrast, the nature of the dermal staining was unclear. The EM rash of LD patients is devoid of neutrophils (170,171,186),

but is marked with infiltrating lymphocytes and occasional macrophages (187). Macrophages can produce calprotectin (1,188-190), and in other reports of inflammation (non-LD), CD68 positive macrophages and CD8 positive lymphocytes have been shown to express calprotectin (190,191). We observed both of these immune cell markers in the dermis of LD patients (Figs. 2-3 and 2-4 and Tables 2-1 and 2-2). In double labeling studies, the LD patient with the lowest dermal S100A8 (patient A) showed negligible co-localization of S100A8 with either CD8 or CD68 markers (Figs. 2-3 and 2-4; Tables 2-1 and 2-2). By comparison, the two patients with high dermal S100A8 (patients B and C) showed marked (25-40%) co-localization of S100A8 with the macrophage CD68 marker (Fig. 2-4 and Table 2-2). There was also some co-localization of S100A8 with CD8, but the cells numbers were comparatively low and restricted to patient B (Fig. 2-3 and Table 2-1). It is important to note that a fraction of S100A8 positive cells were neither positive for CD68 nor CD8 and analysis of other immune markers such as CD163 proved negative (Fig. S2-2). Additional cell types currently of unknown nature must contribute to calprotectin in the infected dermis (see *Discussion*). Regardless of the nature of these cells, our studies demonstrate that calprotectin can exist at sites of primary *Bb* infection in the skin, even in the absence of neutrophils, providing evidence that calprotectin may be important for fighting *Bb* at the site of infection.

Calprotectin effects on Bb growth in culture and Bb metals

We next addressed how calprotectin impacts *Bb* growth and metal homeostasis using laboratory cultures of the spirochete and recombinant human calprotectin. Growth of *Bb* in laboratory cultures requires a specialized medium (BSK II) rich in rabbit serum and albumin, whereby the spirochete grows optimally between 30^{o}C – 37^{o}C and doubles once every 12-24 hours(192,193). Consistent with previous studies(146,156), *Bb* growth

is strongly inhibited by CP at concentrations greater than 100 µg/mL (Fig. 2-5A). These levels of CP are significantly lower than what has been reported for several other bacteria grown in different media including *Helicobacter pylori* (153), *Staphylococcus sp, Pseudomonas aeruginosa* and *Escherichia coli*.(139), but within the range for other organisms including *Listeria monocytogenes*, *Streptococcus mutans* (155) and *Candida albicans*(194). To determine if the BSK II medium affects the bioactive dose of calprotectin, *E. coli* susceptibility to calprotectin was examined in this serum rich medium. As seen in Fig. 2-5B, growth of *E. coli* grown in BSK II is inhibited by >0.5 mg/mL calprotectin, nearly five times the toxic dose of calprotectin for *Bb* grown in BSK II (Fig. 2-5A). Thus, *Bb* seems to have a particularly high sensitivity to growth inhibition by calprotectin, at least compared to *E. coli.*

calprotectin can sequester transition metals using two high affinity metal binding sites and we tested whether this metal binding property was important for the *Bb* growth inhibition observed. To accomplish this, we used a mutant of calprotectin, termed ΔS1ΔS2, that lacks transition metal binding capabilities. Specifically, four of the six metal coordinating histidines of site 1 were mutated to asparagine and the three histidines and single aspartic acid of metal binding site 2 were mutated to asparagine and serine, respectively (139). As seen in Fig. 2-6A, this ΔS1ΔS2 calprotectin mutant showed no toxicity to *Bb*. Additionally, we examined the effects of individual mutations at site 1 versus site 2 and find that calprotectin toxicity was also greatly reversed with ΔS2 calprotectin mutated at site 2 (Fig. 2-6B). By comparison, ΔS1 calprotectin defective in site 1 effectively attenuated *Bb* growth at 125 µg/mL, similar to WT calprotectin (Fig. 2-6B), although ΔS1 calprotectin did show some loss of toxicity at the lower dose of 80 µg/mL. Thus, of the two metal binding sites, site 2 appears most critical for inhibiting *Bb* growth in culture, with site 1 contributing less to toxicity.

Mn binds to calprotectin specifically through site 1 and since the ΔS1 mutant is still toxic to *Bb*, this suggests that calprotectin does not inhibit the growth of *Bb* by withholding Mn. To investigate this, we examined total Mn levels in *Bb* by ICP-MS. As seen in Fig. 2-7A, there was no decrease in Mn in *Bb* cells cultured at the mean inhibitory concentration of calprotectin (80 μg/mL). If anything, Mn levels rose (Fig. 2-7A). We also examined activity of the Mn dependent superoxide dismutase SodA, a biomarker of intracellular Mn in *Bb*.(158,162,164) Although the equivalent SodA in *Staphylococcus aureus* is inactivated by calprotectin in culture (138,152), we observed no such inhibition of SodA in *Bb* when cells were cultured (Fig. 2-7B). Altogether, the findings of Fig. 2-6B, 2-7A and 2-7B demonstrate that calprotectin inhibits *Bb* growth without withholding Mn from the bacteria.

In complex growth media such as BSK II, the binding of metals to calprotectin is affected by the relative bioavailability of the transition metals Mn, Zn, Cu and Fe. As seen in Table S2-1, and consistent with previous findings(169), BSK II media contains Mn and Zn levels that approximate that of the TSB-based medium employed in earlier studies involving CP (26,27,139,143). However, Fe and Cu are higher in BSK II, with contributions from serum (e.g., heme, ferritin, transferrin and cupro-ceruloplasmin) and albumin(195-197). It was therefore possible that the lack of Mn withholding by calprotectin was due to poor availability of Mn compared to these other metals. To address this possibility, we used *E. coli* as an indirect approach to monitoring calprotectin sequestration of metals from BSK II. *E. coli* is reportedly susceptible to metal withholding by calprotectin (27,139,143), and any loss in *E. coli* Mn would be indicative of calprotectin binding to Mn in BSK II. As seen in Fig. 2-7C, calprotectin treatment of *E. coli* resulted in a pronounced decrease in intracellular Mn, at both the 80 μg/mL mean inhibitory dose for *Bb* and at the higher 350 μg/mL dose that approximates the mean

inhibitory dose for *E. coli*. This lowering of intracellular Mn in *E. coli* impacted Mn availability for SOD enzymes. Like *Bb, E. coli* expresses a Mn dependent SodA in addition to an Fe containing SodB. These SODs can be discerned by differential sensitivity towards H_2O_2 inactivation (Fig. 2-7D)(158). As seen in Fig. 2-7E, the activity of the Mn requiring SodA was greatly attenuated in BSK II cultures treated with calprotectin, even at the 80 μg/mL dose, which has no effect on the activity of *Bb* SodA (Fig. 2-7B). In spite of potentially competing Fe, Cu and Zn ions, calprotectin has the capacity to sequester Mn in BSK II medium. However, *Bb* seems refractory to this Mn sequestration by calprotectin.

Rather than Mn, calprotectin may withhold Zn from *Bb*. In fact, Montgomery and colleagues reported reversal of calprotectin toxicity in *Bb* cultures treated with 3 μM Zn, suggestive of Zn withholding (146). However, we failed to observe any reversal of calprotectin toxicity with similar Zn supplements (Fig. S2-3A) and Zn supplements up to 25 μM (BSK II has ≈3 μM Zn, Table S2-1) did not change the mean inhibitory concentration of calprotectin towards *Bb* (Fig. S2-3B). To directly test whether calprotectin withholds Zn from *Bb,* we measured total Zn in the spirochete by ICP-MS. As seen in Fig. 2-8A, there was no diminution in Zn in *Bb* when cultured with the mean inhibitory dose of calprotectin. In fact, Zn levels dramatically rose >10 fold. A similar rise was seen with Cu, while Fe levels were below limits of detection with or without calprotectin treatment (Fig. S2-4A). By comparison, *E. coli* cultured at its mean inhibitory dose of 350 μg/mL calprotectin exhibited a striking decrease in intracellular Zn (Fig. 2-8B). At the lower 80 μg/mL dose of calprotectin that is non-toxic to *E. coli*, there was no withholding of Zn and, if anything, Zn levels slightly rose, although this was minor (≈50%) (Fig 2-8B). The growth inhibition of *E. coli* by high levels of calprotectin (350 μg/mL) clearly correlates with calprotectin withholding of both Mn and Zn. Additionally,

we observed withholding of *E. coli* Fe and Cu micronutrients at this mean inhibitory concentration of calprotectin (Fig. S2-4B,C) and a decrease in Fe-SodB activity (Fig 2-7E). This loss of Fe and Cu micronutrients for *E. coli* may also contribute to the growth inhibition. Compared to these effects on *E. coli*, calprotectin inhibits *Bb* growth at lower doses and in the absence of any obvious withholding of the metal nutrients for *Bb*, Mn and Zn.

Calprotectin interactions with Bb

In cases where calprotectin withholds metals from microbes, metal depletion can be accomplished without physically contacting the organism, examples including *S. aureus, Streptococcus pyogenes, Streptococcus pneumoniae* and the fungal pathogen *C. albicans* (29,149,198). Calprotectin simply acts by modifying the extracellular environment through metal sequestration. However, there are rare reports of calprotectin directly interacting with microbes, e.g., *Neisseria* species and *Finegoldia magna* (149,199,200). We investigated whether the same is true for *Bb*. As seen in Fig. 2-7B, bottom panel, a doublet protein of ≈11-13 kDa was evident in whole cell lysates of calprotectin treated *Bb* cells, but not in lysates from control untreated *Bb*. Upon closer inspection, this doublet was seen to co-migrate with S100A8 (10.8 kDa) and S100A9 (13.2 kDa) subunits of calprotectin (Fig. 2-9A, left panel), and the 13 kDa species cross-reacted with an anti-S100A9 antibody on immunoblots (Fig. 2-9A, right panel). The appearance of calprotectin in whole cell lysates of *Bb* did not reflect non-specific precipitation or aggregation of the protein, as calprotectin was retained following extensive washing of *Bb* cells and required the presence of *Bb* cells. As seen in Fig. 2-9B, calprotectin was undetectable in lysates of *E. coli* cultured in the same BSK II

medium, despite higher levels of calprotectin used to treat *E. coli* (350 µg/mL) versus *Bb* (80 µg/mL).

We next tested whether calprotectin association with *Bb* required transition metal binding sites 1 and/or 2. As seen in Fig. 2-9C top and middle panels, the ΔS2 and ΔS1ΔS2 mutants of calprotectin were absent in lysates of *Bb*, despite equivalent amounts of calprotectin protein added to the culture (Fig. 2-9C bottom). The only calprotectin mutant recovered in *Bb* cell lysates was ΔS1 calprotectin, although the level of calprotectin recovered with the ΔS1 mutant was less than that of WT calprotectin. Together these results demonstrate that calprotectin interactions with *Bb* relies heavily on site 2, and to a lesser extent, on site 1. It is noteworthy that these results completely parallel findings with calprotectin toxicity where growth inhibition is strongly dependent on site 2, and partly dependent on site 1 (Fig. 2-6B). Thus, toxicity against *Bb* is dependent on the ability of calprotectin to physically associate with the spirochete.

Microscopy analyses of intracellular Zn and Bb morphology with calprotectin treatment

Since calprotectin is abundantly recovered with *Bb*, it was possible that the aforementioned elevation in *Bb* Zn (Fig. 2-8A) could be attributable to Zn bound to calprotectin. In fact, we observed a near stoichiometric ratio of *Bb*-associated calprotectin versus the rise in *Bb*-associated Zn (e.g., 30 nmoles CP/10^9 cells versus 32 nmoles Zn/10^9 cells, see *Experimental*). If the Zn measured by ICP-MS is largely bound to calprotectin, it remained possible that calprotectin was in fact depleting Zn bioavailability inside *Bb* cells. To address this, we employed the fluorescent Zn probe zinquin, which was previously used by Gherardini and colleagues to tract available Zn in

Bb (165). Zinquin has an affinity constant for Zn in the nanomolar range and is believed to report on loosely bound or accessible Zn pools(201,202). To validate zinquin as a reporter for *Bb* Zn, we used the metal chelator TPEN (*N*,*N*,*N*',*N*'-tetrakis(2-pyridylmethyl ethylenediamine), which has an affinity constant for Zn in the femtomolar range (203). *Bb* cells were grown with relatively non-toxic levels of 3 μM TPEN (Fig. S2-5) followed by staining with zinquin and the PKH red dye for whole cell membranes. As seen in Fig. 2-10A, zinquin fluorescence in *Bb* was greatly diminished in TPEN cultured cells. By comparison, there was no detectable loss in zinquin fluorescence in cells cultured at the mean inhibitory dose of calprotectin (Fig. 2-10B). This finding supports the notion that calprotectin inhibits *Bb* growth through a mechanism that does not involve Zn starvation.

How can the growth of *Bb* be inhibited? Several agents that inhibit *Bb* growth, such as certain antibiotics or other stress conditions, can induce the morphological cyst-like states known as 'round bodies" or 'blebs' (204-207). The round body consists of a spherical membrane-bound structure, while a bleb, which may be an intermediate between the spirochete and round body, consists of a short spirochete with a terminal rounded structure (207). These cyst forms have decreased metabolic activity, potentially as a means to enhance survival, but have the ability to revert to the spirochete in the absence of the stressor(205,207). We observed that when growth was inhibited by calprotectin, *Bb* retained its characteristic spiral spirochete conformation (Fig. 2-10B and 2-11A left) by dark field microscopy. However, upon immediate dilution by 10-fold in water, calprotectin treated cells rapidly converted into blebs, as well as occasional round bodies (Fig. 2-11A right, 2-11B). The control cells not treated with calprotectin remained in the elongated spiral spirochete conformation under the same short exposures to hypotonic conditions (Fig. 2-11), consistent with findings by Alban *et al.*(205). Rapid conversion to cysts with calprotectin treated *Bb* was seen in cultures diluted in water, but

not with cells diluted in phosphate buffer saline (Fig. S2-6). We conclude that calprotectin interactions with *Bb* affects the spirochete in a manner that increases sensitivity towards hypotonic stress (see *Discussion*).

Altogether, the *in vitro* culture studies demonstrate that calprotectin inhibits *Bb* growth through a mechanism that does not involve the traditional withholding of Mn and Zn micronutrients as has been described for other microbes. Instead, calprotectin physically interacts with the *Bb* spirochete and results in an increased propensity for *Bb* cyst formation.

Discussion

The canonical mode of action of calprotectin in fighting pathogens involves withholding essential metal micronutrients. In the case of *Bb*, calprotectin exerts its antimicrobial effects without starving the pathogen of Zn and/or Mn micronutrients. Here we provide an example of where calprotectin inhibits bacterial growth without any obvious effects on metal accumulation. In fact, *Bb* appears to be particularly resilient to the Mn withholding effects of CP, at least compared to *E. coli* examined under parallel conditions. *Bb* expresses at least two Mn uptake systems (160,161) and is capable of accumulating high levels of Mn that are needed to support SodA activity (158,162). The low level of calprotectin that inhibits *Bb* growth may not adequately compete with the *Bb* uptake systems for accumulating Mn, even though this level of calprotectin effectively competes with the Mn uptake systems of *E. coli*. Like *Bb, Salmonella* and *S. aureus* have been shown to be resistant to calprotectin mediated Mn depletion through the use of strong Mn uptake systems (151,179). *Bb* may use potent metal uptake systems for both Mn and Zn to combat metal depletion by calprotectin.

Typically, calprotectin acts at a distance to deplete extracellular metals, but the anti-*Bb* activity of calprotectin involves the direct association of the protein with the bacteria. Examples of calprotectin directly interacting with bacterial microbes are rare. In certain strains of the bacterial pathogen *Finegoldia magna*, calprotectin binds to a surface protein called protein L that protects the cell from the anti-microbial effects of calprotectin. In *F. magna* strains that lack protein L, calprotectin associates with the membrane and causes cell wall/membrane disintegration (149). Interestingly, *Neisseria sp* bind metal bound calprotectin through the CpbA receptor and use this calprotectin as a nutrient Zn source (199,200). *Bb* does not express orthologues of protein L or CpbA and the mechanism of the CP-*Bb* interactions is not understood. In addition to bacteria, calprotectin and other S100 proteins can bind directly to certain parasitic species. Calprotectin has been shown to interact with the surface of adult *Onchocerca volvulus* and with *Echinococcus granulosus,* although it remains unclear how this affects the growth of the worms (208,209). In addition to calprotectin, the related Zn binding S100A12 protein physically interacts with both *O. volvulus* (210) and the nematode *Brugia malayi* (211,212). As is the case with calprotectin and *Bb*, S100A12 inhibits the growth of *B. malayi* without metal withholding. Rather, S100A12 binding to the parasite disrupts the contractile elements, affecting worm motility (211,212). Overall, these studies with parasitic worms and the spirochete *Bb* suggest that calprotectin can inhibit pathogen growth through mechanisms that involve physical interactions with the microbe, not metal withholding. In the case of *Bb*, our studies do not discern between calprotectin binding strictly to the cell surface versus calprotectin uptake into the cell. We consider the latter possibility unlikely as other cases of calprotectin interactions with microbes involve cellular membranes (149,199,200).

How does the interaction with calprotectin inhibit *Bb* growth? Since growth inhibition tracks with an increased sensitivity towards hypotonic conditions, one possibility is that calprotectin may somehow affect the membrane, as evidenced by *Bb* cyst formation upon immediate dilution in water. Although such hypotonic conditions are not likely to be encountered *in vivo,* the osmotic sensitivity observed *in vitro* may be indicative of issues with membrane or osmolyte balance. Regardless of the mechanism, the physical association of calprotectin with *Bb* seems to require metals, such as Zn, Mn, Cu, and Fe, as intact metal binding sites are necessary for CP-*Bb* interactions. Moreover, the binding of calprotectin to *Bb* correlates with high levels of Zn and Cu that associate with the microbe, presumably reflecting Zn-CP and Cu-CP bound to *Bb* (Figs. 2-8A and S2-4A). Therefore, we propose the following model: calprotectin binds to transition metals, helping to stabilize calprotectin and/or induce its tetramerization, as has been shown for Zn (132,135). Metal binding to site 2, and to a lesser extent, site 1, then promotes calprotectin association with *Bb*, although it is currently unknown if this association is through the cell membrane of if calprotectin is internalized. Once associated, calprotectin may affect the membrane in a way that inhibits microbial growth in the absence of metal withholding. Additional studies are required to define the role of each metal site in promoting calprotectin interactions with *Bb* as well as determine the molecular targets in *Bb* that account for calprotectin binding and growth inhibition.

When does *Bb* encounter calprotectin *in vivo*? With persistent infections, where *Bb* accumulates in joints and synovial fluid, the spirochete is likely to encounter calprotectin secreted by infiltrating neutrophils (146,156). In the skin, a primary organ of *Bb* infection, there is no infiltration of neutrophils; however, we show here that a non-neutrophil source of calprotectin is prevalent in the EM rash. We observe cells expressing S100A8 in keratinocytes of the epidermis as well as scattered S100A8

producing cells of dermal layer. Keratinocytes are well known to secrete calprotectin (173-176) and a punctate pattern of dermal S100A8 staining has also been observed in other cases of skin inflammation and wound healing, although the nature of these specific dermal cells was unclear (175,181,183). We have identified a defined number of dermal calprotectin positive cells as CD68 expressing monocytes/macrophages. Although the level of calprotectin produced by these cells in the skin may not be as high as that derived from neutrophils, *Bb* is sensitive to much lower doses of calprotectin compared to other bacteria. When the antimicrobial action of calprotectin involves metal withholding, very high levels of calprotectin are required to deplete the extracellular environment of Zn and/or Mn. By comparison, much lower doses of calprotectin can inhibit *Bb* growth by physically interacting with the microbe without the need to modify the bioavailability of environmental metals.

Conclusion

Calprotectin is known to inhibit the growth of diverse microbial pathogens by withholding metal micronutrients and this mechanism of antimicrobial activity has become near dogmatic. Here, we provide evidence for the first time that this protein can inhibit bacterial growth without starving the microbe of essential metals. The capacity of calprotectin to act as an antimicrobial is indeed complex and depending on the microbe and host niche, circumstances beyond nutritional immunity should considered.

Materials and Methods

Ethics Statement

Individuals with EM were enrolled in prospective studies (NCT00132327 and NCT00028080) approved by the Institutional Review Board at the National Institute of Allergy and Infectious Diseases. All participants were adults (at least 18 years old) who provided written informed consent.

Skin Biopsy Samples

Specimens of skin from 3 patients with EM were obtained by 4-mm punch biopsy. Specimens were obtained from the advancing border of primary EM lesions before the start of antibiotic therapy. The sample for histology was placed in 4% formaldehyde, embedded in paraffin, and stained with hematoxylin and eosin. Control skin samples were obtained from surgical specimens of anonymous patients undergoing surgery for other purposes.

Tissue slice preparation and microscopy

Sections were deparaffinized and rehydrated using successive 5-minute washes: two washes of a xylene isomer mixture (Sigma Aldrich), two of 100% ethanol (EtOH), one of 95% EtOH, 70% EtOH, 50% EtOH, ddH_2O, and 1XPBS. Slides were then placed in 10 mM sodium citrate (pH 6.0) in a polypropylene container and put in boiling water for 10 minutes. Samples were then cooled to room temperature. Slides were then rinsed with ddH_2O and then 1X PBS for 5 minutes each. Slides were blocked in 2% Normal Goat Serum (G9023-10mL Sigma), 1% Bovine Serum Albumin for 30 minutes. The highly specific anti-S100A8 antibody (GTX54721 Gene Tex)(213) was diluted 1:100 in

blocking buffer. Anti-CD8 antibody (M7103 Dako) was used at a dilution of 1:50 and anti-CD68 (790-2931 Ventana) was used at a concentration of 0.4 µg/mL. A dilution of 1:50 was used for Anti-CD163 (BM4041 Acris). Slides were incubated with primary antibody overnight at 4^{o}C prior to being washed three times in 1XPBS for 10 minutes. Secondary antibodies goat anti-rabbit 488 (ab150077 Abcam) and goat anti-mouse 594 (ab150116 Abcam) were applied at a dilution of 1:1000 for 1 hour at room temperature. Slides were then washed two times in 1XPBS for 5 minutes each before being stained with DAPI for 5 minutes. Slides were washed once in 1XPBS for 5 minutes before being mounted on with a coverslip using FlourSave Reagent (Calbiochem). Images were taken on a Zeiss AxioObserver Z1 with Apotome microscope at 20X magnification. Larger images (Fig. S2-1) were imaged at 10X and stitched together. Multiple images (approximately 10) from a single section of each sample were analyzed for S100A8 quantification. Cell counts were quantified using ImageJ. For quantification, TIFF files exported from Zeiss ZEN software were converted to 8-bit greyscale. Contrast was enhanced 5%. Pictures were thresholded to 35 before the colors were adjusted to RGB and the channels were merged. Multiple images (approximately 10) from a single section of each sample were analyzed for S100A8 quantification. A one-way ANOVA with Tukey post-test was applied. Analysis was carried out in GraphPad Prism v5.0 Software.

Bacterial strains, growth medium and growth conditions

Bb strain 297(214) and *E. coli* strain DH5α were cultured in BSK II medium (pH 7.6) containing 6% (v/v) rabbit serum (193,215). *E. coli* was chosen for comparative analyses based on its documented susceptibility towards metal withholding effects of CP(26,27,139,143), its well-defined Mn and Fe containing superoxide dismutase enzymes(158,216) and its ready availability as a BSL1 laboratory organism. *Bb* cultures

were supplemented with 0.05 mg/mL rifampicin, 0.1 mg/mL phosphomycin, and 5 µg/mL amphotericin(215), and were maintained at 34°C; growth was monitored by counting spirochetes under dark field microscopy (Nikon Eclipse 80i). *E. coli* was cultured without antibiotics at 37°C and growth monitored by absorbance at 600 nm.

For calprotectin toxicity studies, triplicate 200 µl cultures of *Bb* were inoculated at $1x10^4$ cells/mL in 96-well flat-bottom plates in 80% BSK II medium with 6% rabbit serum/20% calprotectin buffer (20 mM Tris pH 7.5, 100 mM NaCl,10 mM BME, 3 mM $CaCl_2$) containing human recombinant WT or mutant calprotectin. The metal content of this medium is shown in Table S2-1. Mn and Zn levels are similar to that of the Tryptic Soy Broth (TSB) based media previously used in studies of microbial toxicity to calprotectin(26,27,139,143), and the levels of calcium are sufficient to activate CP (26,141,143). The presence of BME does not affect cell growth in BSK II medium. Cells were enumerated following 6-7 days of growth. *E. coli* sensitivity towards calprotectin was tested similarly using cells inoculated at $1x10^7$ cells/mL and grown for 5-6 hours. In both cases, cell reached late log phase growth following 7-9 cell doublings in the presence of calprotectin. Preparative *Bb* cultures for biochemical analyses were seeded at $1x10^5$ cells/mL; calprotectin was added when cultures reached ≈$5x10^5$ cells/mL and growth proceeded until untreated controls reached 10^7-10^8 cells/mL. Cultures of *E. coli* for biochemical analyses were seeded in BSK II at $8x10^7$ cells/mL and grown to ≈2 x 10^9 cells/mL.

Biochemical analysis

All samples of recombinant WT and mutant calprotectin were prepared according to our standard published protocols (138,139). *Bb* or *E. coli* cells for biochemical analyses were harvested by centrifugation at 3,000 x g at 4°C for 50 or 20 minutes,

respectively. Cell pellets were washed twice in either cold 1 mM Tris, 10 mM EDTA, pH 7.8 or in *Bb* washing buffer (20mM HEPES, pH 7.6, 100mM NaCl, 10mM EDTA)(157) followed by washing twice in cold MilliQ water. The nature of washing did not alter the level of calprotectin associated with *Bb.* For metal analysis of *Bb* by ICP-MS, pellets containing $2x10^8$-$1x10^9$ cells were resuspended in 500 µL of 67-70% (v/v) nitric acid (J.T. Baker, Ultrex II Ultrapure Reagent) and heated at 80°C for 1 hour. Cell debris was removed by centrifugation at 20,000 x g for 5 minutes and the supernatant was diluted 1:14 in MilliQ water prior to analysis by ICP-MS in semi-quantative mode (Agilent 7700x, University of Maryland, School of Pharmacy, Mass Spectrometry Center). With *E. coli*, $6x10^9$-$1x10^{10}$ cells were digested in 500 µL of 20% (v/v) nitric acid overnight at 90°C and diluted 1:10 in MiliQ water in preparation for ICP-MS as described above. As blank controls, BSK II medium (no cells) was incubated in parallel and subjected to the identical centrifugation, washing and acid treatments. Any metal values of these blanks were subtracted from cell samples.

For analysis of metals in the growth media, 200 µL of media (80% BSK II medium/20% calprotectin buffer with 3 mM $CaCl_2$) was digested in 1.5 mL of 23% nitric acid for 18 hours at 80°C. Digested samples were diluted to a final volume of 5.5 mL with MiliQ water (~6% final nitric acid concentration), clarified by centrifugation at 4,000 x g for 10 minutes and subjected to ICP-MS as described above. Alternatively, BSK II medium was made 1% in nitric acid and analyzed directly without dilution using an Agilent 7500ce ICP-MS (Johns Hopkins NIEHS Center Core Facility). The metal values representing 80% BSK, 20% 3 mM $CaCl_2$ were similar in the two experiments, and averages over the two trials are presented in Table S2-1.

For preparation of *Bb* and *E. coli* cell lysates, $1x10^8$-$8x10^{10}$ and $3x10^9$-$1x10^{10}$ cells, respectively, were lysed by glass bead homogenization in 150 µL of lysis buffer (10

mM potassium phosphate (KPi) pH 7.8, 5 mM EDTA, 5 mM EGTA, 50 mM NaCl, 0.45% Tergitol-type NP-40 (NP40), 10% glycerol) containing a volume of Zirconium oxide (0.7 mm) or glass (400-600 nm) beads equivalent to the cell pellet. Following vortexing at 3200 RPM for three 3 min cycles, lysates were clarified by centrifugation at 20,000 x g and stored in -80°C.

Denaturing gel electrophoresis on NuPage 4-12% BisTris Gels (Life Technologies) used ≈ 30 µg of protein lysate or 100-500 ng of recombinant calprotectin. Gels were subjected to either Coomassie Brilliant Blue staining or immunoblot analysis using anti-S100A9 antibody (Abcam ab63818) diluted 1:1,000 and Alexa Fluor 680 donkey anti-rabbit secondary (Life Technologies) diluted 1:10,000. To define the molar quantity of calprotectin versus moles of Zn associated with *Bb,* a cell sample of verified Zn content (as determined by ICP-MS) was subjected to electrophoresis and Coomassie staining against known quantities of purified recombinant human calprotectin. calprotectin bands were quantified using ImageJ software and analyzed against the standard curve of recombinant calprotectin.

For SOD activity, 30 to 50 µg of protein lysate was subjected to native gel electrophoresis at 50 mA using 10 or 12% Tris-glycine native gels (Novex). SOD activity was monitored by nitroblue tetrazolium (NBT) staining and Fe-SOD activity eliminated by treating gels with 30 mM H_2O_2 prior to NBT staining as described (158).

For all *in vitro* studies, data were considered statistically significantly different for p values of ≤0.05 using the two-tailed t test as determined by GraphPad Prism v7.

Microscopy of Bb

For examination of *Bb* morphology, cells were examined under dark field microscopy at 40X magnification. Zinquin-dependent fluorescence was monitored by microscopy of *Bb* cells essentially as described.(165) $5x10^7$ *Bb* cells were harvested by centrifugation at 1,000 x g for 10 minutes. Cells were washed twice with HN Buffer (20 mM NaCl, 50 mM HEPES, pH 7.6), resuspended in 500 µL HN buffer and incubated at room temperature for 5 minutes. A 5 mM stock of zinquin ethyl ester (Sigma) dissolved in DMSO was diluted 1:2 in HN buffer and added to cells at a final concentration of 25 µM followed by incubation at 34°C for 30 minutes. Cells were subsequently stained with PKH26 Red Fluorescent dye for membranes (Sigma) using 2 µL of dye diluted according to manufacturer's specifications followed by incubation for 5 minutes at room temperature. The staining was terminated by the addition of 500 µL BSK II medium. Cells were subsequently washed twice in HN Buffer, resuspended in 100 µL HN buffer and subjected to 40X fluorescence microscopy and imaging using a Zeiss Observer.Z1 microscope equipped with an Apotome VH optical sectioning grid.

Table 2-1 Dermal cells positive for S100A8 and CD8.[1]LD patient number or four individual controls/non-LD patients. [2]Total S100A8 or CD8 counted in two individual sections of patient C and a single section from the remaining patients and controls. [3]Number of cells that co-stained with S100A8 and CD8

Sample[1]	S100A8+[2]	CD8+[2]	CD8+/S100A8+[3]
Patient A	147	46	21
Patient B	30	6	1
Patient C	76	6	1
Control 1	1	4	1
Control 2	7	1	0
Control 3	0	0	0
Control 4	19	1	1

Table 2-2 Dermal cells positive for S100A8 and CD68. [1]LD patient number or four individual controls/non-LD patients. [2]Total S100A8 or CD68 counted in two individual sections of patient A and a single section from the remaining patients and controls. [3]Number of cells that co-stained with S100A8 and CD68

Sample[1]	S100A8+[2]	CD68+[2]	CD68/S100A8+[3]
Patient A	102	59	40
Patient B	18	1	0
Patient C	202	78	48
Control 1	3	6	2
Control 2	9	7	3
Control 3	2	1	1
Control 4	13	0	0

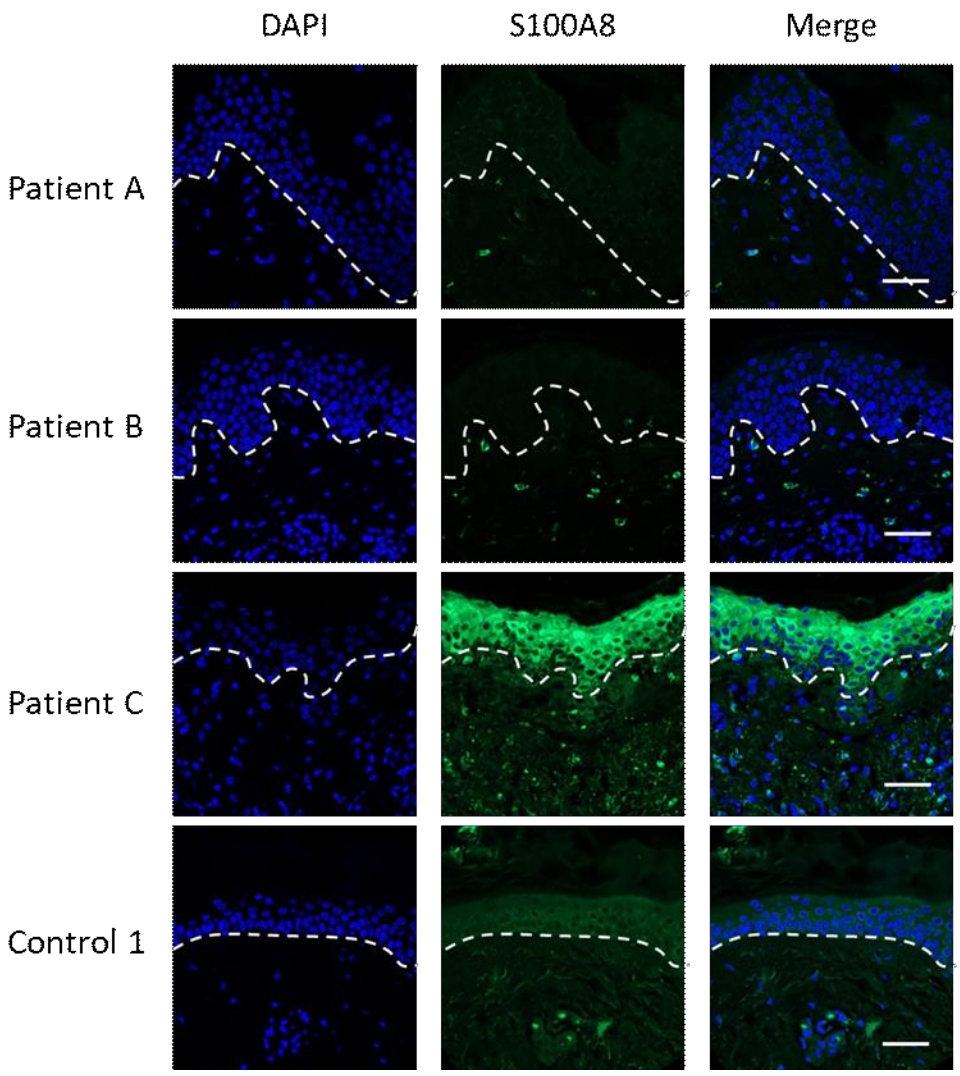

Figure 2-1 Immunofluorescence microscopy imaging of S100A8 expression in the skin of LD patients and controls. Skin tissue sections from the EM rash site of three individual LD patients and one control patient (Control 1) were subjected to immunostaining for S100A8 (green) and nuclei staining with DAPI (blue) before being subjected to fluorescence microscopy at 20X magnification as described in *Experimental*. Dotted lines separate the epidermis from the dermis. Bar represents 50 μm.

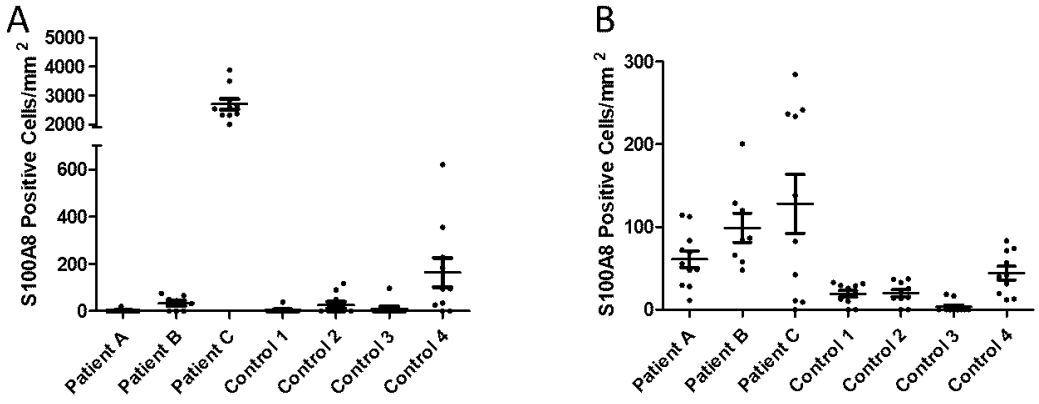

Figure 2-2 Quantification of S100A8 positive cells in the skin of LD patients. S100A8 positive cells were quantified in the epidermis (A) and dermis (B) of skin sections from 3 LD patients and 4 control surgical patients. Results represent cell counts (positive for both DAPI and S100A8) from 8-11 individual images spanning the tissue section of an individual patient. Image numbers: Patient A n=11; patient B n=8; patient C and all four controls n=10. (A) S100A8 staining in the epidermis of patient A is significantly higher than all four controls ($p < 0.001$) and individual patients B and C ($p<0.001$). (B) S100A8 staining in the dermis of patient C is significantly higher than all four controls ($p < 0.01$); the same is true for patient B and controls 1-3 ($p<0.05$).

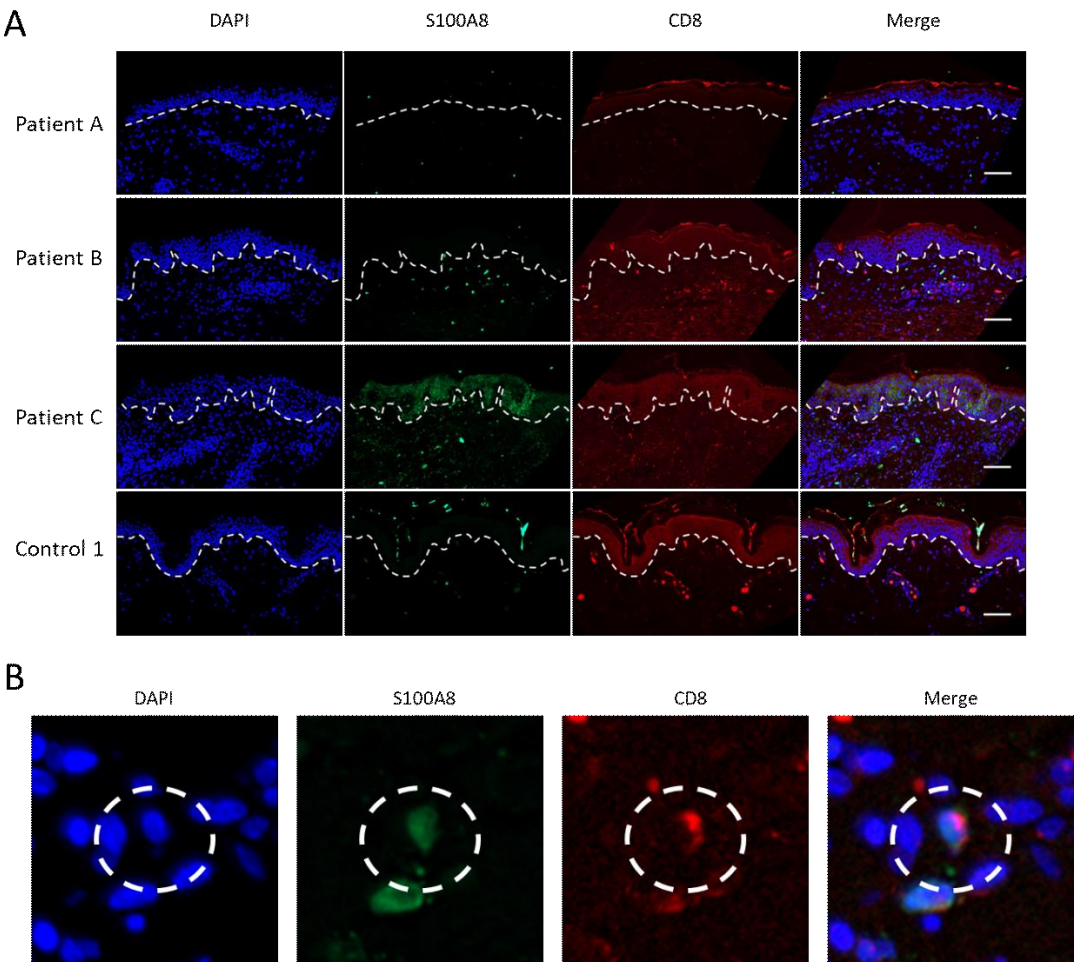

Figure 2-3 Co-localization of S100A8 and CD8 expression in the dermis. (A) Skin tissue sections from the EM rash site of three individual LD patients and one control (control 1) were subjected to immunostaining for S100A8 (green), CD8 (red) and nuclei staining with DAPI (blue) before being subjected to fluorescence microscopy at 20X magnification as in Fig. 1. Dotted lines separate the epidermis from the dermis and bar represents 50 μm. (B) Individual cells co-expressing S100A8 and CD8 were identified by staining with anti-S100A8 (green), anti-CD68 (red) and DAPI (blue) as shown in the dotted circle.

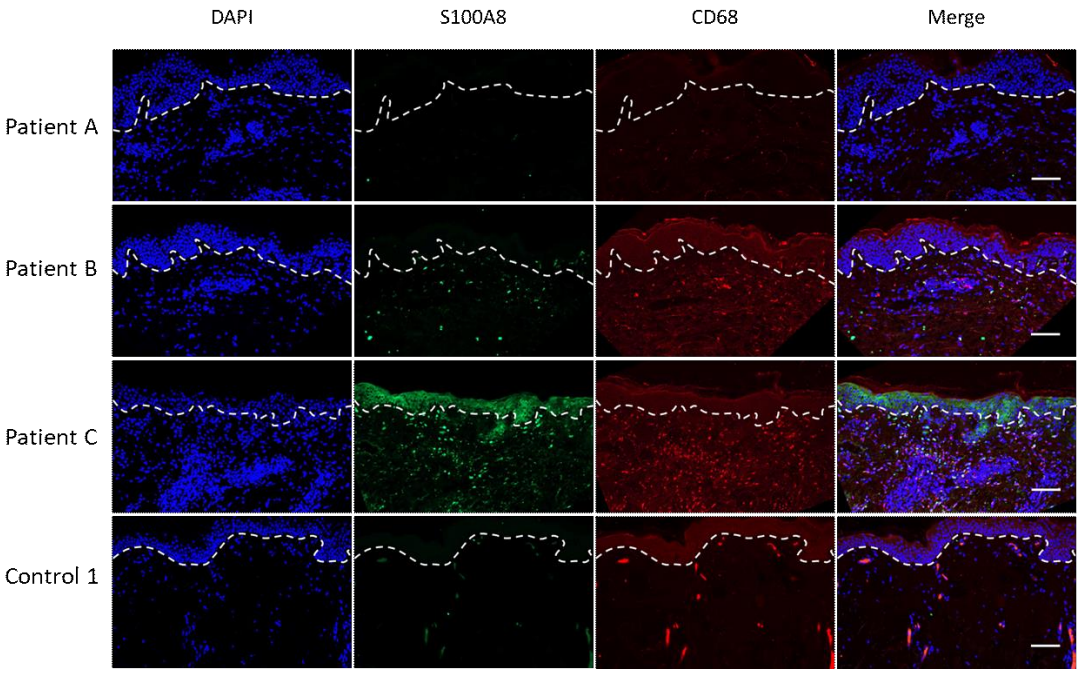

Figure 2-4 Expression of S100A8 and CD68 expression in the dermis. Skin tissue section from the EM rash site of three individual LD patients and one control were subjected to immunostaining for S100A8 (green), CD68 (red) and nuclei staining with DAPI (blue) before being subjected to fluorescence microscopy at 20X magnification as in Fig. 1. Dotted lines separate the epidermis from the dermis and bar represents 50 μm.

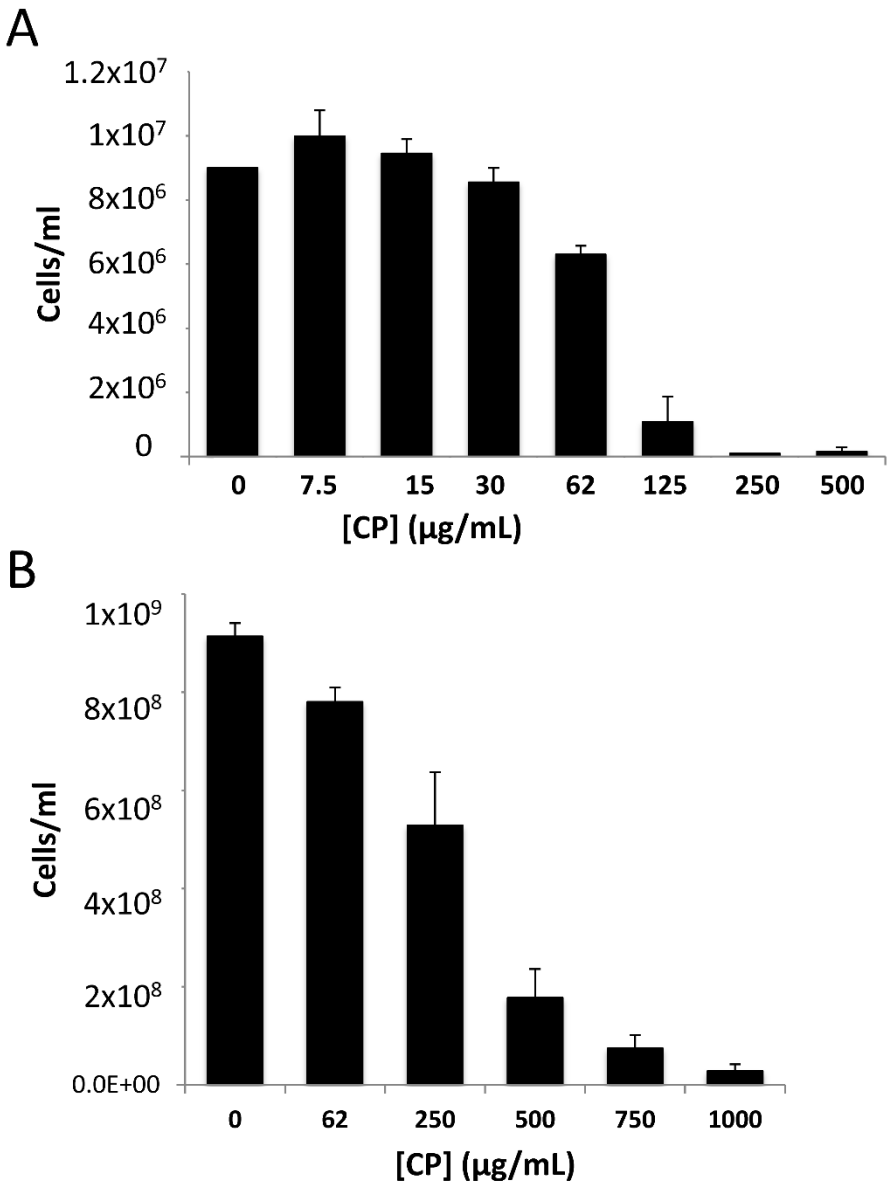

Figure 2-5 Calprotectin mediated growth inhibition of *B. burgdorferi* (*Bb*) versus *E. coli. Bb* (A) or *E. coli* (B) were cultured in BSK II medium as described in *Experimental* in the presence of the indicated concentrations of calprotectin (CP). (A) *Bb* cell number was enumerated under dark field microscopy; results are averages of three biological replicates representative of seven experimental trials. There was essentially no growth at 250 and 500 µg/mL calprotectin and the cell number approximated the original inoculum. (B) *E. coli* cell number was converted from optical density; results are the averages of four biological replicates and are representative of eight experimental trials. Error bars are standard error. Across numerous experimental trials, the mean inhibitory concentration or dose of calprotectin that inhibits growth by 50% for *Bb* and *E. coli* were ≈80 and ≈350 µg/mL, respectively.

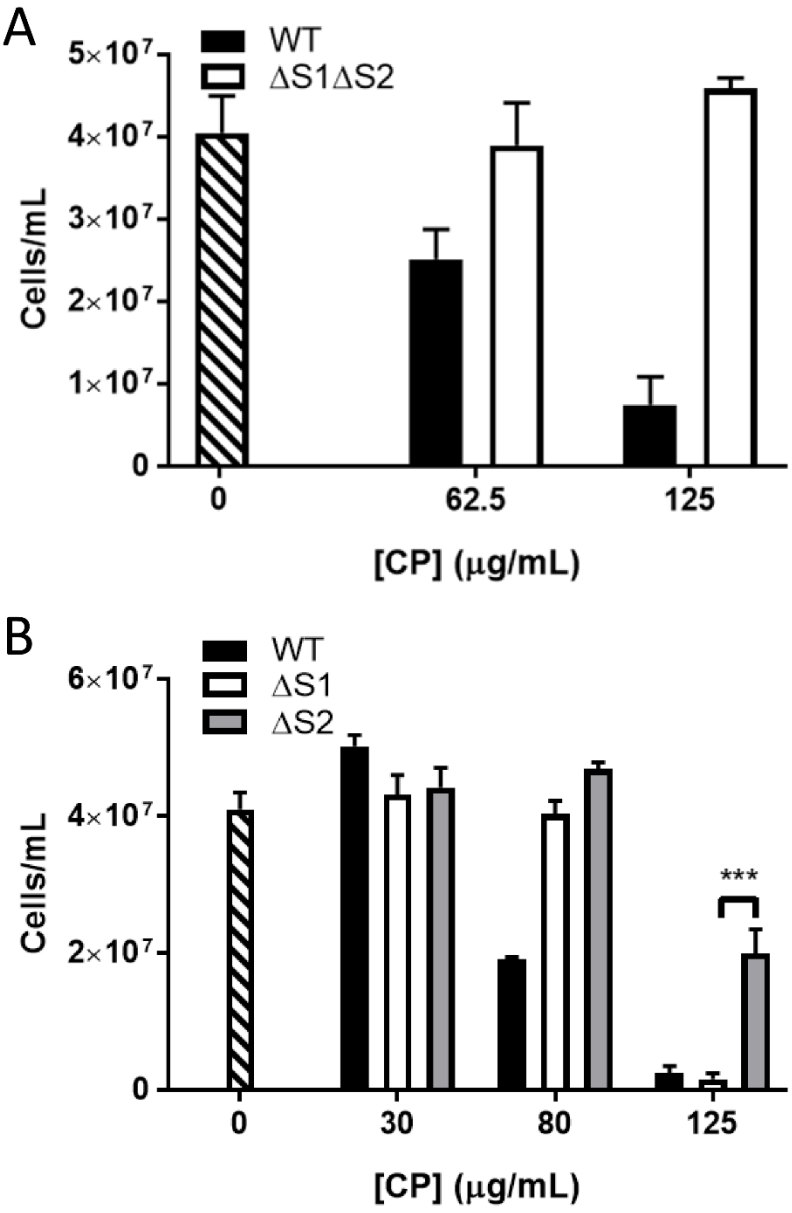

Figure 2-6 Effect of calprotectin metal binding mutants on inhibiting growth of *Bb*. *Bb* cells were grown as in Fig. 5A in the presence of WT calprotectin (CP) (black bar), the indicated metal binding mutants of calprotectin (white and grey bars), or without calprotectin (stippled bar). Results are averages of three biological replicates and are representative of five (A) and three (B) experimental trials; error bars are standard error. The difference in growth inhibition between ΔS1 and ΔS2 calprotectin at 125 μg/mL is statistically significant; ***p = 0.001.

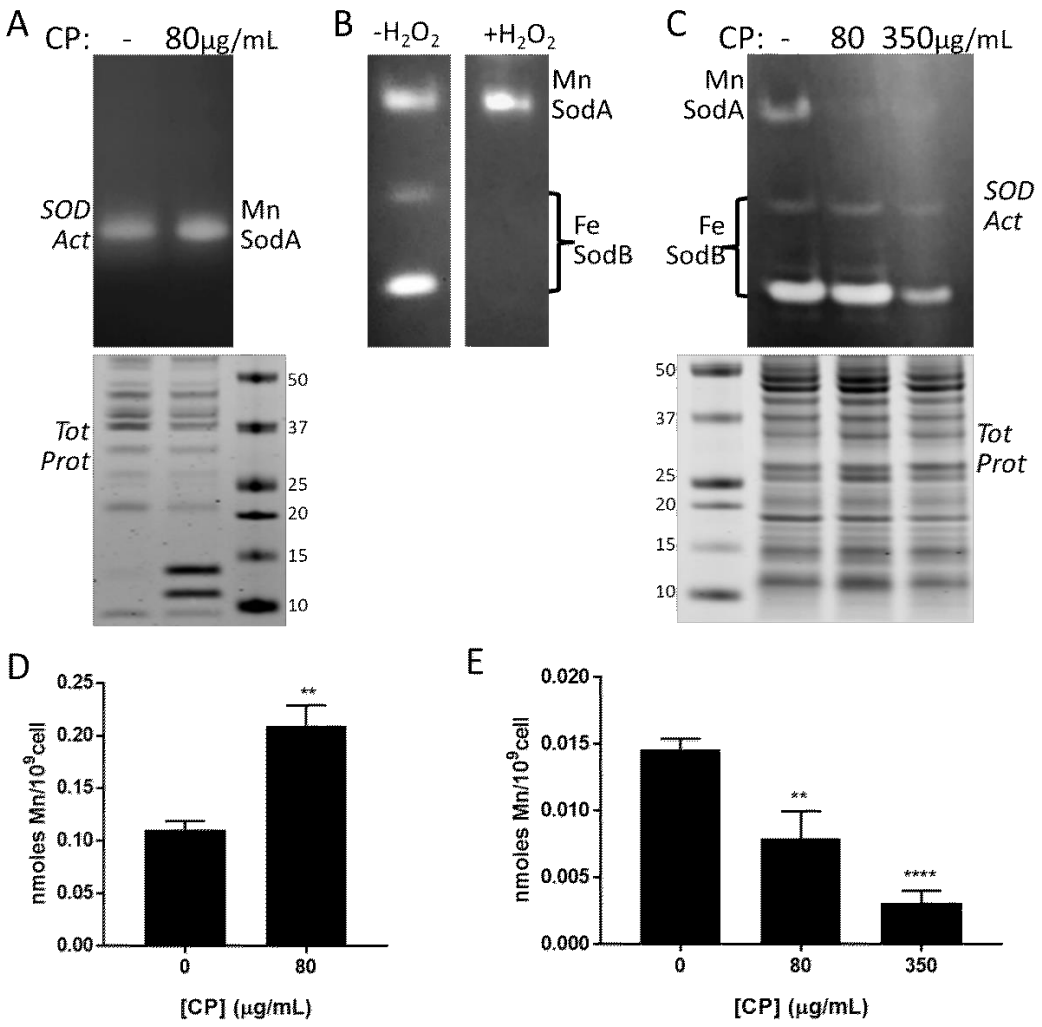

Figure 2-7 Effects of calprotectin on Mn requiring SodA and total cellular Mn in *Bb* versus *E. coli*. *Bb* (A, B) and *E. coli* cells ("*Ec*" C-E) were grown in BSK II supplemented with the designated concentrations of calprotectin (CP). (A,C) Mn levels were measured in *Bb* (A) or *E. coli* (C) cells by ICP-MS. Results are averages of at least five (A) and four (C) replicates over three experimental trials, **p ≤ 0.0035, ****p < 0.0001, where calprotectin treated samples are compared to no calprotectin controls. Error bars are standard error. (B,D,E) Whole cell lysates were analyzed for SOD enzymatic activity by native gel electrophoresis and NBT staining (B top, D, E top). Denaturing gel electrophoresis and Coomassie staining (B bottom, E bottom) were used as a loading control. The positions of SodA and SodB on the native gels are indicated; numbers represent molecular weight markers. Results are representative of five (B) and three (E) experimental trials. (D) The native gel was treated with H_2O_2 where indicated to inactivate Fe containing SodB prior to NBT staining, as described in *Experimental*.

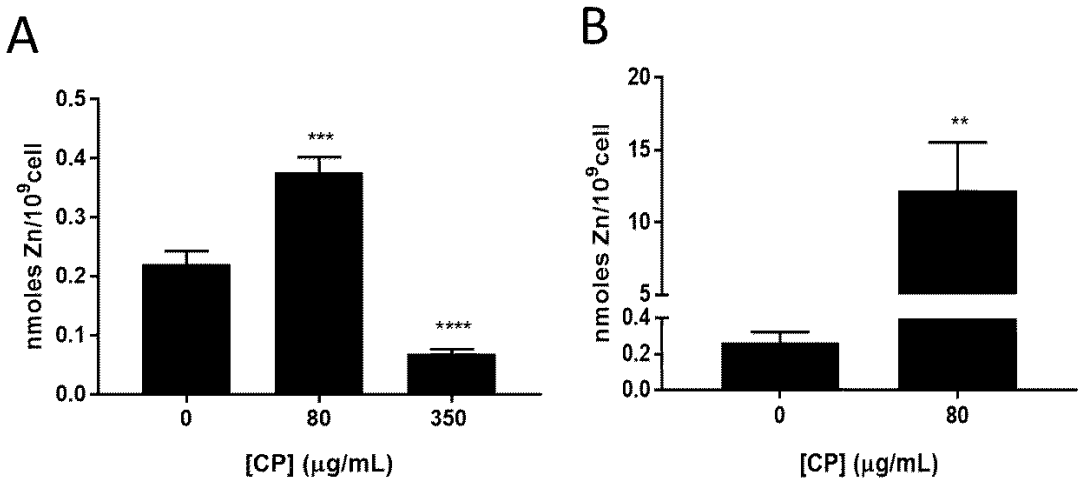

Figure 2-8 Zn and calprotectin in *Bb* versus *E. coli.* Total Zn levels were measured by ICP-MS in whole cell samples of *Bb* or *E. coli* grown with the indicated concentration of calprotectin (CP). (A) Results are averages of eight (0 µg/mL CP) and eleven (80 µg/mL CP) replicates over five independent experiments, where the level of Zn in calprotectin treated cell samples ranged from ≈6-30 nmoles/10^9 cells; **p=0.0073. (B) Results are averages of 10 (0 µg/mL CP), 8 (80 µg/mL CP), and 7 (350 µg/mL CP) replicates over four experimental trials, ***p=0.0004; ****p<0.0001.

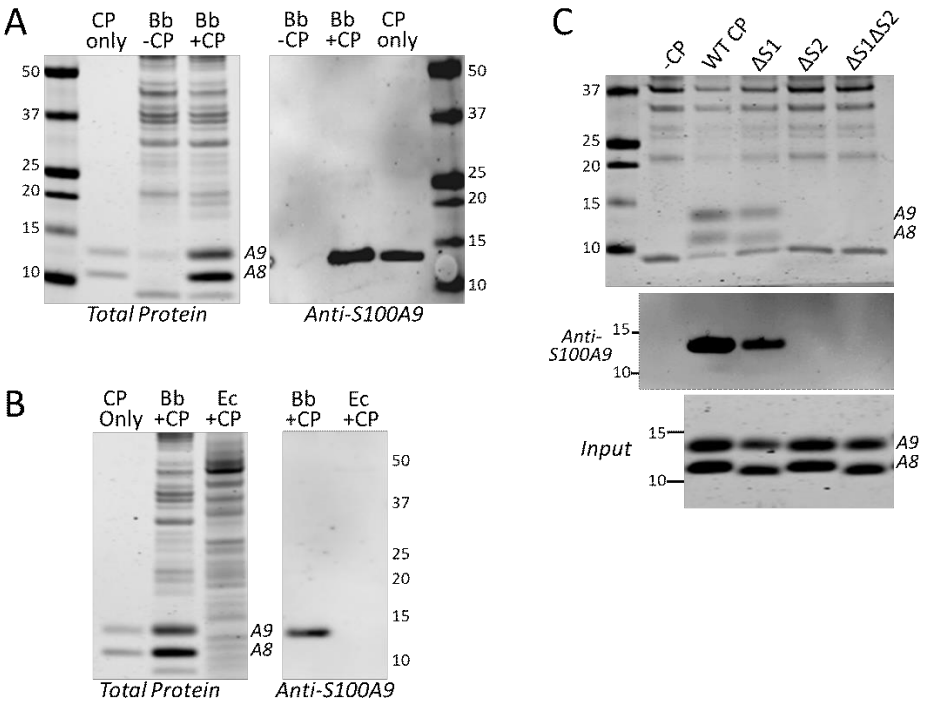

Figure 2-9 Interactions between calprotectin and *Bb*. *Bb* or *E. coli* cells were grown in BSK II in the absence or presence of 80 or 350 µg/mL calprotectin (CP), (A, B). *Bb* was grown with 80 µg/mL of the designated calprotectin mutants (C). Whole cell lysates were subjected to denaturing gel electrophoresis and either Coomassie staining for total protein (A,B left, C top) or immunoblot analysis for S100A9 ("Anti-S100A9"). "CP only" is 500 ng of recombinant human CP. Numbers indicate molecular weight markers and positions of S100A8 and S100A9 are denoted. "Input" shows Coomassie staining of WT and the indicated calprotectin mutants added to *Bb* cultures. Over five experimental trials, the level of ΔS1 calprotectin recovered in *Bb* lysates (as in Fig. 9C top and middle panels) was 42% (± 12%) that of WT CP, while ΔS2 and ΔS1ΔS2 calprotectin were undetected.

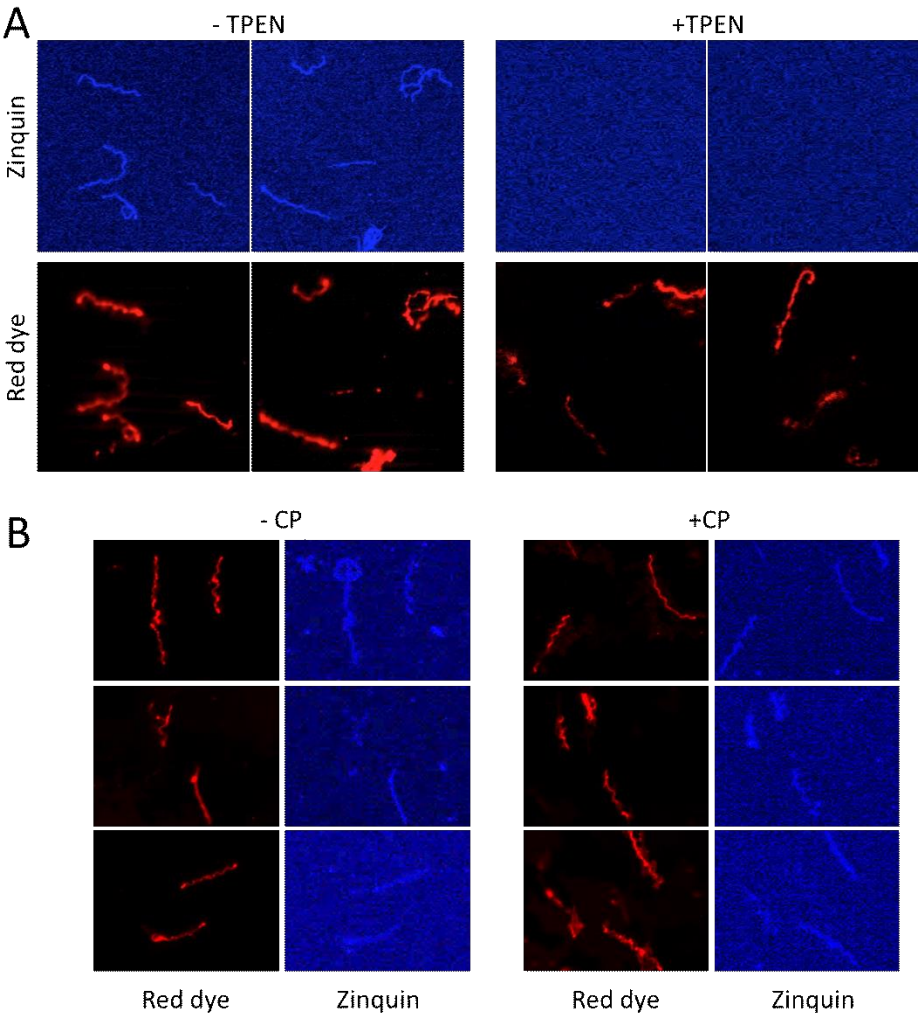

Figure 2-10 Zinquin labeling of *Bb*. *Bb* cells were cultured in the absence (A, left) or presence (A, right) of 3 μM TPEN, a Zn chelator, or in the absence (B, left) or presence (B, right) of 80 μg/mL calprotectin (CP). Cells were prepared for fluorescence microscopy by sequential staining with zinquin and then PKH red dye (for membranes) as described in *Experimental*. Results are representative of 10 (A) and 20 (B) images.

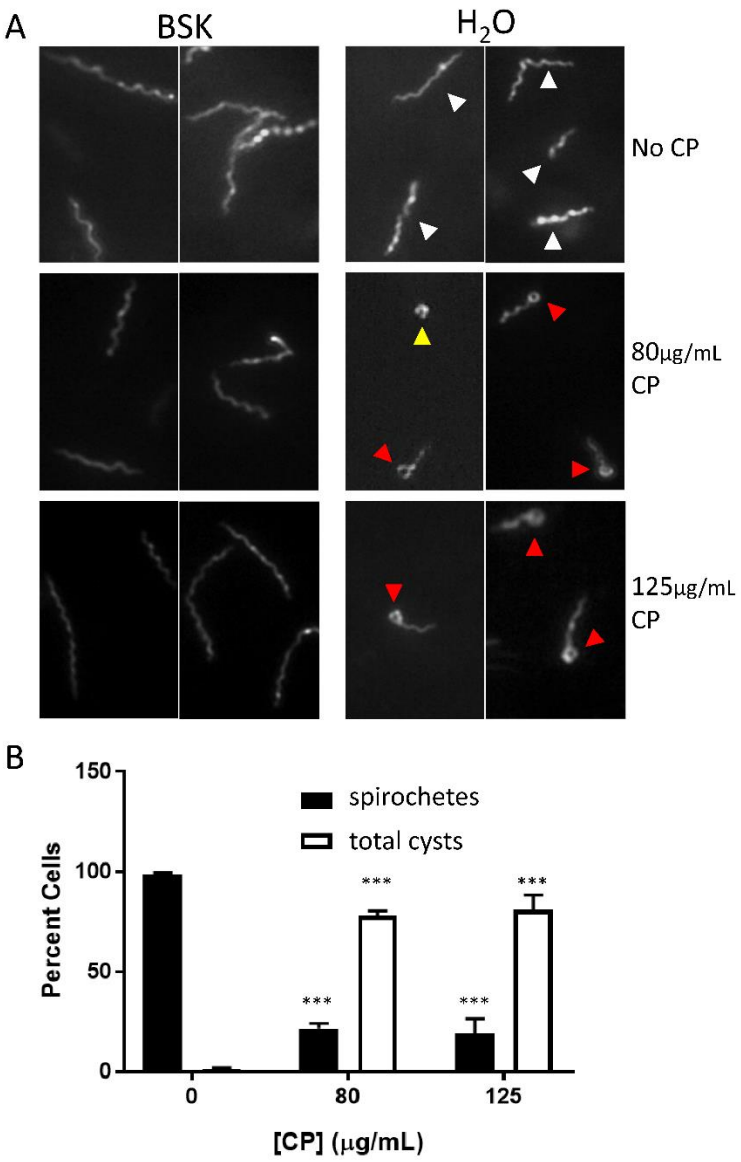

Figure 2-11 Calprotectin and morphology of *Bb*. (A) *Bb* cells cultured with the indicated concentrations of calprotectin (CP) were examined by dark field microscopy either directly in BSK II medium or immediately following a 1:10 dilution in H_2O. Arrows indicate morphology classes: white, elongated spirals; red, cysts with round body tip; yellow, full round body cysts. Similar results were obtained with 1:5 dilution in H_2O (Fig. S5, ESI†). (B) Quantification of cell morphology following dilution in H_2O. Cysts are a combination of the two classes described above where full round bodies are less <5% total cysts. Results represent the averages of >250 cells counted over 3-4 experimental trials. Error bars are standard error. The changes in morphology with 80 and 125 μg/mL calprotectin compared to no calprotectin are statistically significant; ***p<0.001

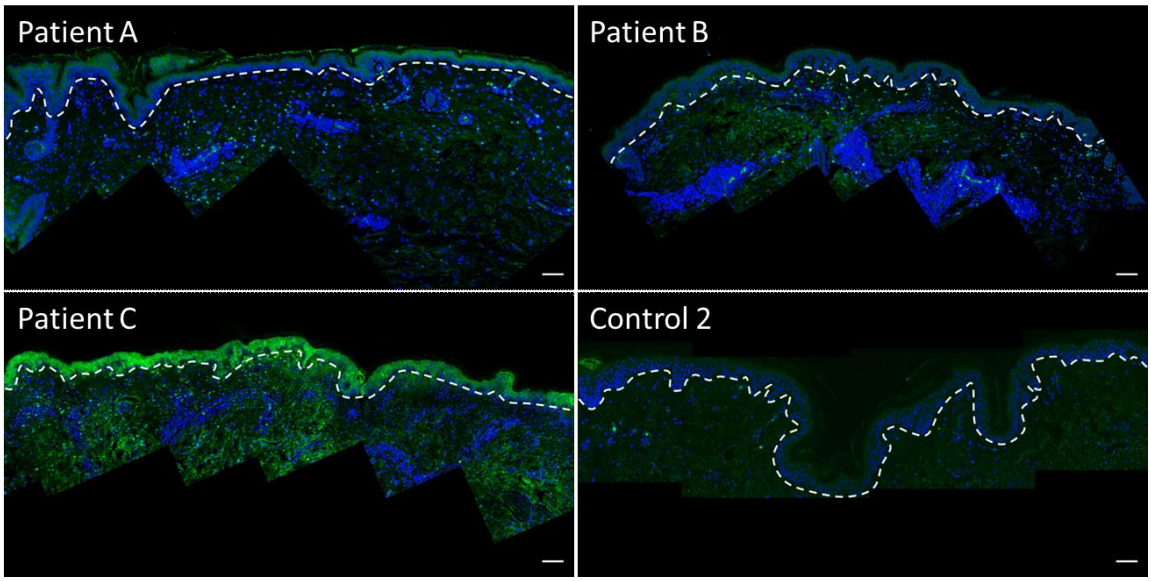

Figure S2-1 Immunofluorescence microscopy imaging of S100A8 expression in the skin of LD patients and controls. Skin tissue sections from the EM rash site of three individual LD patients and on control (Control 2) were subjected to immunostaining for S100A8 (green) and nuclei staining with DAPI (blue) before being subjected to fluorescence microscopy at 10X magnification as described in *Materials and Methods*. Dotted lines separate the epidermis from the dermis and the bar represents 100 μm.

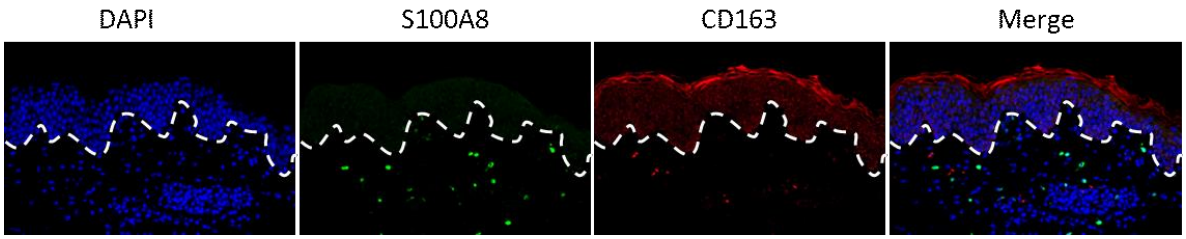

Figure S2-2 Immunofluorescence microscopy of S100A8 and CD163 expression in the dermis. Skin tissue sections from the EM rash site of three individual LD patients and on control (Control 2) were subjected to immunostaining for S100A8 (green) and nuclei staining with DAPI (blue) before being subjected to fluorescence microscopy at 20X magnification as in Figure S2-1. No colocalization was observed between S100A8 and CD163. Results are representative of three images spanning one tissue section each from three LD patients and three controls (patients 2,3,4).

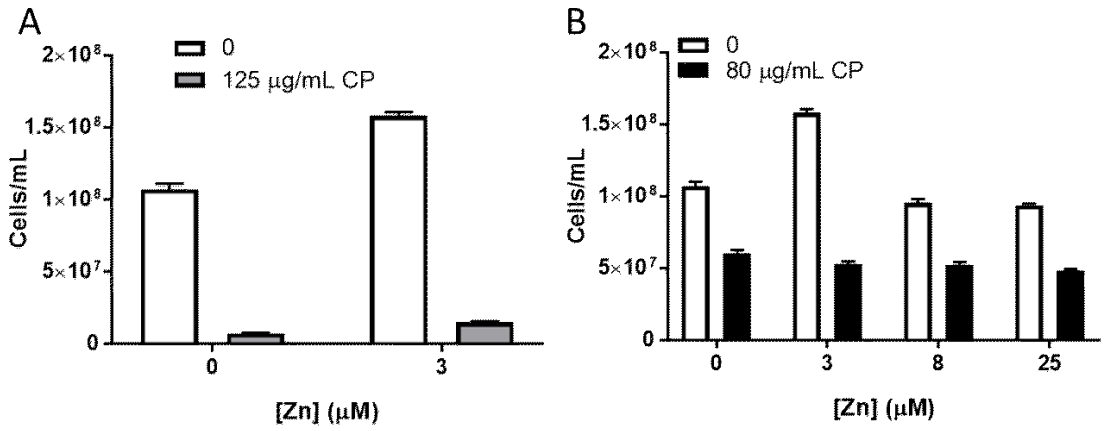

Figure S2-3 Zn does not reverse calprotectin (CP) mediated growth inhibition. *Bb* growth was monitored as in Figure 2-5A in the presence or absence of the designated concentrations of WT calprotectin and the indicated concentrations of $ZnSO_4$. Results are averages of (A) three biological replicates representative of 3 experimental trials, or (B) at least six biological replicates; error bar is standard error. Growth in the presence of 80 µg/mL calprotectin was 56% (±2.4), 33% (±1.5), 55% (±2.7), and 51% (±1.7), that of the no calprotectin control in the cells supplemented with zero, 3.0 µM, 8 µM, and 25 µM $ZnSO_4$ respectively. 3 µM $ZnSO_4$ typically improves growth of *Bb* cultures in BSK II.

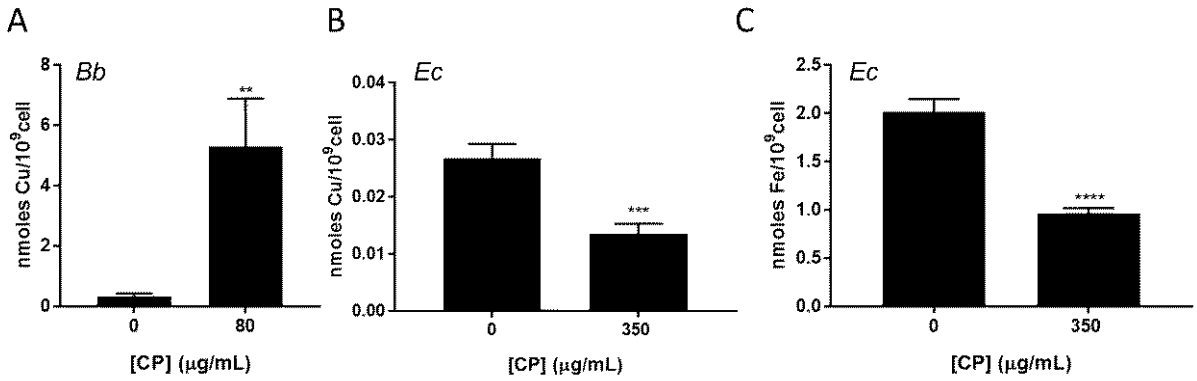

Figure S2-4 Total Cu in *Bb* and *E. coli*. Shown are total Cu (A,B) and Fe (C) levels in whole cell samples of *Bb* incubated with 80 μg/mL calprotectin (CP) (A) or *E. coli* incubated with 350 μg/mL calprotectin (B,C). Metal levels were measured by ICP-MS. Results are averages of eleven replicates over five independent experiments (A) or ten (0 μg/mL) and seven (350 μg/mL) replicates over four independent experiments (B,C). **p=0.0053; ***p=0.0003, ****p<0.0001. Fe levels in *Bb* with or without calprotectin treatment were below the limits of detection.

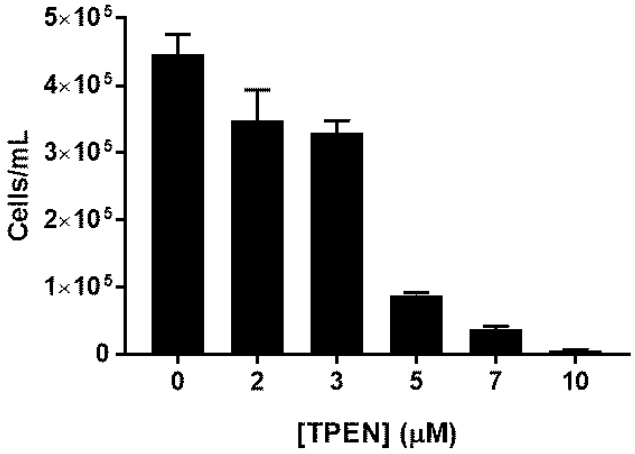

Figure S2-5 Growth of *Bb* in the presence of TPEN. *Bb* growth was monitored as in Figure 2-5A in the presence of increasing concentrations of the metal chelator TPEN. Results are averages of 3 biological replicates; error bar is standard error.

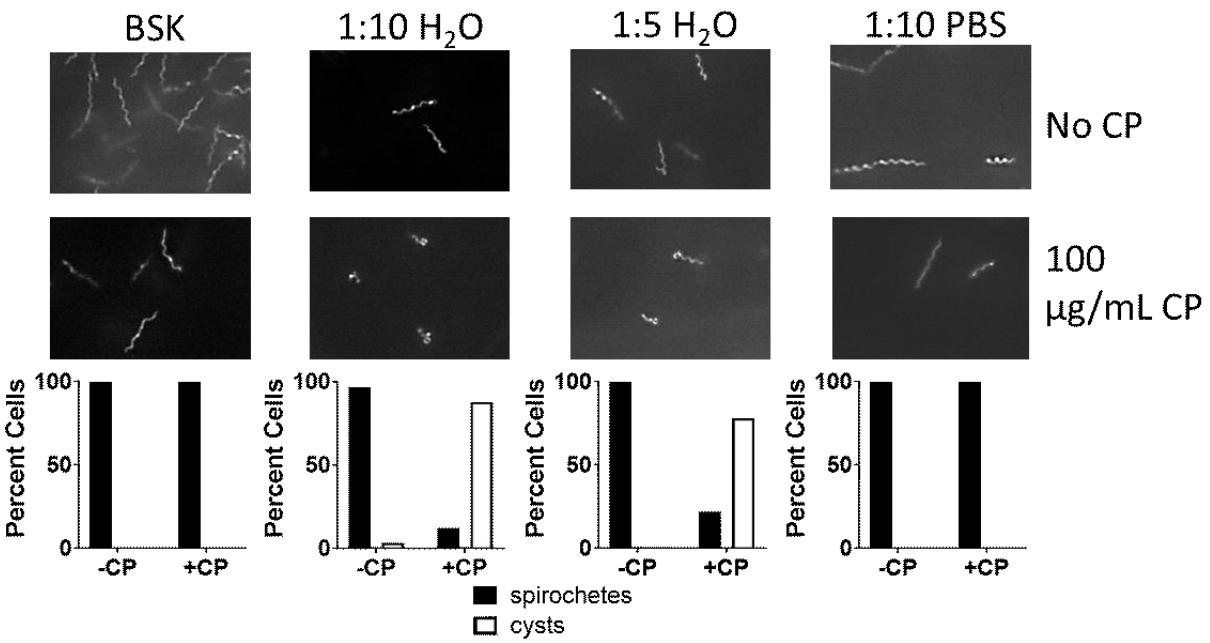

Figure S2-6 *Bb* cell morphology. *Bb* cells grown with or without 100 µg/mL calprotectin (CP) were photographed under dark field microscopy either directly from BSK II medium, or immediately following dilution in H_2O or PBS as indicated. Bottom – quantification of cell morphology as was done in Fig. 2-11B.

Chapter 3

Changes in mammalian copper homeostasis during microbial infection

This chapter was published in *Metallomics* (2020, Mar 25;12(3): 416-426) and is reproduced here with copyright permission from the Royal Society of Chemistry.

Abstract

Animals carefully control homeostasis of Cu, a metal that is both potentially toxic and an essential nutrient. During infection, various shifts in Cu homeostasis can ensue. In mice infected with *Candida albicans*, serum Cu progressively rises and at late stages of infection, liver Cu rises, while kidney Cu declines. The basis for these changes in Cu homeostasis is poorly understood. We show that the progressive rise in serum Cu is attributable to production by the liver of the multicopper oxidase ceruloplasmin (Cp). In *Cp*-/- mice, this elevated Cp helps to recover serum Fe levels at late stages of infection, consistent with a role for Cp in loading transferrin with Fe. Cp also accounts for the elevation in liver Cu seen during infection, but not for the fluctuations in kidney Cu. The Cu exporting ATPase ATP7B is one candidate for kidney Cu control, but we find no change in the pattern of kidney Cu loss during infection of *atp7b*-/- mice, implying other mechanisms. To test whether fungal infiltration of kidney tissue was required for kidney Cu loss, we explored other paradigms of infection. An infection with the intravascular malaria parasite *Plasmodium berghei* caused a rise in serum Cu and decrease in kidney Cu similar to that seen with *C. albicans*. Thus, the dynamics in kidney Cu homeostasis appear to be a feature common to vastly different infection paradigms. The implications for such Cu homeostasis control in immunity are discussed.

Introduction

Transition metals in biology have a dual role: they are essential micronutrients and co-cofactors for many vital enzymes, but also have the potential to become toxic. Cu is a prime example of such double-edged functionality. The metal is a required co-factor for many enzymes involved in oxygen chemistry and electron transfer, including cytochrome C oxidase for mitochondrial respiration, superoxide dismutase enzymes for anti-oxidant defense, and multi-Cu oxidases that couple oxygen reduction to oxidation of a variety of substrates (217,218). At the same time, Cu is potentially toxic through its ability to generate reactive oxygen species (ROS) via Fenton chemistry (219), to mis-metallate non-cupro enzymes (220), and to disrupt Fe-S clusters (31,221,222). Unicellular microbial pathogens that are in direct contact with their environment can be particularly vulnerable to extreme highs and lows in Cu, and during infection the animal host can exploit Cu as weaponry against these microbes (223-226).

The best studied example of Cu in innate immunity involves the Cu burst of macrophages. Macrophages engulf pathogens into the phagolysosome that is essentially an encasement of chemical toxins, including ROS (227), reactive nitrogen species (228,229) and elevated Cu (225,230). The elevation in phagolysosome Cu involves both increases in Cu uptake through the cell surface CTR1 Cu importer and pumping of Cu into the phagolysosomal compartment by ATP7A (33), one of two mammalian Cu-transporting P-type ATPases (54). In response to Cu elevation in the phagolysosome, successful pathogens have evolved elaborate machineries for Cu tolerance, many of which are virulence factors (34,35,38,112,231,232).

The animal host can also withhold Cu from invaders and this appears to be especially true in the case of eukaryotic pathogens such as fungi, which heavily rely on Cu as a micronutrient due to numerous intracellular cuproenzymes (223,233). Interestingly, the macrophage that can attack pathogens with excess Cu can also starve

certain microbes of Cu nutrients. When the pulmonary pathogen *Histoplasma capsulatum* invades macrophages, intraphagolysomal Cu is initially elevated, but at later stages, phagolysosomal Cu diminishes to levels that induce Cu starvation stress in the fungus (44,234). Another pulmonary fungal pathogen, *Cryptococcus neoformans,* also encounters extreme highs and lows in Cu during invasion of host. In the lung, pulmonary macrophages attack the *C. neoformans* with high Cu, but upon dissemination to the brain and cerebrospinal fluid, the fungus is deprived of Cu and activates Cu limitation stress responses (48,50,106). The ability to sense Cu limitation and overcome Cu starvation is also important for *Aspergillus fumigatus* virulence in mice (111).

Another fungal pathogen that is subject to fluctuations in host Cu is *Candida albicans. C. albicans* is a common component of human flora that can cause life-threatening systemic infections (235,236). In a murine model of disseminated candidiasis, the kidneys, which are the main target organ of infection (237), display biphasic changes in Cu. At early stages of *C. albicans* infection, kidney Cu rises, then progressively falls at later stages (30,43,46). These changes in host Cu are sensed by the invading fungi, and *C. albicans* responds first by upregulating Cu export, followed by a Cu starvation stress response involving upregulation of Cu import and downregulation of the major Cu protein, Cu/Zn SOD1 (43,46). *C. albicans* also infects the spleen and liver in this model of candidiasis, and like the kidney, spleen Cu also displays a biphasic response of initially elevated Cu, followed by Cu loss, while liver Cu initially remains stable then rises later during infection (43). The fluctuations in kidney Cu during infection are particularly surprising, in that in uninfected animals, kidney Cu typically remains constant relative to other tissues in cases of Cu deficiency or Cu excess (238-241). The mechanism by which kidney Cu fluctuates during *C. albicans* infection is not known. ATP7B, one of two Cu transporting ATPase of mammals, is seen to rise in the kidney during *C. albicans* invasion (46), although the contribution of ATP7B to changes in

kidney Cu during infection has not been examined. Furthermore, it is not known whether the fluctuations in kidney Cu are the direct result of tissue infiltration by the pathogen or are part of a more global immune response of the host. It is noteworthy that the loss in kidney Cu is paralleled by a dramatic and progressive rise in serum Cu (43). The basis of this rise is unknown, and whether it is connected to fluctuations in the kidney is unclear.

Here we explore the basis for these changes in host Cu during *C. albicans* infection. Our findings show that the progressive rise in serum Cu is due to increased liver production of ceruloplasmin (Cp), a multi-Cu oxidase and ferroxidase produced in the liver. This increased Cp production was found to be unconnected to changes in kidney Cu but rather was necessary to control circulating pools of Fe during infection. Furthermore, we demonstrate that the changes in kidney Cu are not due to direct invasion of the tissue by a microbe, since similar fluctuations in Cu without kidney invasion were seen with the malaria parasite *Plasmodium berghei* which remains intravascular. Thus, these changes in host kidney Cu appear to be part of a global immune response. Our findings reveal organ-specific changes in host Cu homeostasis as a generalized component of host immunity.

Results and Discussion

The accumulation of Cu-ceruloplasmin in serum of mice infected with C. albicans

Infection of 9-week-old BALB/c mice with *C. albicans* via lateral tail vein was associated with a progressive increase in total serum Cu over 72 hours post-infection (Fig. 3-1A). The progressive rise in serum Cu was observed in males and females and in different strains of mice (BALB/c and C57BL/6) (30,43). The basis of the serum Cu increase during this model of candidiasis was not understood. We considered that this

rise in Cu might reflect elevations in the multicopper oxidase ceruloplasmin (Cp), an acute phase protein in the serum (19) that normally accounts for 40-70% of total serum Cu (195). Analysis of serum Cp by immuno-blotting revealed an increase in Cp up to 72 h post infection (Fig. 3-1B, C). Since Cp circulates as both apo and Cu-loaded protein (242), we measured Cp activity as an indicator of metallated protein using the o-dianisidine dihydrochloride oxidation assay (243,244). As seen in Fig 3-1D, there was a dramatic rise in o-dianisidine reactivity during infection that increased progressively up to 72 h. Comparison of serum Cu and serum o-dianisidine reactivity revealed a strong correlation (Fig. 3-1E), indicating that the elevated serum Cu seen during *C. albicans* infection is attributable to serum Cp.

Although serum o-dianisidine reactivity is typically used as indicator of Cp activity (244), other factors can react with o-dianisidine including the closely related multicopper oxidase hephaestin (245) or diamine oxidases (244). To determine whether CP is the main contributor to the observed oxidase activity, we infected $Cp^{-/-}$ null mice with *C. albicans* and measured changes in Cu and oxidase activity in the mouse serum. The infected $Cp^{-/-}$ mice showed fungal burden in kidneys similar to the infected WT C57BL/6 mice (Fig. 3-2A), but had larger weight loss compared to the WT at 72 h (Fig. 3-2B), indicating Cp may play some role in guarding against infection in this model. Nevertheless, mouse survival was not substantially affected by $Cp^{-/-}$ deletion, and these mice therefore provided a valuable model to directly test the contribution of Cp to changes in serum Cu. As seen in Fig. 3-2C, the WT C57BL/6 mice exhibited the characteristic rise in serum Cu over 72 h of infection. By comparison, the $Cp^{-/-}$ mice had very low basal serum Cu that failed to rise during the course of infection. These findings support the results of Fig. 3-1, and demonstrate that the strong elevation in serum Cu during disseminated candidiasis can be attributed to Cu containing Cp.

Where is the Cu-ceruloplasmin coming from in this mouse model of candidiasis? Cp can be secreted from a variety of tissues and cells including macrophages, mononuclear cells, the mammary gland, the choroid plexus, and the kidney (246-249), although a principle source is the liver (250). To test whether the Cu-loaded Cp that hyperaccumulates during disseminated candidiasis is derived from the liver, we used mice containing a liver specific deletion in ATP7B, the P-type Cu ATPase in the secretory pathway that provides Cp with Cu (59). These *Atp7b*$^{\Delta Hep}$ mice hyperaccumulate Cu in the liver and Cp circulates in largely the apo form as determined by a native gel assay (251). Consistent with these previous findings, we observe that uninfected *Atp7b*$^{\Delta Hep}$ mice show low Cp activity as revealed by o-dianisidine reactivity (Fig. 3-3A). These mice also exhibit very low basal levels of serum Cu in uninfected mice (Fig. 3-3B). Figure 3C shows that infection with *C. albicans, Atp7b*$^{\Delta Hep}$ mice showed no visible signs of increased disease severity and no significant changes in kidney fungal burden. Interestingly, serum Cu and Cp activity in *Atp7b*$^{\Delta Hep}$ mice remained exceptionally low during the course of infection compared to the dramatic rises in WT litter mate controls (Fig. 3-3A, B). Despite no increase in Cp activity, the *Atp7b*$^{\Delta Hep}$ mice showed elevations in Cp protein by immunoblot, similar to levels seen in WT mice (Fig. 3-3D). Thus, the elevated Cp that accumulates in infected *Atp7b*$^{\Delta Hep}$ mice appears to be apo and inactive. These studies show that the high level of Cu-loaded and enzymatically active Cp that accumulates in the serum of *C. albicans* infected mice is derived from the liver and is dependent on hepatic ATP7B.

Ceruloplasmin and transferrin Fe during C. albicans infection

While many roles have been ascribed to Cp, a major function is to act as a ferroxidase for ferrous iron to facilitate loading of Fe^{+3} onto serum transferrin (8,129). A

previous study has shown that in the mouse tail vein model for disseminated candidiasis, infection with *C. albicans* led to a great reduction in transferrin-Fe levels at 24 h post-infection, presumably due to release of the pro-inflammatory hormone hepcidin that triggers an anemia of inflammation response (252,253). We corroborated these findings and observed a 3-fold drop in total Fe and transferrin-Fe 24 h post infection in BALB/c mice (Fig. 3-4A,B). Unexpectedly however, the mice seemed to recover over time and serum Fe and transferrin saturation were partially restored 72 h post infection (Fig. 3-4A-B). A similar U-shape curve in serum Fe during *C. albicans* infection could be seen in Wt C57BL/6 mice (Fig. 3-4C). This recovery in serum Fe at later stages of fungal infection had not been previously described and we tested whether Cp was involved. As seen in Fig. 4C, the basal level of serum Fe in uninfected $Cp^{-/-}$ mice was much lower than age-matched controls, consistent with previous results (8,254). Notably, this low level of serum Fe in $Cp^{-/-}$ mice appeared to remain relatively constant over the course of infection (Fig. 3-4C). Based on these findings, it appears that the marked elevation of Cp during infection can help in the recovery of serum Fe deficiency during later stages of infection.

The parallel inductions of Cp and hepcidin during infection seem at odds with one another: while hepcidin works to reduce serum Fe levels, Cp can increase serum Fe through transferrin loading. Our findings suggest a model in which Cp induction serves to restrict the extent of anemia of inflammation induced by hepcidin, which might otherwise be detrimental to the host. However, we cannot exclude other possible roles for Cp during infection. Cp has been shown to play a role in many physiological processes, and the ability of Cp to act as an antioxidant has been well characterized (19,255-257). However it can also act in the oxidation of molecules such as hormones (258) and nitric oxide oxidation (259,260). One or more of these alternative biochemical activities may also contribute to Cp function as an acute phase protein. Regardless of its

precise activity during infection (recovery in serum Fe versus alternative oxidation reactions), Cp seems to contribute to animal fitness during disseminated candidiasis, as witnessed by the larger weight loss in *Cp*$^{-/-}$ mice compared to WT controls (Fig. 3-2B).

Changes in tissue Cu during C. albicans infection and ceruloplasmin

Aside from the rise in serum Cu, infection with *C. albicans* leads to specific changes in Cu content of tissues including the liver and kidney (30,43,46). We sought to test whether these changes in tissue Cu are connected to the strong elevation in serum Cu and serum Cp.

With regard to the liver, total Cu levels significantly increase by 72 h in the murine model of disseminated candidiasis (43). Why the liver accumulates elevated Cu during infection was unknown. As one possibility, Cu may be elevated to meet the demand for liver production of Cu-Cp. We tested this hypothesis using *Cp*$^{-/-}$ null mice. As seen in Fig. 3-5A, WT C57BL/6 and *Cp*$^{-/-}$ null mice have similar basal levels of total liver Cu prior to infection. Following 72 h of infection, C57BL/6 mice exhibited a rise in liver Cu similar to that previously seen with infected BALB/c mice (43). By comparison, liver Cu 72 h post infection remained essentially unchanged from basal levels in the *Cp*$^{-/-}$ null mice (Fig. 3-5A). Thus, liver production of Cp occurs in parallel with the increase in liver Cu observed.

While hepatic Cu steadily increases during *C. albicans* infections, renal Cu levels increase at 24 h followed by a decrease at 72 h (30,43,46), and a similar phenomenon has been reported for the spleen (43). The reduction in renal Cu is not due to urinary losses during infection (43), and is concomitant with high liver production of Cu-Cp (Fig. 3-1B-D). Could these events be linked? There is precedence for cross tissue communication in Cu homeostasis, e.g., cardiac Cu deficiency signals Cu mobilization

from other tissues (261,262). It was therefore possible that during infection, the need to produce Cu-Cp in the liver might signal compensatory Cu losses from other tissues. We used *Cp*$^{-/-}$ mice to address whether CP production is sufficient to trigger Cu changes in extra-hepatic tissues. In WT C57BL/6 mice, kidney Cu levels fall at 72 h, as previously reported (30,43,46) (Fig. 3-5B, left). However, the same change in kidney Cu during infection was also observed in *Cp*$^{-/-}$ mice (Fig. 3-5B, right). These studies exclude liver production of Cu-Cp as a signal to drive Cu loss from the kidney.

The decreases in kidney Cu accumulation at late stages of *C. albicans* infection could result from either reductions in Cu uptake or through increases in Cu export, e.g., through Cu exporting ATPases, ATP7A or ATP7B (54,263,264). Brown and colleagues have shown that levels of both the Cu import protein CTR1 and Cu export proteins ATP7A and ATP7B increase throughout the kidney during *C. albicans* invasion, but the effect was most prominent with ATP7B (46). We examined whether this elevation in ATP7B was responsible for the fluctuations in kidney Cu by examining kidney Cu levels in whole animal *Atp7b*$^{-/-}$ mice. As seen in Fig. 5C, kidney Cu levels in the *Atp7b*$^{-/-}$ mice were observed to drop at 72 h infection, similar to wild type littermate controls. Thus, ATP7B is not responsible for the changes in Cu homeostasis seen during *Candida* infection. It therefore remains possible that the changes in kidney Cu result from alterations in ATP7A or the CTR1 Cu importer. Whether or not ATP7A or CTR1 contribute to fluctuations in kidney Cu awaits the generation of kidney-specific deletions or conditional alleles of the corresponding genes, as both genes are essential for mouse viability (265,266).

Host Cu responses in a distinct model of infection: Plasmodium berghei

The fluctuations in renal Cu during *C. albicans* infection are remarkable, in that under non-infectious conditions, kidney Cu remains relatively constant compared to other tissues in cases of Cu deficiency or Cu excess (53). As one possibility, the loss in kidney Cu could represent a special case of *C. albicans* infiltrating and damaging the tissue. The kidney is the site of highest fungal burden in the mouse model of disseminated candidiasis (237) and the Cu response may simply be a localized effect of colonization. To address whether kidney infiltration triggers Cu loss, we investigated host Cu changes in mice infected with a pathogen that does not predominantly invade the kidney. We chose the intravascular malaria parasite *P. berghei* that infects erythrocytes, preferentially reticulocytes (267) but not kidney cells nor endothelium, and does not produce kidney lesions as found with *Candida* infections (268). During blood stream infection with *P. berghei,* we observed elevations in serum Cu (Fig. 3-6A) and Cp activity (Fig. 3-6B) similar to that seen with *C. albicans* infection (Fig. 3-1A, D). Most interestingly, we also observed a decrease in kidney Cu levels at later stages of infection (Fig. 3-6C). The loss in kidney Cu with *P. berghei* is similar that seen during *C. albicans* infections (Fig. 3-5B,C and (30,43,46)), albeit on a longer timeline. Thus, the kidney Cu response to infection does not appear to be a specific effect of infiltration of this organ by the fungal pathogen, but rather a more global response to systemic infections.

Nutritional immunity for Copper?

Why do kidney Cu levels decrease during infection? This appears to represent a specific host response to infection or inflammation because such changes in kidney Cu are typically not seen under non-infection conditions of Cu excess or Cu deficiency (53,238,240,241,269). The loss in tissue Cu could be a nutritional immunity response of

the host, i.e., an intentional attempt to thwart pathogen growth by starving the microbe of its Cu nutrients. Indeed *C. albicans* is subject to Cu starvation when it invades the kidney and responds by increasing fungal Cu uptake and sparing utilization of Cu as a co-factor (43,46). This withholding of Cu from *C. albicans* reflects a type of nutritional immunity that is unlike similar mechanisms involving calprotectin sequestration of Mn and Zn (29,151), in that the Cu limitation is tissue wide rather than localized to sites of infections (43,46). However, since the loss in kidney Cu is also observed with an infectious agent that does not infiltrate the kidney, it more likely represents a global response to infection and inflammation rather than localized nutritional immunity (Fig. 6C). As an alternative possibility, the loss in kidney Cu may not reflect a bona fide nutritional immunity response, but rather a shift in prioritization of whole animal Cu away from the kidney and towards the liver to meet demands for Cu-Cp production. If this model is correct, the mobilization of kidney Cu is not a direct response to increases in liver Cu and liver Cp, as kidney Cu still declines in the $Cp^{-/-}$ mouse. A similar model invoking cross-tissue redistribution of Cu has been used to explain mobilization of Cu from the liver towards the heart during cardiac Cu deficiency (261,262). How such cross-tissue Cu homeostasis is communicated is still unknown. The identification of Cu homeostasis signals during inflammation in future studies would greatly enhance our understanding of the complex roles this metal plays during microbial infection.

Conclusions

Previous work has shown that Cu homeostasis changes dramatically during *C. albicans* infections. Specifically, it had been shown that serum and liver Cu levels increase while the kidney displayed a biphasic response, rising early in infection and falling at later time points. The nature of this decline in Cu levels was unknown, however,

at the same time as kidney Cu is declining, serum Cu and liver Cu increased and others have shown that the protein levels of Cu transporter ATP7B increased in the kidney as well. We investigated both of these events and found that the increase in serum and liver Cu was due to Cp and that deletion of Cp had no effect on kidney Cu loss. Similarly, deletion of ATP7B also had no effect on kidney Cu loss in this infection model. These results suggest that another Cu transport protein is playing a role or that some other mechanism is compensating during our deletion studies. In this report, we also provide the first evidence that this decline in kidney Cu occurs with another pathogen and that it occurs in an infection paradigm where the kidney itself is not colonized. This finding is of particular interest because it shows that this phenomenon in not *Candida* specific and most likely happens in a large variety of infection conditions. The result also suggests that the kidney is receiving some signal to initiate Cu loss. While that signal is still unknown, future studies to uncover the signal could greatly improve our understanding of Cu redistribution during infection.

Materials and methods

Mouse models of infection

All mouse studies were carried out in accordance with the National Institutes of Health guidelines for the ethical treatment of animals. The protocol was approved by the Institutional Animal Care and Use Committee of the Johns Hopkins University medical institutions, mouse protocol number MO13M264 (*C. albicans* infection) and number MO19H11 (*P. berghei*).

For the lateral tail vein model of disseminated candidiasis, studies involved both male and female mice and no sex differences were noted with in any of the experiments presented in this work, consistent with previous findings on mouse tissue and serum Cu

during *C. albicans* infection (30,43). *C. albicans* strain SC5314 was used for all studies. Fungal cells were grown to stationary phase overnight in a yeast extract, peptone, and 2% (wt/vol) dextrose-based media (YPD). Cells were harvested and washed 2x in phosphate buffered saline (PBS) and cell density determined by optical density at 600 nm (OD_{600}). The cell concentration of the inoculum was confirmed by cell enumeration on a hemocytometer (Hausser Scientific). $5x10^5$ *C. albicans* cells suspended in 100 µL PBS were injected into the lateral tail vein of 9-11-week-old BALB/c or C5BL/6J strains of mice or the indicated mutants. Mice were sacrificed at 24, 48 and 72 hours after infection. Blood was collected and allowed to clot on ice before isolation of serum by centrifugation at 1000 x g for 10 minutes. Organs were perfused with PBS as previously described (43) and kidneys and liver were collected and processed for CFUs and metal analysis. The $Cp^{-/-}$ mice have been previously described (8). The liver specific $Atp7b^{\Delta Hep}$ and global knockout $Atp7b^{-/-}$ mice have been previously described (241,251).

To measure colony forming units during *C. albicans* infection, perfused tissues were weighed before homogenization by mechanical force in 1 mL of PBS. After homogenization, samples were serially diluted in PBS and plated onto YPD medium with 1% Penicillin, 1% Streptomycin (Quality Biological Inc., 120-095-721).

For *P. berghei* experiments, 7-week-old female BALB/C mice were infected by injection of $1x10^6$ parasites of *P. berghei* strain ANKA into the peritoneum of mice as previously described (270). Mice were sacrificed at 7 and 14 days post infection. Blood and PBS perfused kidneys were collected at the time of sacrifice and processed for metal analysis identically to *C. albicans* infected samples.

Biochemical analyses of serum and tissues

Serum was diluted 1:50 in MilliQ water and Cu content was measured on a PerkinElmer Life Sciences AAnalyst 600 graphite furnace atomic absorbance spectrometer (AAS). Tissue samples were weighed and digested overnight at 90°C in 1 mL of 20% (vol/vol) Ultrex II Ultrapure nitric acid. Samples were diluted to 2% nitric acid and Cu content was measured via AAS.

To monitor serum oxidase activity, o-dianisidine dihydrochloride was used as substrate as previously described (243). In a 96 well plate (Falcon, 353072) the following was combined in duplicate samples: 3.75 µL serum, 56.5 µL of 10 µM diethylenetriameinepentaacetic acid in a 0.1 M sodium acetate buffer at pH 5.5, and 30 µL of 2.5 mg/mL o-dianisidine dihydrochloride (Sigma Aldrich, D3252-25G). Samples were incubated at 37°C and following 5- and 60-minute time points, 150 µL 9 M sulfuric acid was added and absorbance measured at 540 nm using Synergy HT (Biotek) to yield A_5 and A_{60}, respectively. Oxidase activity in units/L was calculated as $(A_{60} – A_5) \times 113.6$.

Serum Fe (SI) and unsaturated iron binding capacity (UIBC) were determined using a ferrozine based assay (Pointe Scientific, I7504-60) in a 96 well plate format. To measure SI, 100 µL of 220 mM hydroxylamine hydrochloride in pH 4.5 acetate buffer with surfactant was combined with 20 µL of either serum sample, water, or 500 ug/dL ferrous chloride Fe standard in hydroxylamine hydrochloride. The absorbance at 560 nm (A_{560}) was measured on an Eon plate reader (Biotek) (A_1 reading). 2 µL of 16.7 mM ferrozine in hydroxylamine hydrochloride was then added, following by incubation at 37°C for 10 minutes and A560 measurements (A_2 reading). SI in µg/dL was calculated as $(A_{2serum} - A_{1serum})/(A_{2standard} - A_{1standard}) \times 500$. For UIBC, 80 µL of 500 mM Tris, pH 8.1 with surfactant and 0.05% (w/v) sodium azide was mixed with 60 µL of water, 20 µL of serum sample and 40 µL of the aforementioned Fe standard, or 20 µL of water and 40 µL of Fe standard. A_{560} was measured (A1). 2 µL of 16.7 mM ferrozine in hydroxylamine

hydrochloride was added and incubation proceeded at 37°C for 10 minutes followed by A560 measurements (A2). UIBC in µg/dL was calculated as 500-($A_{2sample}$-$A_{1sample}$)/($A_{2standard}$-$A_{1standard}$) x 500. Total iron binding capacity (TIBC) was calculated as SI + UIBC. Transferrin saturation was then calculated as SI/TIBC x 100.

Ceruloplasmin protein levels were determined by immunoblot. 5 µL of serum was loaded onto a 4-12% Bis-Tris gel (Thermo Fisher). Blots were probed with anti-ceruloplasmin (Abcam, Ab19171) at a 1:10,000 dilution and secondary Alexa Fluor 680 donkey anti-goat (Invitrogen, #A-21084) at 1:10,000 dilution. For albumin, 1 µL of serum was run on a 4-12% Bis-Tris gel (Thermo Fisher) and stained with Coomassie brilliant blue (Fisher Biotech, BP101-50). Densitometry quantification of Cp and albumin was determined using ImageJ version 1.49 (NIH software).

All statistical calculations were made using RStudio. One-way ANOVAs with Tukey post-test were used when comparing multiple groups with one independent variable, and two-way ANOVA with Tukey post-test was used to compare group means with two independent variables. Two tailed student's T tests were used when comparing two groups. Least squares analysis using the lm function was used to determine the slope and intercept of the line in Fig. 1E. The values plotted are individual mice where the middle line represents the mean and the error bars are showing the standard error of the mean (SEM).

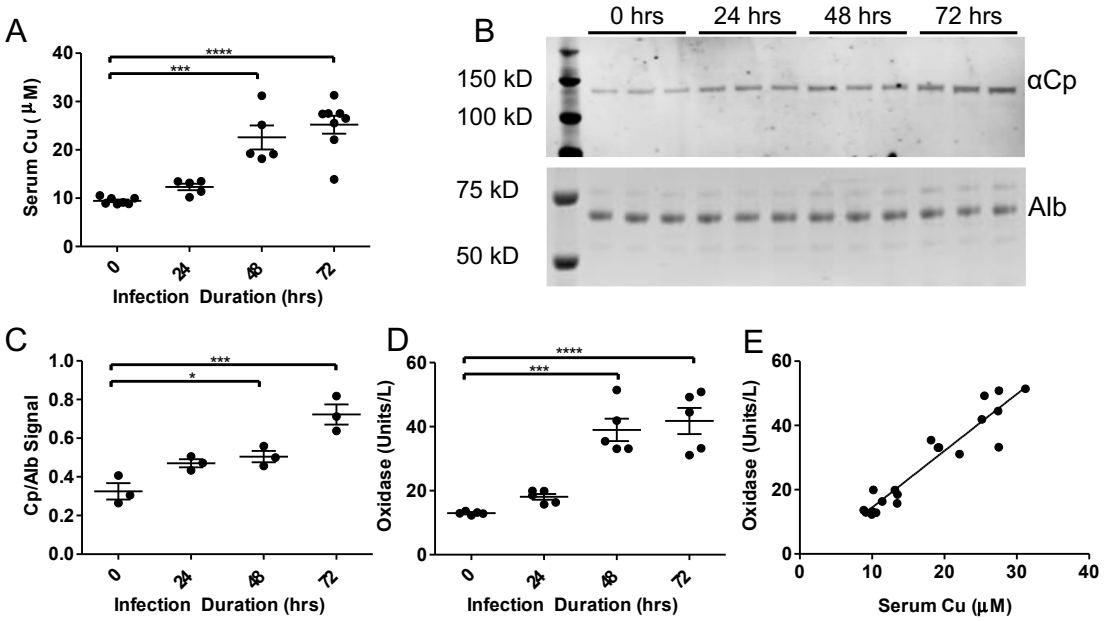

Figure 3-1 The rise in serum Cu in *C. albicans*-infected mice is attributable to holo-Ceruloplasmin. Nine-week-old female BALB/c mice were infected with Candida albicans strain SC5314 and sacrificed at the indicated time points. Blood was harvested at sacrifice and serum was isolated. (A) Serum Cu during infection for 5-8 mice per group.***P<0.001, ****P< 0.0001 as determined by one-way ANOVA with Tukey post-test. (B) Ceruloplasmin (Cp) levels in serum were assayed via immunoblot (B top) and normalized to albumin levels visualized by Coomassie blue staining (B bottom). Results are from three mice per group and the intensity of bands was measured by densitometry (C). *P<0.05, ***P<0.001 as determined by one-way ANOVA. (D) Oxidase activity of Cp was assayed via o-dianisidine dihydrochloride oxidation. Results shown are from 5 mice per group. ***P<0.001,**** P< 0.0001 as determined by one-way ANOVA with Tukey post-test. (E) Correlation between oxidase activity (from D) and serum Cu (from A), slope= 1.76+/- 0.14, intercept=-3.23+/- 2.66, R2=0.894, p=2.03x10-10. Line parameters and statistics determined by lm function in RStudio. Values from individual mice are plotted with middle line representing the mean with error bars showing +/- SEM.

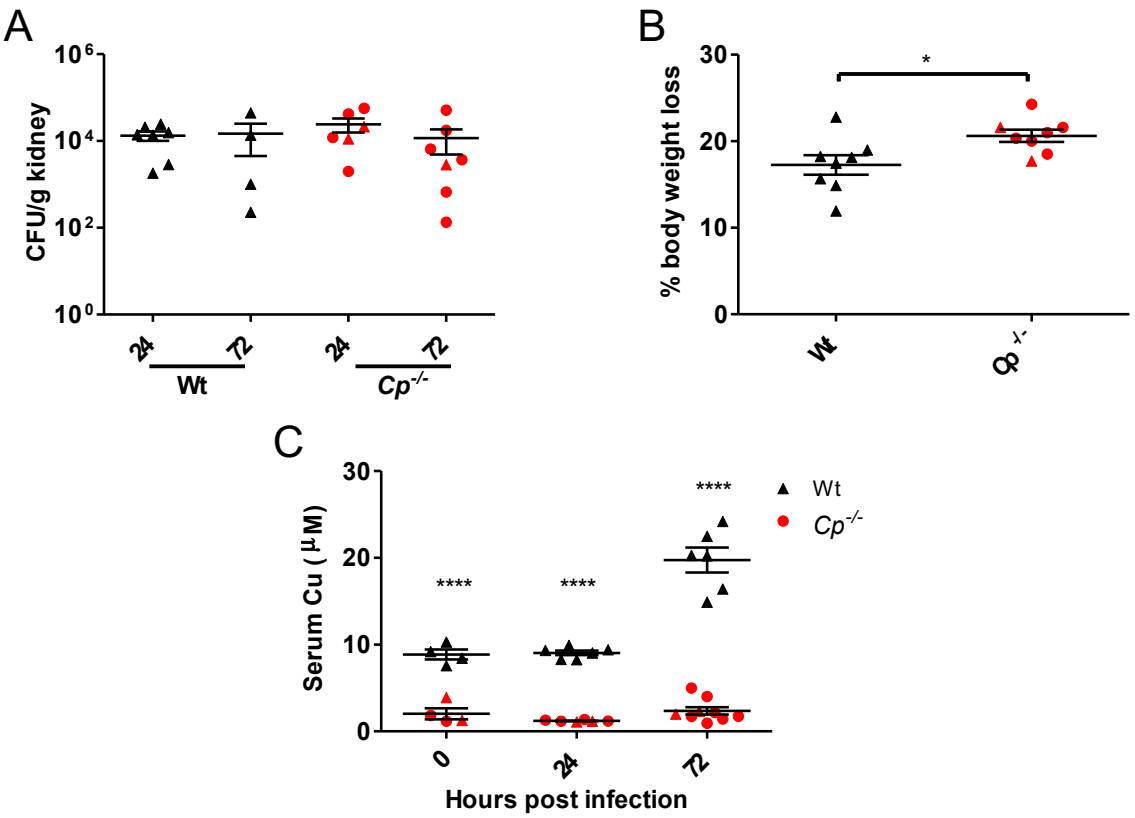

Figure 3-2 The effects of aceruloplasminemia on serum Cu, weight loss and renal lesions during infection. Male (triangles) and female (circles) 11-week-old *Cp*$^{-/-}$ null mice and age matched Wt controls were infected with *C. albicans* as in Fig. 1. (A) Colony forming units (CFU) in the kidneys harvested at the indicated time points in hours; n= 4-7 mice per group. Analysis via two-way ANOVA showed no statistically significant difference between WT and *Cp*$^{-/-}$ mice. (B) Weight loss at 72 hours post infection is significantly higher in *Cp*$^{-/-}$ mice as determined via two-tailed Student's t-test, n=8 mice per group, *P=0.0281. (C) Total serum Cu levels are significantly higher in WT mice compared to *Cp*$^{-/-}$ mice as determined by two-way ANOVA with Tukey post-test; 4-9 mice per group ****P<0.0001. This two-way ANOVA test showed no statistically significant difference in serum Cu levels of the *Cp*$^{-/-}$ mice during infection. Asterisks above data in C indicate statistical significance of the difference between Wt and Cp$^{-/-}$ at that time point. Values for individual mice are plotted with middle line representing the mean with error bars showing +/- SEM.

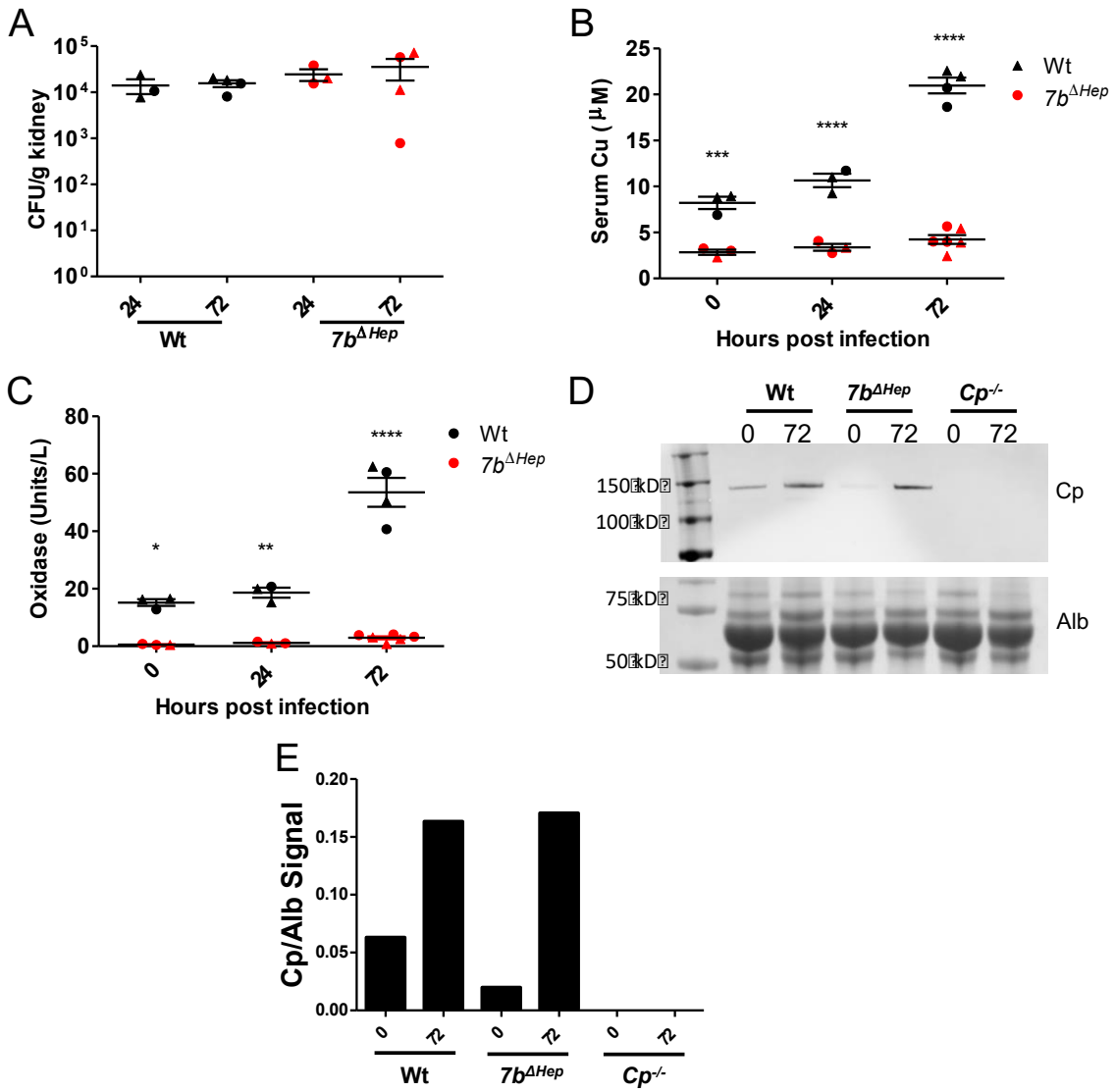

Figure 3-3 During infection with *Candida albicans,* serum ceruloplasmin is produced in the liver. Male (triangles) and female (circles) 11-week-old *Atp7b*$^{\Delta Hep}$ (7b$^{\Delta Hep}$, red) mice and Wt littermate controls (black) were infected with *C. albicans*. (A) Mean oxidase activity of mouse serum as measured by o-dianisidine dihydrochloride oxidation; n=3-6 mice per group. *P=0.013; **P=0.0030; **** P< 0.0001. (B) Serum Cu levels from 3-6 mice per group. ***P=0.00061; ****P<0.0001. (C) There was no significant difference in kidney CFUs between Wt and *Atp7b*$^{\Delta Hep}$ mice in 3-4 mice per group analyzed. (D) Ceruloplasmin in serum at 0 and 72 hours detected by immunoblot with albumin as loading control. (A-C) Statistical significance was determined by two-way ANOVA with Tukey post-test. Asterisks above data in A,B,C indicate the statistical significance of the difference between Wt and *Atp7b*$^{\Delta Hep}$ at that time point. Values plotted are individual mice with middle line representing the mean with error bars showing +/- SEM.

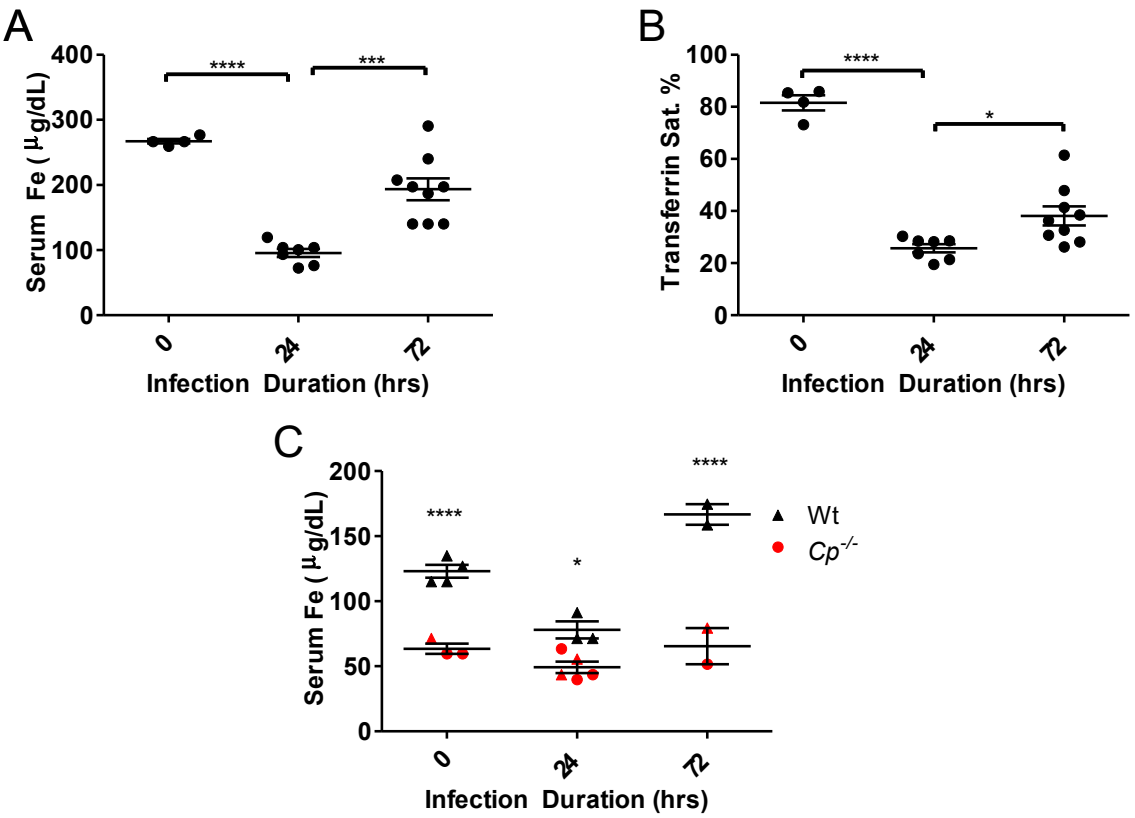

Figure 3-4 Changes in serum Fe during infection. Total serum Fe and transferrin Fe were measured in 9-week-old BALB/C (A-B) and 11-week-old C57BL/6 mice and *Cp* $^{-/-}$ mutants (C). (A-B) Total serum Fe and transferrin saturation were determined in serum of 4-9 mice per group at the indicated time points. *P <0.05; ***P<0.001; ****P<0.0001 (C). Total serum Fe was determined in the serum of 2-5 Wt and *Cp* $^{-/-}$ mice per group at the designated time points. *P <0.05; ***P<0.001. Statistical significance determined by one-way ANOVA with Tukey post-test for (A-B) and two-way ANOVA with Tukey post-test for (C). Sex of mice denoted by given markers: male (triangles) and female (circles). Values plotted are individual mice with middle line representing the mean with error bars showing +/- SEM.

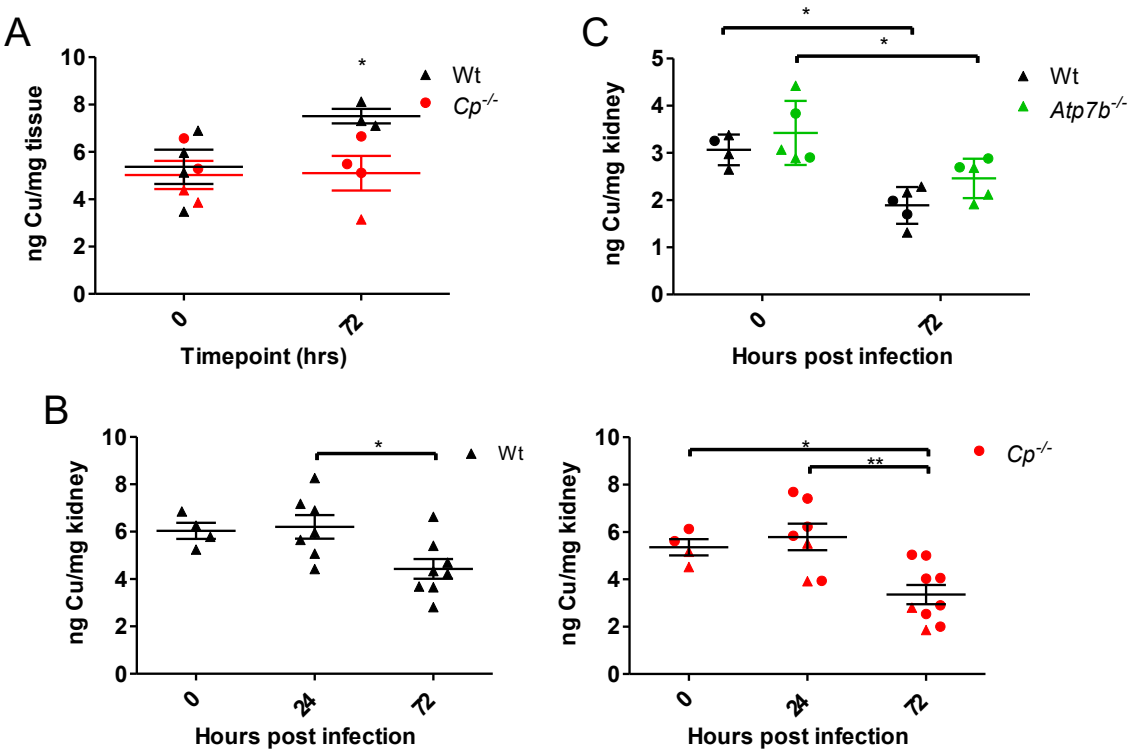

Figure 3-5 Presence of ceruloplasmin and ATP7B affect liver Cu but not kidney Cu. Liver and kidney Cu content as measured by AAS in *Cp*$^{-/-}$ and *Atp7b*$^{-/-}$ mice. (A) Liver Cu in Wt and CP$^{-/-}$ mice; 3-4 mice per group. *P=0.038. (B) Kidney Cu determined by AAS in 4-8 Wt C57BL/6 mice per group (left panel) and 4-9 *Cp*$^{-/-}$ mice per group (right panel). *P<0.05; ***P<0.001. (C) Kidney Cu levels in 4-5 Wt and *Atp7b*$^{-/-}$ mice per group during infection. *P<0.05. Statistical significance determined by two tailed Student's t-test (A,C) and one-way ANOVA with Tukey post-test for (B). Values plotted are individual mice with middle line representing the mean with error bars showing +/- SEM.

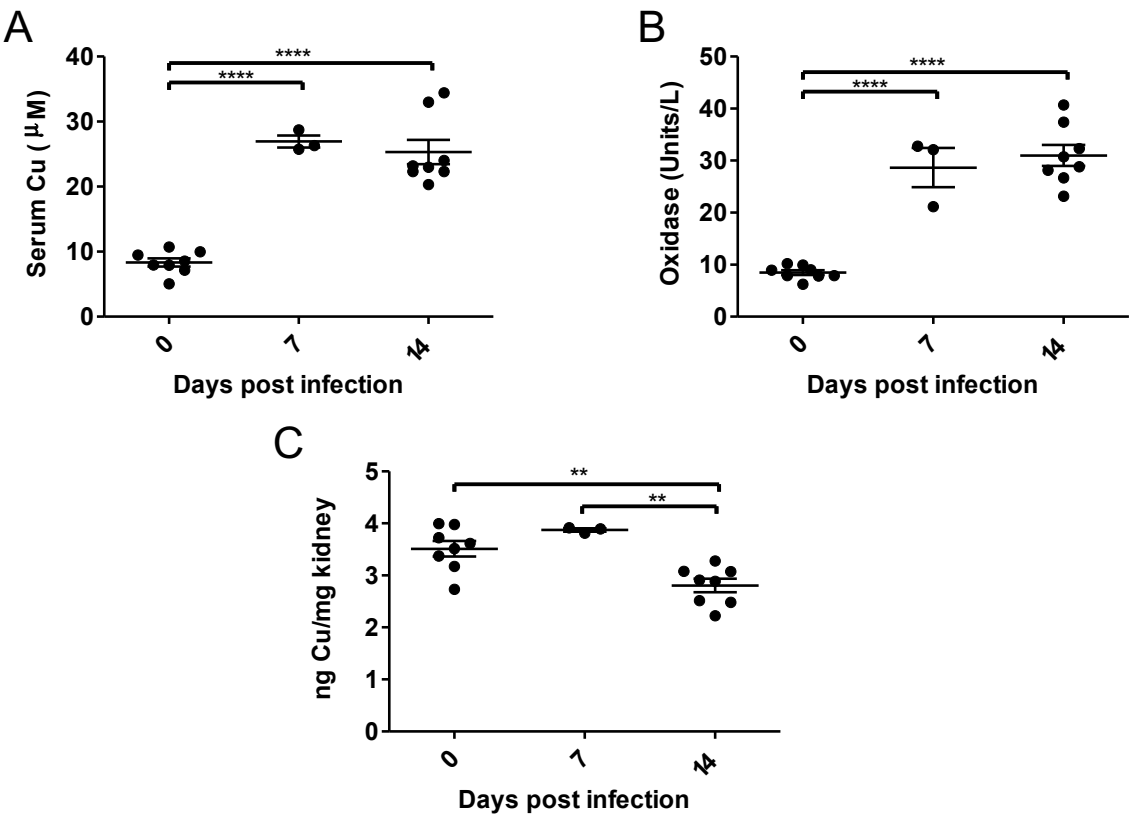

Figure 3-6 Changes in serum and kidney Cu during infection with *Plasmodium berghei.* Seven-week-old female BALB/c mice were infected with *P. berghei* and sacrificed at the indicated time points. Results shown are pooled from two experiments with 8 control mice, 3 mice sacrificed at day 7, and 8 mice after 14 days. (A) Serum Cu measurements of *P. berghei* infected mice. ****P<0.0001. (B) Oxidase activity of *P. berghei* infected serum in 19 mice. **** P< 0.0001. (C) Kidney Cu levels of *P. berghei* infected mice. **P<0.01. Statistical significance determined by one-way ANOVA with Tukey post-test for (A-C). Values plotted are individual mice with middle line representing the mean with error bars showing +/- SEM.

Chapter 4:

Expanded role of the Cu-sensing transcription factor Mac1p in *Candida albicans*

This chapter was published in *Molecular Microbiology* (2020, Aug 18; 2020;10.1111/mmi.14591) and is reproduced here with copyright permission from the Wiley Online Library.

Abstract

As part of the innate immune response, the host withholds metal micronutrients such as Cu from invading pathogens, and microbes respond through metal starvation stress responses. With the opportunistic fungal pathogen *Candida albicans*, the Cu sensing transcription factor Mac1p governs the cellular response to Cu starvation by controlling Cu import. Mac1p additionally controls reactive oxygen species (ROS) homeostasis by repressing a Cu-containing superoxide dismutase (*SOD1*) and inducing Mn-containing *SOD3* as a non-Cu alternative. We show here that *C. albicans* Mac1p is essential for virulence in a mouse model for disseminated candidiasis and that the cellular functions of Mac1p extend beyond Cu uptake and ROS homeostasis. Specifically, *mac1*Δ/Δ mutants are profoundly deficient in mitochondrial respiration and Fe accumulation, both Cu-dependent processes. Surprisingly, these deficiencies are not simply the product of impaired Cu uptake; rather *mac1*Δ/Δ mutants appear defective in Cu allocation. The respiratory defect of *mac1*Δ/Δ mutants was greatly improved by a *sod1*Δ/Δ mutation, demonstrating a role for *SOD1* repression by Mac1p in preserving respiration. Mac1p down-regulates the major Cu consumer SOD1 to spare Cu for respiration that is essential for virulence of this fungal pathogen. The implications for such Cu homeostasis control in other pathogenic fungi are discussed.

Introduction

Transition metals represent a double-edged-sword to biological systems; they are required for life but also can become toxic if not properly managed. Because of this dual nature, homeostasis of transition metals in biological systems is tightly controlled. Cu is one such metal that has this dual property of being both essential and potentially toxic. Cu is required as a redox cofactor for numerous enzymes involved in oxygen chemistry, but can also have deleterious side chemistry (217-219,221,222). Unicellular microbes are particularly vulnerable to fluxes in environmental metals and have evolved sophisticated means of regulating Cu homeostasis.

In the bakers' yeast *S. cerevisiae* Cu homeostasis is controlled by two Cu binding transcription factors: Ace1p and Mac1p (88). Ace1p senses high, toxic Cu concentrations and activates Cu detoxification machinery involving genes encoding Cu-binding metallothioneins (89,271). In times of Cu limitation, Mac1p activates transcription of genes for Cu uptake including the high affinity Cu permeases and cupric reductases (272). Variations on this theme of sensing and responding to extremes in Cu can be found throughout yeast species. The pulmonary fungal pathogen *Cryptococcus neoformans* uses the Cu-sensing transcription factor Cuf1p which bears homology to both *S. cerevisiae* Ace1p and Mac1p. Cuf1p activates both Cu uptake and Cu detoxification genes in response to Cu limitation and Cu excess, respectively (47,48,104,105). On the other hand the pathogenic and saprotrophic fungi *Aspergillus fumigatus* has retained separate Ace1/Mac1 systems but in this fungus, AfMac1p has evolved to independently upregulate genes involved in Fe uptake as well as Cu uptake (45,110,111,113). The opportunistic human fungal pathogen *Candida albicans* also has separate Mac1p and Ace1p Cu regulators and the core functions of Mac1p have been retained, namely transcriptional activation of Cu uptake genes including the *CTR1* Cu

permease and *FRE7* cupric reductase (121). However, *C. albicans* Mac1p has additionally evolved to regulate anti-oxidant systems including superoxide dismutase enzymes (SOD).

SOD metalloenzymes utilize redox active co-factors such as Mn and Cu to disproportionate superoxide anion free radicals and therefore play important roles in metabolism of reactive oxygen species (ROS) (273). Eukaryotes typically contain a Cu/Zn-SOD1 in the cytosol and mitochondrial intermembrane space, and a distinct Mn-SOD2 in the mitochondrial matrix. Mitochondrial SOD1 and SOD2 ensure protection against respiratory chain superoxide, while cytosolic Cu/Zn-SOD1 can participate in cell signaling involving ROS (62,67,123,274-278). Apparently unique to *C. albicans* and closely related fungi is a second Mn containing Sod3p in the cytosol (126). During Cu limitation, *C. albicans* Mac1p transcriptionally represses Cu-Sod1p and induces Mn-Sod3p to maintain cytosolic levels of SOD (43,68,123). Additionally, Mac1p induces a mitochondrial alternative oxidase (*AOX2*) to compensate for loss of mitochondrial Cu/Zn SOD1 (121,123). *C. albicans* Mac1p clearly participates in ROS homeostasis as well as Cu uptake.

The Mac1-Cu response is utilized by *C. albicans* during pathogenesis. In a murine model of disseminated candidiasis, where the kidney is the major target organ, kidney Cu levels fluctuate such that at early time points Cu levels are high, but decrease later in infection (30,43,46,127). *C. albicans* is able to sense these changes in Cu and exhibits abundant expression of *SOD1* at early stages of infection, and then repression of *SOD1* and transcriptional induction of *SOD3* and *CTR1* later in infection when Cu levels decrease (30,43,46). Clearly *C. albicans* senses a Cu starved microenvironment in murine kidneys and is responding using Mac1p. It was not known if this Mac1p response plays a role in virulence in this model. Furthermore, the full impact of Mac1p on cell physiology is not understood. Is the function of Mac1p limited to cell surface Cu

uptake and ROS homeostasis? It was unclear what, if any, additional genes are Mac1p targets in *C. albicans.*

In these studies, we investigate the requirement for *C. albicans* Mac1p in pathogenesis and its expanded role in regulating metal homeostasis and anti-oxidant enzymes. We find that Mac1p does indeed contribute to pathogenesis in a murine model of disseminated candidiasis and that its cellular function extends beyond Cu uptake and reactive oxygen homeostasis. Cells lacking Mac1p are severely compromised in both mitochondrial respiration and Fe accumulation, both a product of disrupted Cu homeostasis. Loss of Cu uptake in *mac1*Δ/Δ mutants cannot totally explain these deficiencies; rather *mac1*Δ/Δ mutants are defective in intracellular distribution of Cu to essential targets including Cu-requiring cytochrome oxidase (COX) for respiration. We provide evidence that Mac1p control of anti-oxidant genes through down-regulation of *SOD1* not only maintains oxidative stress protection, but also spares Cu for mitochondrial COX. Mac1p helps maintain respiration essential for pathogenesis in the face of limiting host copper.

Results and Discussion

The mac1 strain has a virulence defect in a murine model of disseminated candidiasis

We sought to determine whether the Mac1p response to Cu during *C. albicans* invasion of the kidney was essential for pathogenesis. For these studies, we generated a *mac1*Δ/Δ mutation in a *C. albicans* clinical isolate lacking auxotrophic markers. Both *mac1*Δ/+ heterozygous and *mac1*Δ/Δ homozygous mutations were generated in the SC5314 background using the SAT1 flipper technique (279). We validated that *mac1*Δ/Δ

homozygotes, but not *mac1Δ/+* heterozygotes, behaved similarly to a *mac1Δ/Δ* homozygous deletion in the SN152 background (43), and are unable to switch from Cu containing Sod1p to Mn containing Sod3p during Cu starvation, as induced by the Cu(I) chelator bathocuproinedisulfonic acid (BCS) (Fig. 4-1A, lane 7). This defect was corrected by integrating a single copy of *MAC1* into its native locus (Fig. 4-1A, lane 9). We used both the *mac1Δ/Δ* deletion strain and the reintegrated *MAC1* rescue for virulence studies in a murine model of disseminated candidiasis where the kidneys are the major target organs and where tissue Cu levels decline during infection (30,43,46,127,237). As seen in Fig. 4-1B, female mice infected with WT *C. albicans* by lateral tail vein injection succumbed to the infection by 9 days. The *mac1Δ/Δ* strain displayed a stark virulence defect (Fig. 4-1B) with *mac1Δ/Δ* infected mice displaying a mean survival of 15 days post-infection. Virulence was fully restored by reintegration of *MAC1* (Fig. 4-1B). Thus, Mac1p plays an important role in fungal virulence in disseminated candidiasis. Recent studies by Khemiri have shown role for *C. albicans* Mac1p in adherence to a human colon epithelial cell line *in vitro*, consistent with the importance of Mac1p in fungal growth and cell invasion (280).

The effects of mac1Δ/Δ mutations on fungal copper accumulation and mitochondrial respiration

The basis for the virulence defect of *mac1Δ/Δ* strains was unclear. We therefore examined in detail the effects of *MAC1* loss in cultures of *C. albicans in vitro*. Aside from regulating *SOD1* and *SOD3*, Mac1p has been reported to induce the Cu permease gene *CTR1* when cells are deprived of extracellular Cu (121). To directly monitor *CTR1* expression we examined transcript levels by qRT-PCR. In enriched YPD media that was not depleted for Cu, *CTR1* mRNA levels in the *mac1Δ/Δ* mutant were significantly lower

than that of WT cells (Fig. 4-2A). Therefore Mac1p not only upregulates *CTR1* with Cu starvation, but is also needed for basal levels of *CTR1* expression when extracellular Cu is available. Consistent with this low basal level of *CTR1* expression, *mac1Δ/Δ* mutants displayed ≈25-30% of the total intracellular Cu of WT cells (Fig. 4-2B, also see Figs. 4-3C and 4-4A). This low level of intracellular Cu in *mac1*Δ/Δ cells is similar to WT cells treated with 400 μM of the Cu chelator BCS (Fig. 4-2B).

We tested whether this low level of intracellular Cu in *mac1*Δ/Δ mutants impacted mitochondrial respiration, a Cu-dependent process essential for virulence *of C. albicans* (80,281,282). Cytochrome c oxidase (COX) of the electron chain is a Cu-requiring complex (217,218) and can be monitored by measuring the rate of cyanide sensitive-oxygen consumption. As seen in Fig. 4-2C, COX-respiration in the *mac1Δ/Δ* strain was drastically reduced compared to the WT strain. This defect is indeed due to Cu deficiency, as oxygen consumption levels were restored to WT levels in cells supplemented with high Cu in the growth medium (Fig. 4-2C).

Since *C. albicans* is dependent on respiration for growth *in vivo* (80,281,282), we tested whether the lowered oxygen consumption in *mac1Δ/Δ* cells impacted respiration-dependent growth *in vitro*. *C. albicans* relies on respiration in the presence of non-fermentable carbon sources such as glycerol and ethanol. As seen in Fig. 4-2D top*,* *mac1*Δ/Δ strains failed to grow when glycerol and ethanol are provided as sole carbon sources, compared to growth on glucose that supports both fermentation and respiration. This requirement of Mac1p for growth on non-fermentable carbon sources is consistent with findings of *mac1*Δ/Δ mutants in an independent *C. albicans* strain background (BWP17) (120). As with oxygen consumption, the respiratory defect of *mac1Δ/Δ* mutants was totally rescued by supplementation with Cu salts (Fig. 4-2D bottom). Thus, the respiratory deficiency of *mac1Δ/Δ* mutants as seen in Fig. 4-2C is

indeed sufficient to block respiration-dependent growth as might occur *in vivo* during infection.

To test if low intracellular Cu by itself can explain the respiratory deficiency of *mac1*Δ/Δ cells, we quantified COX-respiration in WT cells that accumulate virtually identical low levels of total intracellular Cu through treatment with 400 μM BCS (Fig. 4-2B). Surprisingly, these Cu-depleted WT cells showed no defect in respiration (Fig. 4-2E). Unlike *mac1Δ/Δ* mutants, COX-respiration in WT cells appears resilient to Cu deprivation. Hence, the respiration defect of *mac1Δ/Δ* mutants cannot be explained by low levels of total intracellular Cu. Instead, the mutants may be unable to properly allocate Cu to COX in the mitochondria.

*Contribution of SOD1 to the respiratory defect of mac1*Δ/Δ *cells*

We addressed whether the apparent *mac1*Δ/Δ defect in Cu allocation to COX is due to improper regulation of *SOD1*. Sod1p is an abundant cellular protein that can account for 10-20% of the total intracellular Cu in yeast strains (283). Since *mac1*Δ/Δ mutants cannot repress *SOD1* gene expression, Sod1p polypeptide levels remain unaffected in these Cu starved cells (Fig. 4-1A, lane 7, and (43)). Most importantly, Sod1p retains a certain level of activity in *mac1*Δ/Δ cells (Fig. 4-3A, lane 3). In spite of very low intracellular Cu, Sod1p is still receiving Cu in *mac1*Δ/Δ cells.

To test whether the residual Cu bound to Sod1p in *mac1Δ/Δ* mutants is preventing Cu activation of COX, we generated a *mac1Δ/Δ sod1Δ/*Δ double mutant using a CRISPR based approach for *C. albicans* (284). When we assayed COX respiration, we found that deletion of *SOD1* significantly ameliorated the oxygen consumption defect of *mac1Δ/Δ* mutants (Fig. 4-3B). This rescue of respiration by the *sod1*Δ mutation occurred without any increases in total intracellular Cu (Fig. 4-3C).

Therefore, the presence of residual Sod1p in Cu-starved *mac1Δ/Δ* cells appears to function as a Cu sink, sequestering Cu away from COX. This notion of Sod1p limiting Cu accessibility to COX is consistent with our previous studies in WT cells where inappropriate over-expression of *SOD1* lowered COX respiration (123). We conclude that Mac1p in *C. albicans* has evolved to maintain COX activity essential for growth and pathogenesis in at least two ways: by inducing Ctr1p-dependent Cu transport and by down-regulating Sod1p, a major Cu consumer. The regulation of anti-oxidant enzymes by *C. albicans* Mac1p not only serves to maintain oxidative stress protection and ROS signaling during Cu starvation (68,123), but also facilitates Cu sparing for COX to help maintain mitochondrial respiration. A similar mechanism may extend to other organisms as well. In *C. neoformans,* the Cuf1p Cu sensor represses Cu/Zn SOD1 during Cu starvation (105), which may also be part of a Cu sparing pathway for maintaining respiration or other essential Cu-dependent processes. The notion of Cu sparing for mitochondrial respiration has also be proposed for certain marine microorganisms. During Cu limitation, the photosynthetic algae *Chlamydomonas reinhardtii* degrades Cu containing plastocyanin for photosynthesis and Cu is prioritized for mitochondrial COX (285-287). Down regulation of plastocyanin during Cu limitation has also been observed in diatoms (288).

Evidence for non-Sod1 factors in Mac1p-maintenance of respiration

It is important to note that loss of *SOD1* only partly rescues COX-dependent respiration in *mac1Δ/Δ* mutants, but does not restore oxygen consumption to WT levels (Fig. 4-3B). Is this level of restored oxygen consumption sufficient to support respiration-dependent growth? As seen in Fig. 4-3D*,* deletion of *SOD1* did not restore growth of *mac1Δ/Δ* strains on non-fermentable carbon sources without Cu supplements (Fig. 4-3D

column 1); however the *mac1Δ/Δ sod1Δ/*Δ mutant did exhibit improved growth compared to the *mac1Δ/Δ* strain when low levels of Cu salts were added to the growth media (Fig. 4-3C, column 2-6). Thus, loss of *SOD1* can improve respiration-dependent growth of a *mac1*Δ/Δ strain, but only under specific conditions of Cu availability. We also tested the effects of Sod1p loss in the disseminated model of candidiasis, where respiration is essential for virulence (80,281,282) and where the kidney is the major site of infection (237). Previous studies have shown that Cu availability becomes low in the kidney during *C. albicans* invasion (30,43,46,127), and with these Cu-limited conditions, loss of *SOD1* may not be sufficient to support respiration-dependent growth. Indeed, as shown in in Fig. 4-3E, there was no significant difference between mouse survival in mice infected with *mac1Δ/Δ* or *mac1Δ/Δ sod1Δ/Δ* strains. However, as a potential caveat to these studies, *sod1*Δ/Δ strains by themselves are defective in virulence in this mouse model (64) and consistent with this, we observed a slight trend towards decreased virulence in the *mac1Δ/Δ sod1Δ/Δ* strain compared to the single *mac1*Δ/Δ mutant. In any case, our cell culture studies (Fig. 4-3C and 4-3D) demonstrate that Mac1p repression of *SOD1* is just one method for preserving COX-respiration and other factors may contribute as well.

mRNA profile changes associated with mac1Δ/Δ *mutations*

To search for other factors that may contribute to the *mac1Δ/Δ* defect, we used an RNA-seq approach to identify possible targets of Mac1p regulation. For these studies, we compared *mac1Δ/Δ* to WT cells treated with 400 μM of the Cu(I) chelator BCS. As seen in Fig. 4-4A, these two experimental groups have similarly low levels of intracellular Cu (see also Fig. 4-2B). Any variations in gene expression patterns can

therefore be ascribed specifically to the loss of Mac1p*,* not variations in Cu accumulation.

The possible targets of Mac1p-repression were defined as those genes repressed ≈ 3-fold or greater with BCS, but either unchanged or elevated in a *mac1Δ/Δ* strain. As shown in Fig. 4-4B, only three genes fit this category and of these, the most strongly repressed by Cu starvation is *SOD1*. Similar findings were obtained with *C. neoformans,* where the most prominent target of Cuf1-repression during Cu starvation is *SOD1* (105)*.* In the case of *C. albicans,* other genes down-regulated by BCS but not in *mac1*Δ/Δ mutants include *AAH1*, which encodes an adenine deaminase that is differentially regulated in biofilms (289,290), and *FGR23,* a member of the FGR family that has been implicated in the regulation of filamentous growth (289) (Fig. 4-4B). Neither *AAH1* or *FGR23* are predicted to encode cuproproteins. Mac1p is known to repress *SOD1* through a Mac1p binding consensus site in an intron, 147 nucleotides downstream of the translational start site (43) (Fig. 4-4B). Across the various known *C. albicans* Mac1p targets, the putative binding consensus sequence is XTTGCKCR where X, K, and R are preferably a T, T, A respectively (121,280). Using this sequence as a reference, neither *AAH1* nor *FGR23* have an obvious Mac1p consensus sequence within the coding region. In fact, no consensus sequences could be identified within 1000 bps either upstream or downstream of *AAH1* and *FGR23.* It is therefore possible that *SOD1* is the only gene repressed by Mac1p in *C. albicans*, highlighting the importance of *SOD1* repression during Cu starvation. As a possible caveat to our search of consensus sequences, *C. albicans* Mac1p may be promiscuous in its DNA recognition site, as has been observed for *C. neoformans* Cuf1p (105) and *A. fumigatus* Mac1p (110,113).

We also interrogated possible gene targets of Mac1p activation. Such genes should be upregulated upon treatment with BCS but not in *mac1*Δ/Δ strains. Indeed, we

identified many previously published activated gene targets of Mac1p as being uniquely induced by Cu chelation including *CTR1, FRE7, FRE30, SOD3, AOX2,* and *MAC1* (Fig. 4-4C) (43,121,280). Aside from these genes for Cu uptake and genes that substitute for Sod1p loss (*AOX2* and *SOD3),* a number of other loci were specifically induced by Cu starvation in WT cells, but not in *mac1*Δ/Δ strains. These are summarized in the Venn diagram of Figure 5A showing gene ontology (GO) terms of genes that were upregulated more than three-fold in BCS versus *mac1*Δ/Δ cells. Unique to BCS treatment were genes encoding hexose sugar transporters. Upon sequence analysis, none of these genes had obvious Mac1p binding consensus sequences. We have previously shown that *sod1*Δ/Δ deletions induce hexose transporters, reflecting a role of Sod1p in glucose signaling (68). The total absence of Sod1p in BCS-treated WT cells (Fig. 4-1A) likely accounts for induction of sugar transporters with Cu starvation. We also observed genes for adhesion and hyphal growth induced in BCS-treated WT cells, but not in *mac1*Δ/Δ cells e.g., *ECE1, HWP1, ALS3* (Table S4-1). This is consistent with some development of filamentation observed with Cu-starved WT cells, but not in the *mac1*Δ/Δ strain (Fig. S4-1). Interestingly, Cu starvation has been reported to induce filamentation in *C. albicans* in a Mac1p-dependent manner through an unknown mechanism (120,291).

Fe-starvation state of mac1Δ/Δ *mutants*

RNA-seq analysis indicated that *mac1*Δ/Δ mutants are not only starved for Cu but also Fe. Specifically, we observed a large number of genes induced in *mac1*Δ/Δ cells consistent with a transcriptional Fe-starvation stress response. Gene Ontology (GO) analysis revealed that many genes induced in the *mac1*Δ/Δ strain were related to ribonucleoprotein complex biogenesis, which is regulated by the HAP43/CCAAT binding protein Fe regulatory complex of *C. albicans* (292). We observed strong induction of

genes involved in reductive Fe uptake, heme acquisition and the siderophore transporter *SIT1* (Fig. 4-5B), all of which are known be induced under Fe starvation stress conditions (293). While this manuscript was in its final stages of preparation, Khemiri et. al. published a study showing a similar high induction of specific Fe transport genes in *mac1*Δ/Δ cells from the background strain SN125 (280).

Regulation of Fe transport genes has also been reported with *A. fumigatus* Mac1p (Afmac1), however the role of Afmac1 in Fe homeostasis appears opposite to that of *C. albicans* Mac1p. AfMac1 is an activator of Fe uptake genes and loss of Afmac1p results in a decreased expression of Fe transporters (113), unlike the pronounced induction of the Fe transport regulon with *C. albicans mac1*Δ/Δ mutations (Fig. 4-5B). *C. albicans* Mac1p is either a repressor of Fe uptake or the effects of *mac1*Δ/Δ are an indirect consequence of Cu starvation. We favor the latter. Cu is important for Fe acquisition and in yeast species including *C. albicans,* FET multicopper oxidases drive Fe uptake into the cell (294,295). Consistent with this requirement for Cu in Fe uptake we find that *C. albicans mac1*Δ/Δ mutants accumulate extraordinarily low levels of intracellular Fe (Fig. 4-6A), explaining the strong induction of the Fe starvation stress response at the mRNA level (Fig. 4-5B). Moreover, this Fe deficiency of *C. albicans mac1*Δ/Δ mutants is totally reversed by Cu supplements (Fig. 4-6A), unlike AfMac1p control of *A. fumigatus* Fe transport which occurs independent of Cu status (113). With *C. albicans*, the Fe starvation stress state of *mac1*Δ/Δ mutants appears secondary to defects in Cu homeostasis and the inability of these cells to populate FET oxidases with Cu.

Fe and Cu deficiency and the respiratory defect of mac1Δ/Δ *mutants*

With such low Fe in *mac1Δ/Δ* mutants, we questioned if limited Fe bioavailability could be contributing to the respiration defect of these cells. Both Complex I and Complex II of the electron transport chain make use of Fe-S clusters (296) and Complex II, III, and IV all make use of Fe in the form of heme (297). To test the impact of low Fe on *mac1Δ/Δ* respiration, we sought to uncouple the Fe and Cu deficiencies of this mutant. Through Fe titrations we found that supplementation of 350 μM ferrous ammonium sulfate to the growth media restored Fe levels in the *mac1Δ/Δ* mutant to near WT levels (Fig. 4-6B), with no elevation in intracellular Cu (Fig. 4-6C). This restoration of intracellular Fe pools also alleviated the Fe starvation stress response of this mutant as demonstrated by reversal of the strong *mac1Δ/Δ* induction of the *CFL4* and *SOD4* gene targets of the Sef1/Sfu1p Fe regulatory system (Fig. 4-6D,E) (293). However, amelioration of the *mac1Δ/Δ* Fe deficiency had no effect on the poor respiration of these mutants (Fig. 4-6F), compared to the strong rescue of respiration with Cu supplements (Fig. 4-2C). The *mac1Δ/Δ* respiratory phenotype is overwhelmingly driven by deficiencies in Cu, not Fe.

Evidence for mac1Δ/Δ *defects in Cu allocation for Fe uptake*

It is important to note that the Fe starvation state of *mac1Δ/Δ* cells cannot wholly be explained by low total Cu. The same Fe stress response is not mirrored in WT cells treated with BCS (Fig. 4-5A,B), even though these cells accumulate similarly low levels of Cu (Fig. 4-2B, 4-4A). Only a small number of the Fe transport genes were induced in BCS-WT cells, including *CFL2*, *CFL5, FET31,* and the level of induction was greatly reduced compared to that of *mac1Δ/Δ* cells (Fig. 4-5B). Just *SOD4,* which is not involved in Fe transport but is part of the Fe starvation regulon (293,298,299), is induced to

similar levels in BCS-treated WT versus *mac1*Δ/Δ cells (Fig. 4-5B). Furthermore, BCS-treated WT cells accumulate substantially higher levels of Fe compared to *mac1*Δ/Δ cells (Fig. 4-7A). These comparisons to Cu-starved WT cells demonstrate that the severe Fe deficiency of *mac1*Δ/Δ cells is not simply due to low total Cu. As with COX respiration, the *mac1*Δ/Δ mutant appears impaired in proper allocation of Cu for Fe uptake.

Since the respiratory defect of *mac1Δ/Δ* cells was improved upon loss of the Sod1p Cu consumer (Fig. 4-3B), we tested if a deletion in *SOD1* would likewise restore Fe accumulation. Significantly and unlike respiration, deletion of *SOD1* had no effect on the Fe deficiency of the *mac1*Δ/Δ mutant (Fig 4-7B). Mac1p repression of *SOD1* helps spare Cu for respiration but not for Fe uptake. Other Cu consumers may be preventing Cu allocation for Fe uptake and one family of genes that are suspect are the FETs themselves. *Candida* has 5 annotated FETs: Fet3p, Fet31p, Fet33p, Fet34p, and Fet99p (300). Of these, Fet34p and Fet99p are reported to be the most important for Fe acquisition (295) and both of the corresponding genes are strongly induced in *mac1*Δ/Δ strains as part of the Fe starvation stress response (Fig. 4-5B). Of the FETs less critical for Fe uptake (Fet3p, Fet33p, Fet31p; (295)), *FET31* is 100x fold induced in *mac1*Δ/Δ mutants, while *FET3* and *FET33* are not substantially changed (Fig. 4-5B). It is possible that Cu binding to highly abundant Fet31p may preclude proper Cu allocation to the more essential FETs for Fe uptake. Other possible Cu consumers of the cell include the putative amine oxidases Amo1p and Amo2p and although neither is induced in *mac1*Δ/Δ strains (Table S4-1), they may contribute to poor Cu availability. Additionally, we cannot exclude the possibility that Cu is sequestered in organelles such as the vacuole, or that a certain as-of-yet unknown Cu chaperone for Fet34p or Fet99p may be defective in *mac1*Δ/Δ strains. Lastly, it is important to note that while Sod1p contributes to the respiratory defect of *mac1*Δ/Δ strains, Sod1p by itself cannot account for the deficiency. A *sod1*Δ/Δ deletion only partly restores oxygen consumption in *mac1*Δ/Δ cells (Fig. 4-3B)

and other *mac1*ΔΔ defects in Cu allocation, including those described above, may be involved.

Conclusions:

Across numerous fungal species, the Cu sensor Mac1p/Cuf1p controls cell surface uptake of Cu to ensure that intracellular Cu levels remain ample under conditions where extracellular Cu is low (43,45,91,95,104,105,110,111,120,121,301). Our studies demonstrate that in addition to this role in Cu uptake, Mac1p in *C. albicans* participates in Cu allocation and prioritizing Cu for processes such as Fe uptake and cellular respiration. This role in Cu allocation is accomplished in part through down-regulation of a major Cu consumer Sod1p and re-directing Cu towards COX for mitochondrial respiration. Previously, Mac1p control of *C. albicans* anti-oxidant genes *SOD1, SOD3* and *AOX2* was shown to maintain oxidative stress protection and ROS signaling during times of Cu limitation (68,123). We now show this regulation of antioxidant genes has the added purpose of sparing Cu for respiration that is essential for pathogenesis of *C. albicans.* These findings with Mac1p may not be unique to *C. albicans*. *C. neoformans* also represses *SOD1* during Cu limitation(105) and the Cu maybe re-purposed for other cuproenzymes essential for pathogenesis.

Materials and methods

Fungal strains and culture conditions

Cultures of *C. albicans* were maintained at 30°C in YPD (1% yeast extract, 2% peptone, 2% dextrose). Where indicated, cultures were supplemented 400 μM of the Cu(I) chelator BCS. Tests for respiration-dependent growth used non-fermentable

carbon source containing YPGE medium (2% bacto-peptone, 1% yeast extract, 3% glycerol, 2% ethanol) and both YPD and YPGE plates were made with 2% bactoagar. YPD and YPGE plates supplemented with Cu contained 100 μM $CuSO_4$. YPM media (1% yeast extract, 2% peptone, 2% maltose) was used to stimulate flippase activity. When noted, Fe was supplemented to liquid cultures as ferrous ammonium sulfate (Sigma Chemical Co.)) and Cu was added as $CuSO_4$ (Sigma-Aldrich)

C. albicans clinical isolate SC5314 was used as the WT and parental strain from which all mutants were derived. Construction of the *mac1*Δ/Δ mutant by the SAT1-flipper method was as follows using primers described in Table S2: genomic DNA from strain SC5314 was used to amplify *MAC1* residues -441 to -205 and +1423 to +1593. These were inserted respectively into the SacI and NotI and the XhoI and KpnI sites of the pSFS2 plasmid (279), generating plasmid pEC-M1L. The *mac1* deletion cassette from pEC-M1L was mobilized by KpnI and SacI digestion and used to transform SC5314 by electroporation. Cells were plated onto YPD containing 200 mg/mL nourseothricin sulfate (NAT) (Gold Bio), and NAT resistant colonies selected and verified for presence of the NAT cassette by PCR. Positive colonies were then grown overnight in YPM media to induce excision of NAT resistance by flippase. Cells were then plated onto 25 mg/mL NAT containing YPD media and NAT sensitive colonies were selected. The resultant *mac1*Δ/+ heterozygous mutant strain EC003 was verified by PCR. To delete the second allele, *MAC1* sequences -205 to -1 and +1201 to +1419 were amplified by PCR and inserted into the SacI and NotI, and XhoI and KpnI sites in pSFS2 to generate the plasmid pEC-M1S. The deletion cassette from pEC-M1S was liberated with KpnI and SacI digestion and used to transform the *mac1*Δ/+ strain EC003. NAT resistant colonies were selected and NAT resistance excised as above. Deletion of the second *MAC1* allele was verified by PCR, resulting in the *mac1*Δ/Δ strain EC004.

A single copy of *MAC1* was introduced in the *mac1Δ/mac1Δ* strain EC004 as follows: *MAC1* genomic sequences from -205 to +1419 were amplified and inserted into pSFS2 at SacI and NotI sites. *MAC1* residues +1209 to 1419 were inserted into XhoI and KpnI sites of this plasmid to generate the pEC-M1R plasmid, which was then linearized with SacI and KpnI and transformed into the *mac1Δ/Δ* strain EC004, generating the *mac1Δ/Δ::MAC1* re-integrant strain EC005.

A CRISPR protocol optimized for *C. albicans* was used as previously described (284) to generate the *mac1Δ/Δ sod1Δ/Δ* and a *mac1Δ/Δ* control strain using oligonucleotides listed in Table S3. Homozygous null mutations were introduced using a donor DNA oligo 100 bp in length composed of residues -50 to -1 upstream and 50 base pairs directly downstream of the coding regions of *MAC1* and *SOD1*, respectively. Guide RNAs to *MAC1* and *SOD1* were designed using Benching Software. Both *SOD1 and MAC1* were simultaneously deleted in *C. albicans* strain SC5314 to generate strain EC007 and the *mac1Δ/Δ* single homozygous mutant strain EC006 was generated similarly. Strains were confirmed by PCR and DNA sequencing.

Fungal cells were photographed using dark field microscopy using a Nikon Infinity 1 microscope at 40x magnification.

Murine Virulence Studies

Murine studies were carried out according to the National Institutes of Health guidelines for the ethical treatment of animals. This protocol was approved by the Institutional Animal Care and Uses Committee of the Johns Hopkins University medical institutions, protocol number M013M264. Nine-week old BALB/c female mice per strain in groups of ten were infected with $2x10^5$ *C. albicans* cells in 100 µL by lateral tail injection as previously described (302). Female mice were used as no difference

between sexes has been noted in regards to the Cu response seen in the kidney during infection (30,43,127). The fungal cells for infection were obtained by growth overnight in YPD to OD_{600} ~15; cells were harvested by centrifugation, washed twice in sterile 1x phosphate buffered saline (PBS), enumerated on a hemocytometer and diluted to $2x10^6$ cells mL^{-1} in PBS. Mouse survival following injection was monitored daily up to 30 days.

Metal measurements

For Cu analysis, cells were grown in YPD to OD_{600} of ≈2.0. 10-20 OD_{600} cell units were harvested by centrifugation and washed twice with 10 mM Tris, 1 mM EDTA, pH 8, and twice with MilliQ deionized water and cell recovery determined by measuring OD_{600}. Cells were digested with 200 µL 10% nitric acid (Fisher Chemical) at 100°C, diluted to a final concentration of 2% nitric acid in MilliQ water and then Cu content was measured using an AAnalyst graphite furnace atomic absorption spectrometer (AAS) (PerkinElmer). Metal content was normalized to cell number.

For Fe measurements, samples were subjected to a bathophenanthroline disulfonate (BPS) based assay as previously described (303). Cells for Fe analysis were prepared in nitric acid as described above for AAS. A plate-based version of the assay was adopted in which reactions contained 100 µL of standard or cell sample, 75 µL of water, 40 µL of 38 mg ml^{-1} sodium ascorbate, and 32 µL of a 1/3 saturated ammonium acetate solution. A first measurement of absorbance at 535 and 680 nm was then measured on an Eon (Biotek) plate reader. After the first spectrophotometric readings, 3 µL of 34 mg mL^{-1} BPS was added to each well. A second set of absorbance measurements at 535 and 680 nm was then measured. The BPS signal was determined as $X = ((A_{535}\text{-}A_{680})_{sample+BPS} - (A_{535}\text{-}A_{680})_{sample-BPS}) - ((A_{535}\text{-}A_{680})_{blank+BPS} - (A_{535}\text{-}A_{680})_{blank-BPS})$.

Oxygen Consumption Assays for COX respiration

Oxygen consumption measurements were conducted on whole cells similarly to published protocols (123,304) with modifications. Cells were grown in YPD to an OD_{600} of ≈2.0, harvested by centrifugation and resuspended to an OD_{600} of 5.0 and allowed to grow for 1 hour in fresh YPD at 30°C. 500 µL of the 5 mL culture were added to 1 mL of YPD in a Clark-type electrode (Hanstech Oxythem Plus) in a magnetically stirred, thermostatically controlled 1.5 mL chamber at 30°C. Oxygen saturation was measured over the course of 3-5 minutes and the change in oxygen saturation over time was used to determine the oxygen consumption rate. To validate oxygen consumption dependent on COX-mitochondrial respiration, 10 mM potassium cyanide (KCN) was added to inhibit COX respiration as described (304). For all respiration experiments 3 cultures for each strain served as the biological replicates and for each biological replicate 2 technical replicates of oxygen consumption were averaged.

Analyses of SOD protein and enzyme activity

For immunoblots and SOD activity gels, cells were grown to an OD_{600} of ≈2 in 10 mL YPD. 10 OD_{600} cell units were harvested, washed in water and resuspended in 100 µL of a lysis buffer containing 5 mM EDTA, 5 mM EGTA, 50 mM NACL, 10% glycerol, and 0.1% Triton X-100 in 10 mM sodium phosphate, pH 7.8. An equal volume of 0.5 mm zirconium oxide beads (Research Products International) was added and the samples were vortexed three times for a minute and a half at 4°C. Samples were then centrifuged for 10 minutes at 14,000xg. Supernatant was removed and protein concentration was determined via Bradford method. The resultant protein lysates were used for immunoblot analysis and SOD activity.

Immunoblot analysis for Sod1p and Sod3p followed published procedures (305). Briefly 10-15 µg of the samples were subjected to denaturing gel electrophoresis on 4-12% Bis-Tris acrylamide gels (Thermo Fisher). Proteins were then transferred to a PVDF membrane and blocked in 2% non-fat milk (VWR Life Science). Blots were probed with anti-SOD1(306) at a 1:10000 dilution and anti-SOD3 (305) at 1:5000. Primary antibody incubation was followed by incubation with secondary goat anti-rabbit IgG Alexa Flour 680 antibody at 1:10,000 (Thermofisher Scientific). Blots were imaged on an Odyssey infrared imaging system (LI-COR Biosciences) at 700 nm.

For analysis of SOD activity, lysates were run on native non-reducing 10% Tris-glycine gels at 50 mA for 90 minutes at 4^{o}C. Gels were then stained with 35 mL of a potassium phosphate buffered solution containing Nitro Blue Tetrazolium (Sigma-Aldrich), riboflavin (Acros Organics) and 35 µL of TEMED (Invitrogen) as previously published (305). Gels were incubated in this solution for 1 hour in the dark with gentle shaking. Gels were then placed in dH_2O, exposed to light and photographed.

RNA analysis by qRT-PCR and RNA-seq

To prepare RNA for qRT-PCR or RNA-seq, triplicate cultures were grown 16 hours to an OD_{600} of ≈ 2.0 in YPD. RNA was extracted from at least five OD_{600} cell units via an acid-phenol protocol as previously described (307). Briefly cells were lysed for an hour at 65^{o}C with vortexing every 5 minutes in 400 µL of acid phenol pH 4.5 (Ambion AM9720), 350 µL of 3M sodium acetate pH 5.5 (Thermo Fisher Scientific), and 1% SDS. Samples were subjected to three organic extractions with acid-phenol, precipitated by ethanol and nucleic acids treated with DNAse by Rapidout (ThermoFisher Scientific K2981). For qRT-PCR, cDNA was synthesized using a RevertAid First Strand cDNA (ThermoFisher Scientific K1622). cDNA samples were diluted 1:10 in DEPC-treated

water before qRT-PCR analysis with PowerUp SYBR Green Master Mix (ThermoFisher Scientific). qRT-PCR was performed on a QuantStudio 3 (Applied Biosystems) instrument. Cycle threshold values (Ct values) were normalized to *TUB2*. Relative expression was calculated using the dCT method. Amplicons of ~200 bp were obtained from the primers for *TUB2*, *CTR1, CFL4*, and *SOD4* shown in the Table S4-4. For RNA-seq, RNA samples were processed by Novogene Corporation Inc. for paired-end sequencing on an Ilumina HiSeq 2500. Reads were aligned to the *C. albicans* reference genome (SC5314) using TopHat2 (308). Aligned reads were then used to generate read counts for each gene and the DE-seq package from Bioconductor was used for statistical analysis of differential gene expression (309).

Software and Statistics

Differences were considered statically significantly if comparisons for P values were ≤ 0.05 using a one-way analysis of variance (ANOVA) with a Tukey posttest as determined by Graphpad Prism 7. Mouse survival was analyzed using a log rank test (Mantel Cox) to query any statistical differences. A gene was considered differentially expressed if its FDR for differential expression was <0.05. For GO analysis we used the Candida Genome Data Base's GO Term Finder and report GO terms with an FDR of less than 25%.

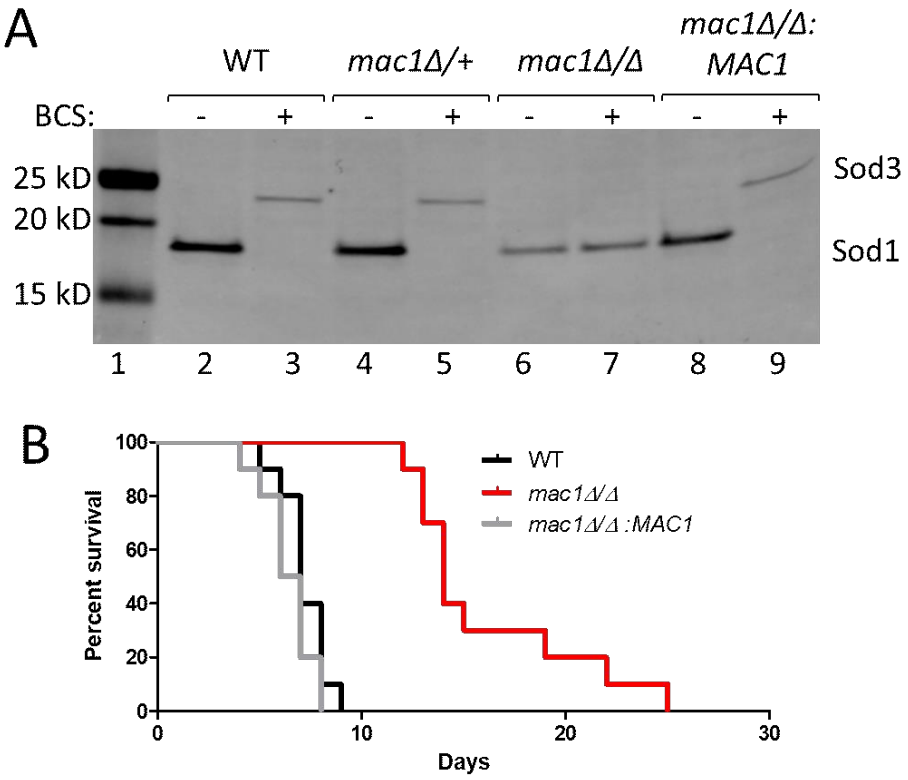

Figure 4-1 Generation of a *mac1Δ/Δ* mutant and virulence in a murine model of disseminated candidiasis. (A) Shown is immunoblot analysis of Sod1p and Sod3p for the indicated *C. albicans* strains using anti-SOD1 and anti-SOD3 antibodies as described in *Experimental Procedures*. (B) Survival curves are shown with groups of 10 female mice infected with $2x10^5$ cells of the indicated strains as outlined in *Experimental Procedures*. There was a statically significant difference ($p<0.0001$) between mice infected with WT and those infected with *mac1Δ/Δ* but not between WT and *mac1Δ/Δ:MAC1* ($p=0.15$). Statistical significance of survival curves was determined by the log-rank (Mantel-Cox) test. Strains utilized: WT, SC5314; *mac1Δ/+,* EC003; *mac1Δ/Δ,* EC004; *mac1Δ/Δ:MAC1,* EC005.

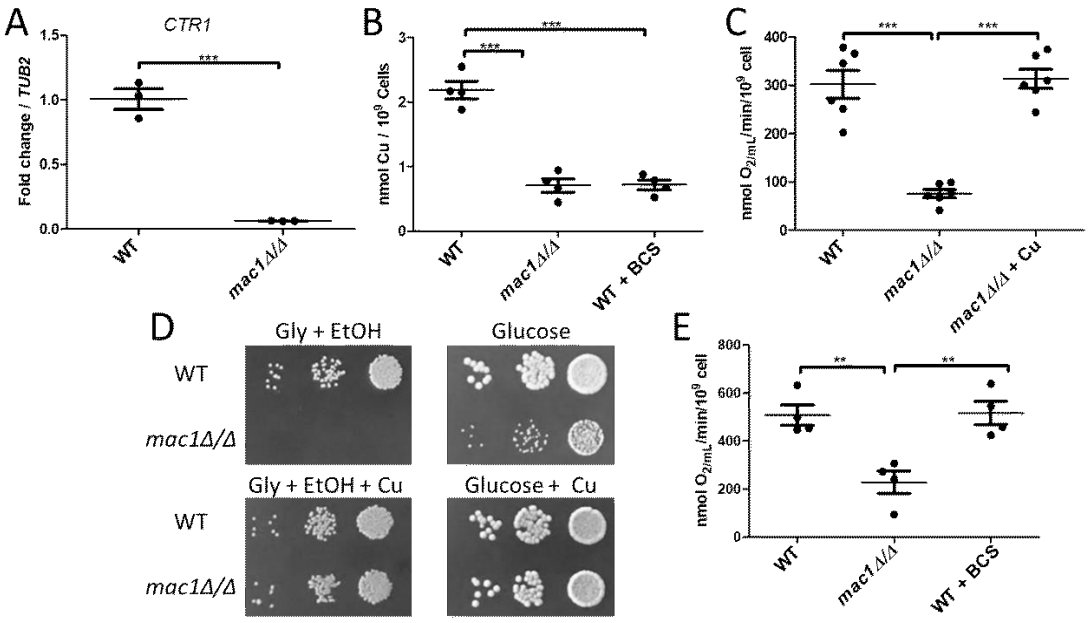

Figure 4-2 The Cu deficiency and respiratory defects of *mac1Δ/Δ* strains. (A) Expression of *CTR1* mRNA was analyzed by qRT-PCR and results normalized to *TUB2.* Results are shown for three independent cultures. Expression of *CTR1* in the *mac1Δ/Δ* strain was significantly different as determined by two-tailed student's T test (p=0.0003). (B) Total cellular Cu levels were measured by AAS in the indicated strains. Shown are the results of 4 independent cultures across 2 experimental trials. (C,E) KCN-inhibitable oxygen consumption was measured by a Clark-type electrode in the indicated strains. "+ Cu" and "+BCS" indicates cells cultured and assayed for oxygen consumption in the presence of 50 μM $CuSO_4$ and 400 μM BCS, respectively. Results are from 4-6 cultures across 2-3 experimental trials. (D) 5 μL of a cell solution containing 0.01 and 0.001 OD_{600}/mL of the designated strains were plated on YPGE ("gly + EtOH") or YPD ("glucose") plates. Where indicated, media was supplemented with 100 μM $CuSO_4$. Statistical significance for B,C,E was determined by one-way ANOVA with Tukey posttest; **p≤0.01, ***p≤0.001. The absence of a bracket indicates that comparisons are not significantly different. Strains utilized are as described in Fig. 1. With all the data points, the wide bar reflects the mean value and the standard error of the mean (SEM) is shown with error bars.

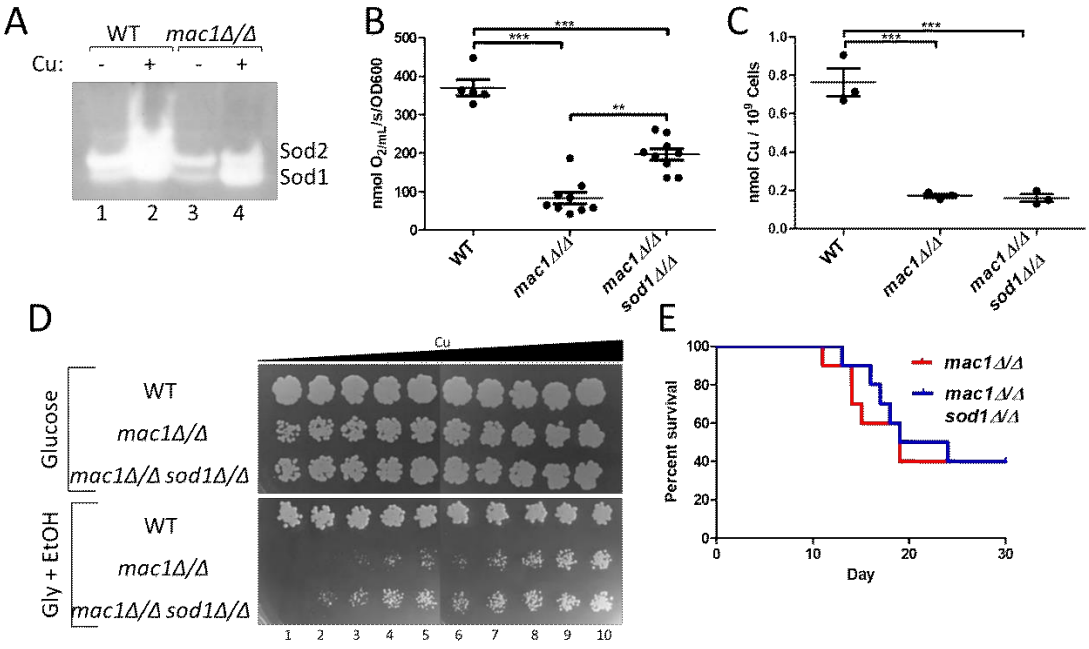

Figure 4-3 Deletion of *SOD1* helps alleviate the respiratory deficiency of the *mac1Δ/Δ* strain. (A) SOD activity was analyzed by the native gel assay as described in *Experimental Procedures.* Shown are results from cells grown in the presence or absence of 1 mM $CuSO_4$. The *mac1*Δ/Δ strain exhibits Sod1 activity even without Cu supplements to the growth media. (B,C) Oxygen consumption (B) and total Cu levels (C) were measured in the indicated strains as described in Fig. 2C and 2B, respectively. Statistical significance was determined by one-way ANOVA with Tukey posttest; **p≤0.01, ***p≤0.001. The absence of a bracket indicates that comparisons are not significantly different. The individual data points represent 5-9 or 3 independent cultures in parts B or C respectively; the wide bar shows the mean and error bars represent SEM. (D) 10 µL of a cell solution containing 0.0005 OD_{600}/mL of the indicated strains in PBS and increasing concentrations of Cu was spotted onto YPD ("glucose") or YPGE ("gly + EtOH"). The cell solutions for columns 2-10 were supplemented with 50 µM, 75 µM, 100 µM, 125 µM, 150 µM, 175 µM, 200 µM, 250 µM¸ and 1000 µM $CuSO_4$, respectively. (E) Shown are survival curves of groups of 10 female mice infected with $2x10^5$ cells of the designated strains. There was no statically significant difference (p=0.51) between female mice infected with *mac1*Δ/Δ and those infected with *mac1Δ/Δ sod1Δ/Δ* strains. Statistical significance of survival curves was determined by the log-rank (Mantel-Cox) test. Strains utilized: WT, SC5314; *mac1*Δ/Δ, EC006; *mac1*Δ/Δ *sod1*Δ/Δ, EC007.

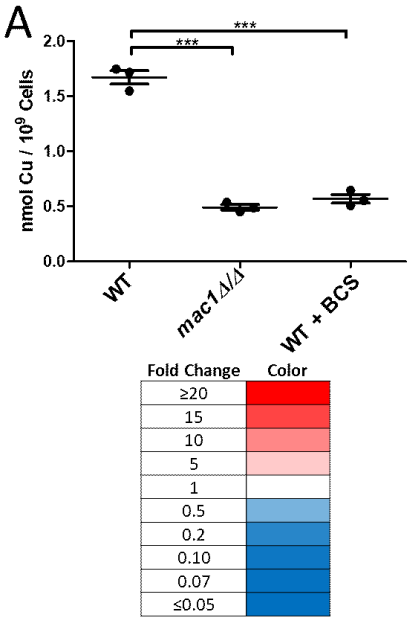

B

Transcript	Wt + BCS	*mac1Δ/Δ*	Sequence	Position
SOD1	0.12	1.42	TTTGCTCA	147
AAH1	0.23	1.22		
FGR23	0.35	1.22		

C

Transcript	Wt + BCS	*mac1Δ/Δ*	Sequence	Position
CTR1	165	0.54	TTTGCTCA	-396
			R-TTTGCTCA	-275
			TTTGCTCA	-237
FRE7	78	0.17	R-CTTGCTCA	-383
			R-TTTGCTCA	-176
			TTTGCTCA	-131
FRE30	70	1.13	TTTGCTCA	-643
			R-TTTGCTCT	-238
			R-ATTGCTCA	-174
SOD3	65	0.20	ATTGCTCA	-153
AOX2	39	3.25	TTTGCTCA	-774
			R-TTTGCTCA	-176
			R-TTTGCTCA	-163
			R-TTTGCTCG	-149
MAC1	6.3	0.06	TTTGCGCA	-167

Figure 4-4 Genes regulated by Cu starvation in a *MAC1*-dependent manner. (A) Intracellular Cu levels are shown for the individual cell samples utilized for RNA-seq analysis (n=3). One-way ANOVA with Tukey posttest was used to determine the statistical significance; ***p≤0.001. The absence of a bracket indicates that comparisons are not significantly different. Within the data points, the bar represents mean with error bars showing the SEM. (B, C) Summary of genes most strongly repressed (B) or induced (C) in WT cells treated with BCS, but not in *mac1Δ/Δ* strains. Comparisons are made to untreated WT control cells. The position and sequence of the Mac1p consensus sites is shown with an “R” designating if they are located on the opposite strand of DNA.

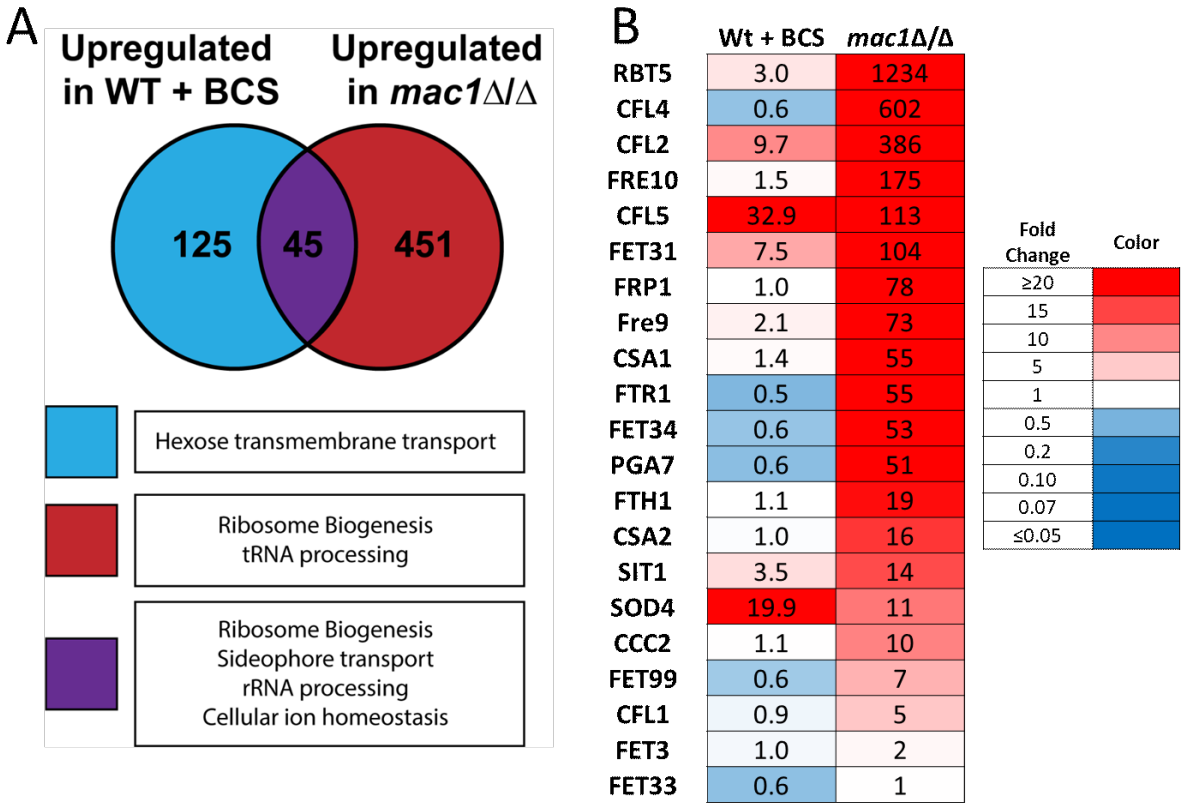

Figure 4-5 Differentially regulated genes by Cu starved WT versus *mac1Δ/Δ* mutants. (A) Shown is a summary of genes upregulated by >3-fold in WT + 400 μM BCS and *mac1Δ/Δ* strains compared to WT untreated control cells. (TOP) Venn diagram shows the total number of genes up-regulated under the two conditions. (BOTTOM) GO analysis shows enrichment of specific gene categories. The genes involved in hexose transmembrane transport were enriched specifically in BCS-treated WT cells with a P-value of 0.00032. Genes associated with ribosome biogenesis and tRNA processing were specifically enriched in *mac1Δ/Δ* cells with P values of 1.99×10^{-75} and 1.68×10^{-8}, respectively. For genes upregulated under both conditions, the GO terms for ribosome biogenesis, siderophore transport, rRNA processing, and cellular ion homeostasis were enriched with P-values of 2.2×10^{-5}, 0.011, 0.026, and 0.096 respectively. (B) Fold change of genes involved in Fe transport are shown for *C. albicans* in WT + BCS and *mac1Δ/Δ* cells compared to untreated WT cells.

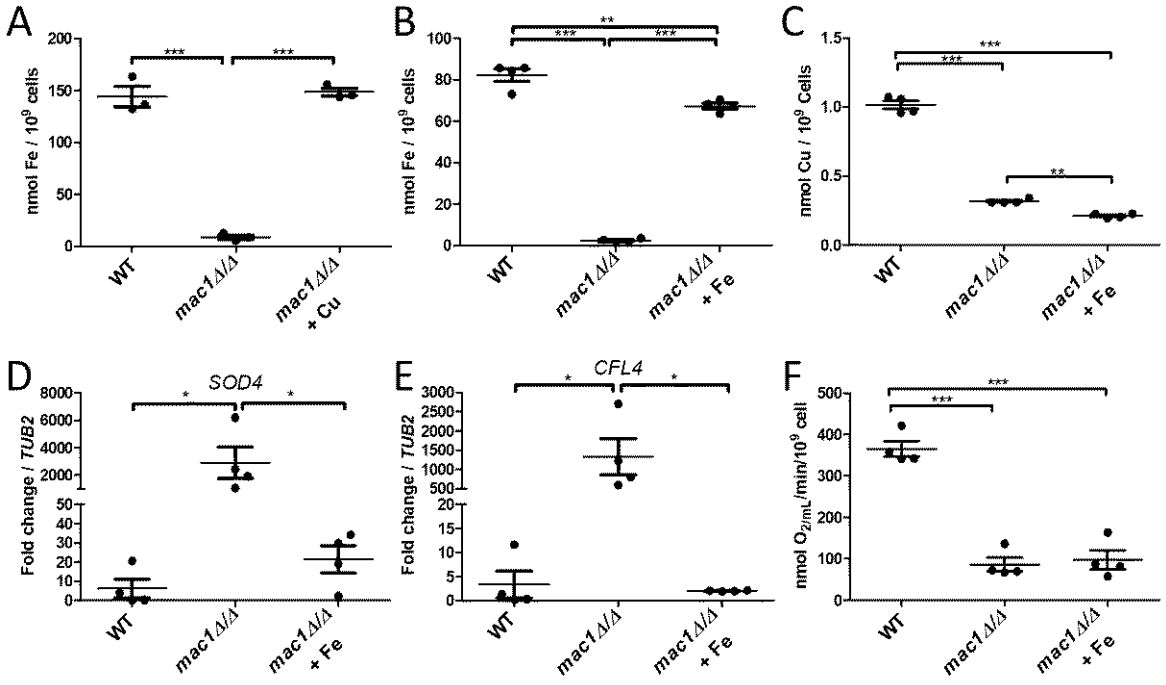

Figure 4-6 *mac1Δ/Δ* mutants are severely starved for Fe. Intracellular levels of Fe (A,B) or of Cu (C) were measured by a colorimetric BPS-based assay or by AAS in the indicated strains as described in *Experimental Procedures*. (D,E) mRNA levels of *SOD4* and *CFL4* was monitored by qRT-PCR in the indicated strains and values normalized to *TUB2*. (F) KCN-inhibitable oxygen consumption was measured as in Fig. 2C. Values are from 3-4 independent cultures over 2 experimental trials. Where designated, cultures were supplemented with either 100 μM $CuSO_4$ ("+ Cu"), 350 μM ferrous ammonium sulfate ("+ Fe") or 400 μM BCS ("+ BCS"). Statistical significance was determined by one-way ANOVA with Tukey posttest; *p≤0.05, **p≤0.01, ***p≤0.001. The absence of a bracket indicates that comparisons are not significantly different. Among the data points, bar represents the mean with error bars showing the SEM. Strains utilized: WT, SC5314; *mac1Δ/Δ,* EC004.

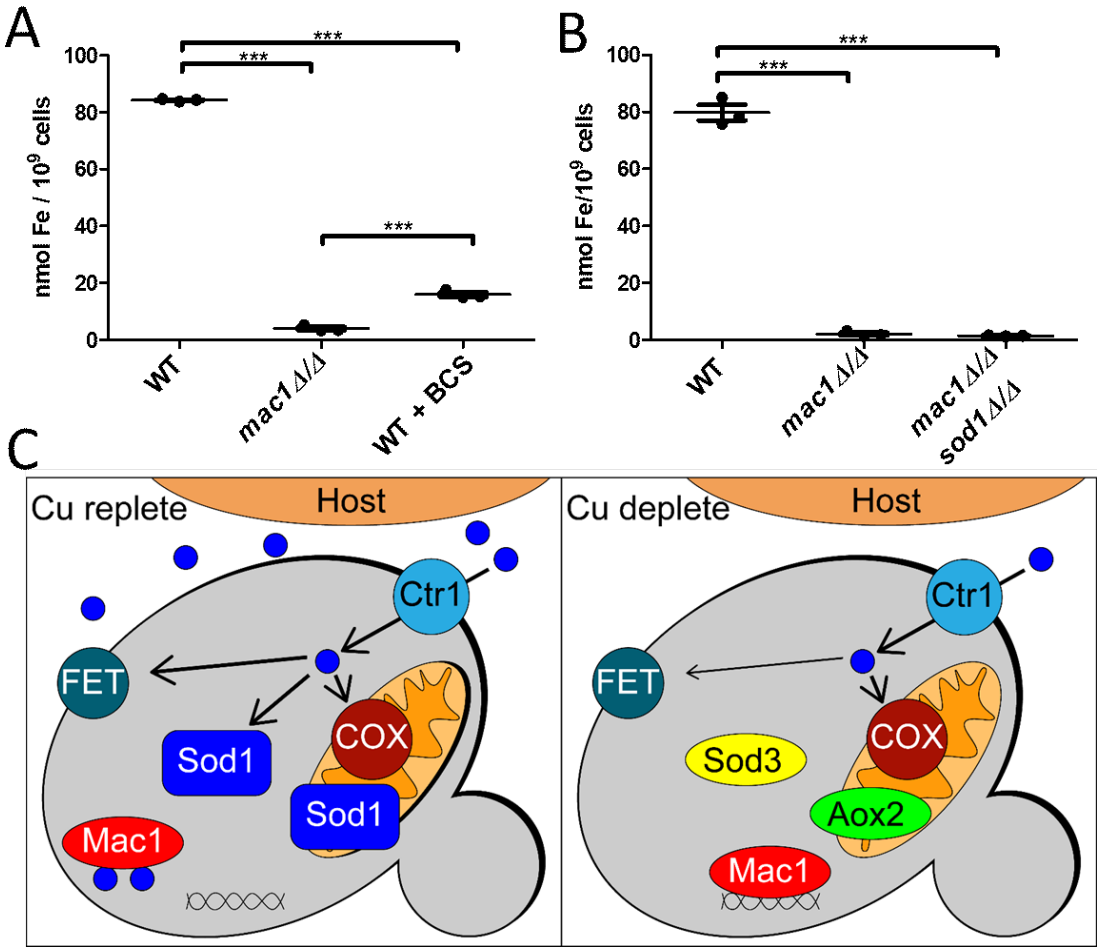

Figure 4-7 The severe Fe deficiency of *mac1Δ/Δ* cells and a proposed model for Mac1p in Cu homeostasis. (A,B) Intracellular Fe concentrations of the indicated strains was measured as in Fig. 6A,B. Statistical significance was determined by one-way ANOVA with Tukey posttest; ***p≤0.001. The absence of a bracket indicates that comparisons are not significantly different. Within the data points representing three independent cultures, wide bar represents mean with error bars showing the SEM. Strains utilized: WT, SC5314; *mac1Δ/Δ,* EC004 (part A) or EC006 (part B); *mac1Δ/Δ sod1Δ/Δ,* EC007. (C) Shown is a model for how *C. albicans* Mac1p regulates Cu homeostasis during infection. In the early stages of kidney infiltration (left), host Cu availability is high and there is sufficient Cu for FET multicopper oxidases for Fe uptake, for Cu/Zn Sod1p and for COX for mitochondrial respiration. At later stages (right), the host limits Cu availability to *C. albicans.* Mac1p is activated and induces Cu import as has been shown for numerous fungi (91,110,120,121,272,310). Additionally, *C. albicans* Mac1p represses *SOD1*, and induces *SOD3* and *AOX2* to maintain ROS homeostasis in the cytosol and mitochondria, respectively. The repression of the major Cu consumer Sod1p serves to maintain high COX respiration in the mitochondria through a Cu sparing mechanism. *C. albicans* Mac1p also helps spare a limited amount of Cu for Fe uptake, through a mechanism that does not involve *SOD1* repression.

Table 4-1 Annotated RNAseq data. Excel file containing the annotated RNA-seq data can be found in this link: Table S4-1

TABLE 4-2 Primers used for Plasmid construction.

Primer Name	Description	Sequence
M1-5L-SacI	*MAC1* -441 to -205 with SacI site for pEC-M1L	GGAGCTCGTTTGACAACTTGCAGAT
M1-5L-NotI	*MAC1* -441 to -205 with NotI site for pEC-M1L	GGCGGCCGCACAAGGGAGGGATCAGGA
M1-5S-SacI	*MAC1* -205 to -1 with SacI site for pEC-M1S	GGAGCTCAGTTTCACCTAACCATTCCC
M1-5S-NotI	*MAC1* -205 to -1 with NotI site for pEC-M1S	GCGGCCGCTCCTTATTCAGTCTTGCTTT
M1-3L-XhoI	*MAC1* 1423 to 1593 with XhoI site for pEC-M1L	GGCTCGAGCCTGCATACAGCACCAAT
M1-3L-KpnI	*MAC1* 1423 to 1593 with KpnI site for pEC-M1L	GGCTCGAGCCTGCATACAGCACCAAT
M1-3S-XhoI	Amplify *MAC1* 1201 to 1419 with XhoI site for pEC-M1S	GGCTCGAGGACAAGAAGGCAACAAAG
M1-3S-KpnI	Amplify *MAC1* 1201 to 1419 with KpnI site for pEC-M1S	GGGTACCTCATAGTTCCAAATACCAC

Table 4-3 Primers used for CRISPR.

Primer	Sequence
Mac1 gDNA	CGTAAACTATTTTTAATTTGAAAGCAAGACTGAATAAGGAGTTTTAGAGCTAGAAATAGC
SOD1 gDNA	CGTAAACTATTTTTAATTTGCAACATATATATAATTAAAAGTTTTAGAGCTAGAAATAGC
MAC1 dDNA F	TCGTACCTTAAGTTAGACTATTTACAAAAATATTTACATATACAGTTCATCCCCTTATTCAGTCTTGCTTTTTGGAGGGGATCTAGTGACATGTAAACAT
MAC1 dDNA R	AGTTTTACATGTCACTAGATCCCCTCCAAAAAGCAAGACTGAATAAGGGGATGAACTGTATATGTAAATATTTTTGTAAATAGTCTAACTTAAGGTACGA
SOD1 dDNA F	TTCTTGGGTTGGATTGTTGATGATGATGGCAATCTTGGCTCATCTATTCCTTTTAATTATATATATGTTGATAATTGAATTGAATTGAATTGATCTTT
SOD1 dDNA R	AAAGATCAATTCAATTCAATTCAATTATCAACATATATATAATTAAAAGGAATAGATGAGCCAAGATTGCCATCATCATCAACAATCCAACCCAAGAA

Table 4-4 Primers used for qRT-PCR reactions.

Primer Name	Sequence	Reference
TUB2 F	GAGTTGGTGATCAATTCAGTGCTAT	(43)
TUB2 R	ATGGCGGCATCTTCTAATGGGATTT	(43)
CFL4 F	CGAGAGTAAAGAGCCGTTGC	(311)
CFL5 R	CATTGCTGGATGACCACAAG	(311)
SOD4 F	CTTGACGAAGGTGACGATACTGCAA	(298)
SOD4 R	TTAAAGCAGCAACAACACCGGCAAT	(298)
CTR1 F	CAAAAGCTCGTGGAACCGGTAAATC	(43)
CTR1 R	TCAGCAACAAATCTTCCAACACCGG	(43)

Future Directions

The research in this thesis focused on trace elements at the host-pathogen interface with an emphasis on the role of Cu during *C. albicans* infection. While these studies have elucidated important information on the role of metals in both the mammalian host and microbial pathogen, many questions remain unanswered. These questions represent exciting new lines of investigations for the future.

Exploring the role of calprotectin mediated toxicity

In Chapter 2, we describe a role calprotectin mediated toxicity that does not involve metal withholding, but rather growth is inhibited by physical interactions with calprotectin and possible hypo osmotic stress. So far, this alternate toxicity strategy has only been observed with the Lyme disease pathogen *Borrelia burgdorferi.* This type of calprotectin-mediated toxicity might occur in other pathogens, or some combination of metal withholding and physical interaction. Calprotectin toxicity in several other bacterial pathogens and in the fungal *Candida albicans* is mediated by metal withholding, so a first step could be to test whether the alternate mechanism involving physical interactions and cell wall stress occurs in the other microbial species (30,198). The basic experimental setup would be similar to Sohnle et. al with some modifications: first cell growth inhibition by calprotectin would be monitored, then this toxicity would be measured in a system where a calprotectin-impermeable membrane would separate calprotectin from the microbe (198). We would be looking for outcomes where direct contact between calprotectin and microbe is required for growth inhibition.

Understanding Cu homeostasis of the host during infection

Work in this thesis provided evidence that ATP7B and ceruloplasmin are not required for kidney Cu loss during infection. What then is the mechanism by which

kidney Cu loss occurs? We were not able to investigate the CTR1 nor the other P-type ATPase in the kidney, ATP7A, as the corresponding genes are both essential and there are currently no kidney specific mouse models available. Mackie et. al. showed that in the *Candida* infected kidney, murine *CTR1* protein levels rise progressively over the course of infection (46). What is the role of CTR1 in this context? As one possibility, CTR1 expression could reflect an approach by the host to limit Cu in the surrounding kidney tissue. Conversely, CTR1 expression might be a response by the kidney cells to local Cu limitation. Careful monitoring of CTR1 mRNA expression, protein levels, and protein localization during infection could begin to unravel the role of CTR1 in the infected kidney. Does CTR1 help execute global kidney Cu loss? Given that CTR1 functions to import Cu into the cytosol, it seems unlikely that CTR1 alone could mediate kidney Cu loss. However, CTR1 could be working with a Cu exporter to affect global kidney Cu levels.

ATP7A is one Cu exporter that remains highly suspect as a driver of kidney Cu loss during infection. Also, ATP7A might have been compensating for ATP7B loss in the ATP7B$^{-/-}$ mice (Chapter 3, Figure 3-5C). A careful investigation of the localization of ATP7A and ATP7B in a WT infected kidney and in an ATP7B$^{-/-}$ kidney could help expand our understanding of how the kidney might be losing Cu. If either were responsible for kidney Cu changes, I would expect them to localize at the plasma membrane. Specifically, I would be monitoring for ATP7B localization to the basolateral membrane (53,54).

As an alternative to the more descriptive studies outlined above, tissue specific knockouts could be used. CTR1 and ATP7A are prime suspects as drivers of kidney Cu loss and so using a kidney specific knockout of these proteins could reveal their role during kidney infection. These experiments would be carried out similar to those in Chapter 3, where *C. albicans* cells would be injected via the lateral tail vein and organs

would be harvested at 0, 24, and 48 hours. We would monitor kidney Cu, *Candida* colony forming units, and fungal mRNA markers to determine if the loss of these transporters affects kidney Cu loss during infection.

Another key finding was that infection with the malaria parasite *Plasmodium berghei* caused kidney Cu loss. This showed that local infection was not necessary for the phenomenon to occur. This begs the question, what range of infecting organisms signal kidney Cu loss? To begin to answer this question, mice could be challenged with gram-negative or gram-positive bacteria, or with sublethal doses of LPS and kidney Cu could be monitored over time. This experiment would first establish if kidney Cu loss could happen in response to bacterial infection, and in response to known PAMPs in the absence of actual infection. If kidney Cu loss did occur, serum cytokines could be analyzed for potential signaling molecules.

Mechanism of Mac1p mediated *SOD1* repression

In Chapter 4 of this thesis the role of Mac1p in *Candida albicans* was explored. However, there are still some outstanding questions. In *Candida* Mac1p functions as a transcriptional activator of all its targets except for *SOD1.* How does Mac1p repress *SOD1*? It is known that *SOD1* has a Mac1p consensus binding site, which is located in intron located at position +148. Mutation of this Mac1p consensus sequence leads to constitutive expression of *SOD1 (43).* One idea is that Mac1p binds to the *SOD1* locus and drives transcription of a nonfunctional transcript in the 3' to 5' direction relative to *SOD1.* Another hypothesis is that Mac1p binds to the *SOD1* intron and sterically hinders RNA polymerase. The precedent for transcriptional activators functioning as repressors, via a "roadblock" mechanism, has been established in *S. cerevisiae* (312). Both of these ideas could be initially tested using qRT-PCR with a number of primers in the 5' region of

SOD1. If Mac1p were to be driving transcription in the 3' to 5' direction then we could expect to observe elevated levels of a transcript involving residues -1 to -50 of *SOD1.* If on the other hand, SOD*1* is constitutively transcribed but RNA polymerase is blocked by Mac1p binding, then we might expect to see an N-terminal transcript of +1 to +100 that is equally abundant in Cu-replete and Cu-deplete conditions. In these experiments a positive result would be informative but a negative one might not be, as it is possible that mRNA decay could hide the results.

An alternative to the PCR based approach mentioned above would be a Mac1p chromatin immunoprecipitation (ChIP) followed by either qRT-PCR or sequencing. To date, an antibody for *C. albicans* Mac1p does not exist and so one would have to be generated. Ideally, recombinant Mac1p would be expressed and purified in *E. coli* and used to generate a polyclonal antibody. However if efforts to purify recombinant Mac1p failed, a *MAC1* construct could be expressed in *C. albicans* cells with a non-native tag, such as Myc or GFP, similar to what has been done in *S. cerevisiae* (93).Use of a tagged Mac1p avoids the generation of an antibody but would still need to be validated to ensure that the tag does not affect its function or regulation.

Further investigating the role of *Candida albicans* Mac1p in transition metal homeostasis

In an RNA-seq experiment detailed in Chapter 4 of this work, we observed a number of differentially regulated transcripts caused by deletion of Mac1p. Our work and Khemiri et. al. show that a number of Fe related genes as well as new Mac1 targets are upregulated (280). However, to-date no group has observed direct binding of Mac1p to its targets on a large, unbiased scale. We suggest investigating the targets of Mac1p via ChIP-seq to both validate current Mac1p annotated targets as well as potentially

discover new targets. As above, a Mac1p antibody must first be generated and validated before this experiment could be executed.

References

1. Zackular, J. P., Chazin, W. J., and Skaar, E. P. (2015) Nutritional Immunity: S100 Proteins at the Host-Pathogen Interface. *J Biol Chem* **290**, 18991-18998
2. Zygiel, E. M., and Nolan, E. M. (2018) Transition Metal Sequestration by the Host-Defense Protein Calprotectin. *Annu Rev Biochem* **87**, 621-643
3. Nunez, G., Sakamoto, K., and Soares, M. P. (2018) Innate Nutritional Immunity. *J Immunol* **201**, 11-18
4. Weinberg, E. D. (1975) Nutritional immunity. Host's attempt to withold iron from microbial invaders. *JAMA* **231**, 39-41
5. Neale, F. C. (1955) The demonstration of the iron-binding globulin (transferrin) in serum and urine proteins by use of 59Fe combined with paper electrophoresis. *J Clin Pathol* **8**, 334-337
6. Roeser, H. P., Lee, G. R., Nacht, S., and Cartwright, G. E. (1970) The role of ceruloplasmin in iron metabolism. *J Clin Invest* **49**, 2408-2417
7. Nittis, T., and Gitlin, J. D. (2002) The copper-iron connection: hereditary aceruloplasminemia. *Semin Hematol* **39**, 282-289
8. Harris, Z. L., Durley, A. P., Man, T. K., and Gitlin, J. D. (1999) Targeted gene disruption reveals an essential role for ceruloplasmin in cellular iron efflux. *Proc Natl Acad Sci U S A* **96**, 10812-10817
9. Abboud, S., and Haile, D. J. (2000) A novel mammalian iron-regulated protein involved in intracellular iron metabolism. *J Biol Chem* **275**, 19906-19912
10. Donovan, A., Brownlie, A., Zhou, Y., Shepard, J., Pratt, S. J., Moynihan, J., Paw, B. H., Drejer, A., Barut, B., Zapata, A., Law, T. C., Brugnara, C., Lux, S. E., Pinkus, G. S., Pinkus, J. L., Kingsley, P. D., Palis, J., Fleming, M. D., Andrews, N. C., and Zon, L. I. (2000) Positional cloning of zebrafish ferroportin1 identifies a conserved vertebrate iron exporter. *Nature* **403**, 776-781
11. McKie, A. T., Marciani, P., Rolfs, A., Brennan, K., Wehr, K., Barrow, D., Miret, S., Bomford, A., Peters, T. J., Farzaneh, F., Hediger, M. A., Hentze, M. W., and Simpson, R. J. (2000) A novel duodenal iron-regulated transporter, IREG1, implicated in the basolateral transfer of iron to the circulation. *Mol Cell* **5**, 299-309
12. Shike, H., Lauth, X., Westerman, M. E., Ostland, V. E., Carlberg, J. M., Van Olst, J. C., Shimizu, C., Bulet, P., and Burns, J. C. (2002) Bass hepcidin is a novel antimicrobial peptide induced by bacterial challenge. *Eur J Biochem* **269**, 2232-2237
13. Nicolas, G., Chauvet, C., Viatte, L., Danan, J. L., Bigard, X., Devaux, I., Beaumont, C., Kahn, A., and Vaulont, S. (2002) The gene encoding the iron regulatory peptide hepcidin is regulated by anemia, hypoxia, and inflammation. *J Clin Invest* **110**, 1037-1044
14. Nemeth, E., Valore, E. V., Territo, M., Schiller, G., Lichtenstein, A., and Ganz, T. (2003) Hepcidin, a putative mediator of anemia of inflammation, is a type II acute-phase protein. *Blood* **101**, 2461-2463
15. Nemeth, E., Tuttle, M. S., Powelson, J., Vaughn, M. B., Donovan, A., Ward, D. M., Ganz, T., and Kaplan, J. (2004) Hepcidin regulates cellular iron efflux by binding to ferroportin and inducing its internalization. *Science* **306**, 2090-2093
16. Cartwright, G. E., and Wintrobe, M. M. (1952) The anemia of infection. XVII. A review. *Adv Intern Med* **5**, 165-226

17. Fraenkel, P. G. (2017) Anemia of Inflammation: A Review. *Med Clin North Am* **101**, 285-296
18. Cassat, J. E., and Skaar, E. P. (2013) Iron in infection and immunity. *Cell Host Microbe* **13**, 509-519
19. Goldstein, I. M., Kaplan, H. B., Edelson, H. S., and Weissmann, G. (1979) A new function for ceruloplasmin as an acute-phase reactant in inflammation: a scavenger of superoxide anion radicals. *Trans Assoc Am Physicians* **92**, 360-369
20. Dale, I., Fagerhol, M. K., and Naesgaard, I. (1983) Purification and partial characterization of a highly immunogenic human leukocyte protein, the L1 antigen. *Eur J Biochem* **134**, 1-6
21. Steinbakk, M., Naess-Andresen, C. F., Lingaas, E., Dale, I., Brandtzaeg, P., and Fagerhol, M. K. (1990) Antimicrobial actions of calcium binding leucocyte L1 protein, calprotectin. *Lancet* **336**, 763-765
22. Brandtzaeg, P., Dale, I., and Fagerhol, M. K. (1987) Distribution of a formalin-resistant myelomonocytic antigen (L1) in human tissues. II. Normal and aberrant occurrence in various epithelia. *Am J Clin Pathol* **87**, 700-707
23. Johne, B., Fagerhol, M. K., Lyberg, T., Prydz, H., Brandtzaeg, P., Naess-Andresen, C. F., and Dale, I. (1997) Functional and clinical aspects of the myelomonocyte protein calprotectin. *Mol Pathol* **50**, 113-123
24. Dale, I., Brandtzaeg, P., Fagerhol, M. K., and Scott, H. (1985) Distribution of a new myelomonocytic antigen (L1) in human peripheral blood leukocytes. Immunofluorescence and immunoperoxidase staining features in comparison with lysozyme and lactoferrin. *Am J Clin Pathol* **84**, 24-34
25. Teigelkamp, S., Bhardwaj, R. S., Roth, J., Meinardus-Hager, G., Karas, M., and Sorg, C. (1991) Calcium-dependent complex assembly of the myeloic differentiation proteins MRP-8 and MRP-14. *J Biol Chem* **266**, 13462-13467
26. Brophy, M. B., Hayden, J. A., and Nolan, E. M. (2012) Calcium ion gradients modulate the zinc affinity and antibacterial activity of human calprotectin. *J Am Chem Soc* **134**, 18089-18100
27. Brophy, M. B., Nakashige, T. G., Gaillard, A., and Nolan, E. M. (2013) Contributions of the S100A9 C-terminal tail to high-affinity Mn(II) chelation by the host-defense protein human calprotectin. *J Am Chem Soc* **135**, 17804-17817
28. Wang, J., Lonergan, Z. R., Gonzalez-Gutierrez, G., Nairn, B. L., Maxwell, C. N., Zhang, Y., Andreini, C., Karty, J. A., Chazin, W. J., Trinidad, J. C., Skaar, E. P., and Giedroc, D. P. (2019) Multi-metal Restriction by Calprotectin Impacts De Novo Flavin Biosynthesis in Acinetobacter baumannii. *Cell Chem Biol* **26**, 745-755 e747
29. Corbin, B. D., Seeley, E. H., Raab, A., Feldmann, J., Miller, M. R., Torres, V. J., Anderson, K. L., Dattilo, B. M., Dunman, P. M., Gerads, R., Caprioli, R. M., Nacken, W., Chazin, W. J., and Skaar, E. P. (2008) Metal chelation and inhibition of bacterial growth in tissue abscesses. *Science* **319**, 962-965
30. Besold, A. N., Gilston, B. A., Radin, J. N., Ramsoomair, C., Culbertson, E. M., Li, C. X., Cormack, B. P., Chazin, W. J., Kehl-Fie, T. E., and Culotta, V. C. (2018) Role of Calprotectin in Withholding Zinc and Copper from Candida albicans. *Infect Immun* **86**
31. Macomber, L., and Imlay, J. A. (2009) The iron-sulfur clusters of dehydratases are primary intracellular targets of copper toxicity. *Proc Natl Acad Sci U S A* **106**, 8344-8349
32. Wagner, D., Maser, J., Lai, B., Cai, Z. H., Barry, C. E., Bentrup, K. H. Z., Russell, D. G., and Bermudez, L. E. (2005) Elemental analysis of Mycobacterium avium-, Mycobacterium tuberculosis-, and Mycobacterium smegmatis-containing phagosomes indicates

pathogen-induced microenvironments within the host cell's endosomal system. *Journal of Immunology* **174**, 1491-1500
33. White, C., Lee, J., Kambe, T., Fritsche, K., and Petris, M. J. (2009) A Role for the ATP7A Copper-transporting ATPase in Macrophage Bactericidal Activity. *Journal of Biological Chemistry* **284**, 33949-33956
34. Osman, D., Waldron, K. J., Denton, H., Taylor, C. M., Grant, A. J., Mastroeni, P., Robinson, N. J., and Cavet, J. S. (2010) Copper homeostasis in Salmonella is atypical and copper-CueP is a major periplasmic metal complex. *J Biol Chem* **285**, 25259-25268
35. Shafeeq, S., Yesilkaya, H., Kloosterman, T. G., Narayanan, G., Wandel, M., Andrew, P. W., Kuipers, O. P., and Morrissey, J. A. (2011) The cop operon is required for copper homeostasis and contributes to virulence in Streptococcus pneumoniae. *Mol Microbiol* **81**, 1255-1270
36. Johnson, M. D., Kehl-Fie, T. E., Klein, R., Kelly, J., Burnham, C., Mann, B., and Rosch, J. W. (2015) Role of copper efflux in pneumococcal pathogenesis and resistance to macrophage-mediated immune clearance. *Infect Immun* **83**, 1684-1694
37. Achard, M. E., Stafford, S. L., Bokil, N. J., Chartres, J., Bernhardt, P. V., Schembri, M. A., Sweet, M. J., and McEwan, A. G. (2012) Copper redistribution in murine macrophages in response to Salmonella infection. *Biochem J* **444**, 51-57
38. Ladomersky, E., Khan, A., Shanbhag, V., Cavet, J. S., Chan, J., Weisman, G. A., and Petris, M. J. (2017) Host and Pathogen Copper-Transporting P-Type ATPases Function Antagonistically during Salmonella Infection. *Infect Immun* **85**
39. Smith, A. T., Smith, K. P., and Rosenzweig, A. C. (2014) Diversity of the metal-transporting P1B-type ATPases. *J Biol Inorg Chem* **19**, 947-960
40. Solioz, M., Abicht, H. K., Mermod, M., and Mancini, S. (2010) Response of gram-positive bacteria to copper stress. *J Biol Inorg Chem* **15**, 3-14
41. Rensing, C., and McDevitt, S. F. (2013) The copper metallome in prokaryotic cells. *Met Ions Life Sci* **12**, 417-450
42. Nies, D. H., and Herzberg, M. (2013) A fresh view of the cell biology of copper in enterobacteria. *Mol Microbiol* **87**, 447-454
43. Li, C. X., Gleason, J. E., Zhang, S. X., Bruno, V. M., Cormack, B. P., and Culotta, V. C. (2015) Candida albicans adapts to host copper during infection by swapping metal cofactors for superoxide dismutase. *Proc Natl Acad Sci U S A*
44. Shen, Q., Beucler, M. J., Ray, S. C., and Rappleye, C. A. (2018) Macrophage activation by IFN-gamma triggers restriction of phagosomal copper from intracellular pathogens. *PLoS Pathog* **14**, e1007444
45. Park, Y. S., Kim, T. H., and Yun, C. W. (2017) Functional characterization of the copper transcription factor AfMac1 from Aspergillus fumigatus. *Biochem J* **474**, 2365-2378
46. Mackie, J., Szabo, E. K., Urgast, D. S., Ballou, E. R., Childers, D. S., MacCallum, D. M., Feldmann, J., and Brown, A. J. (2016) Host-Imposed Copper Poisoning Impacts Fungal Micronutrient Acquisition during Systemic Candida albicans Infections. *PLoS One* **11**, e0158683
47. Waterman, S. R., Hacham, M., Hu, G., Zhu, X., Park, Y. D., Shin, S., Panepinto, J., Valyi-Nagy, T., Beam, C., Husain, S., Singh, N., and Williamson, P. R. (2007) Role of a CUF1/CTR4 copper regulatory axis in the virulence of Cryptococcus neoformans. *J Clin Invest* **117**, 794-802
48. Waterman, S. R., Park, Y. D., Raja, M., Qiu, J., Hammoud, D. A., O'Halloran, T. V., and Williamson, P. R. (2012) Role of CTR4 in the Virulence of Cryptococcus neoformans. *Mbio* **3**

49. Garcia-Santamarina, S., Probst, C., Festa, R. A., Ding, C., Smith, A. D., Conklin, S. E., Brander, S., Kinch, L. N., Grishin, N. V., Franz, K. J., Riggs-Gelasco, P., Lo Leggio, L., Johansen, K. S., and Thiele, D. J. (2020) A lytic polysaccharide monooxygenase-like protein functions in fungal copper import and meningitis. *Nat Chem Biol* **16**, 337-344
50. Sun, T. S., Ju, X., Gao, H. L., Wang, T., Thiele, D. J., Li, J. Y., Wang, Z. Y., and Ding, C. (2014) Reciprocal functions of Cryptococcus neoformans copper homeostasis machinery during pulmonary infection and meningoencephalitis. *Nature Communications* **5**
51. Lee, J., Petris, M. J., and Thiele, D. J. (2002) Characterization of mouse embryonic cells deficient in the ctr1 high affinity copper transporter. Identification of a Ctr1-independent copper transport system. *J Biol Chem* **277**, 40253-40259
52. La Fontaine, S., and Mercer, J. F. (2007) Trafficking of the copper-ATPases, ATP7A and ATP7B: role in copper homeostasis. *Arch Biochem Biophys* **463**, 149-167
53. Linz, R., Barnes, N. L., Zimnicka, A. M., Kaplan, J. H., Eipper, B., and Lutsenko, S. (2008) Intracellular targeting of copper-transporting ATPase ATP7A in a normal and Atp7b-/- kidney. *Am J Physiol Renal Physiol* **294**, F53-61
54. Lutsenko, S., Barnes, N. L., Bartee, M. Y., and Dmitriev, O. Y. (2007) Function and regulation of human copper-transporting ATPases. *Physiol Rev* **87**, 1011-1046
55. Kuo, Y. M., Gitschier, J., and Packman, S. (1997) Developmental expression of the mouse mottled and toxic milk genes suggests distinct functions for the Menkes and Wilson disease copper transporters. *Hum Mol Genet* **6**, 1043-1049
56. Michalczyk, A., Bastow, E., Greenough, M., Camakaris, J., Freestone, D., Taylor, P., Linder, M., Mercer, J., and Ackland, M. L. (2008) ATP7B expression in human breast epithelial cells is mediated by lactational hormones. *J Histochem Cytochem* **56**, 389-399
57. Bull, P. C., Thomas, G. R., Rommens, J. M., Forbes, J. R., and Cox, D. W. (1993) The Wilson disease gene is a putative copper transporting P-type ATPase similar to the Menkes gene. *Nat Genet* **5**, 327-337
58. Tanzi, R. E., Petrukhin, K., Chernov, I., Pellequer, J. L., Wasco, W., Ross, B., Romano, D. M., Parano, E., Pavone, L., Brzustowicz, L. M., and et al. (1993) The Wilson disease gene is a copper transporting ATPase with homology to the Menkes disease gene. *Nat Genet* **5**, 344-350
59. Terada, K., Nakako, T., Yang, X. L., Iida, M., Aiba, N., Minamiya, Y., Nakai, M., Sakaki, T., Miura, N., and Sugiyama, T. (1998) Restoration of holoceruloplasmin synthesis in LEC rat after infusion of recombinant adenovirus bearing WND cDNA. *J Biol Chem* **273**, 1815-1820
60. Terada, K., Aiba, N., Yang, X. L., Iida, M., Nakai, M., Miura, N., and Sugiyama, T. (1999) Biliary excretion of copper in LEC rat after introduction of copper transporting P-type ATPase, ATP7B. *FEBS Lett* **448**, 53-56
61. Gleason, J. E., Galaleldeen, A., Peterson, R. L., Taylor, A. B., Holloway, S. P., Waninger-Saroni, J., Cormack, B. P., Cabelli, D. E., Hart, P. J., and Culotta, V. C. (2014) Candida albicans SOD5 represents the prototype of an unprecedented class of Cu-only superoxide dismutases required for pathogen defense. *Proc Natl Acad Sci U S A* **111**, 5866-5871
62. Sturtz, L. A., Diekert, K., Jensen, L. T., Lill, R., and Culotta, V. C. (2001) A fraction of yeast Cu,Zn-superoxide dismutase and its metallochaperone, CCS, localize to the intermembrane space of mitochondria. A physiological role for SOD1 in guarding against mitochondrial oxidative damage. *J Biol Chem* **276**, 38084-38089
63. Narasipura, S. D., Ault, J. G., Behr, M. J., Chaturvedi, V., and Chaturvedi, S. (2003) Characterization of Cu,Zn superoxide dismutase (SOD1) gene knock-out mutant of

Cryptococcus neoformans var. gattii: role in biology and virulence. *Mol Microbiol* **47**, 1681-1694
64. Hwang, C. S., Rhie, G. E., Oh, J. H., Huh, W. K., Yim, H. S., and Kang, S. O. (2002) Copper- and zinc-containing superoxide dismutase (Cu/ZnSOD) is required for the protection of Candida albicans against oxidative stresses and the expression of its full virulence. *Microbiology-Sgm* **148**, 3705-3713
65. Cox, G. M., Harrison, T. S., McDade, H. C., Taborda, C. P., Heinrich, G., Casadevall, A., and Perfect, J. R. (2003) Superoxide dismutase influences the virulence of Cryptococcus neoformans by affecting growth within macrophages. *Infect Immun* **71**, 173-180
66. Tsang, C. K., Liu, Y., Thomas, J., Zhang, Y., and Zheng, X. F. (2014) Superoxide dismutase 1 acts as a nuclear transcription factor to regulate oxidative stress resistance. *Nat Commun* **5**, 3446
67. Reddi, A. R., and Culotta, V. C. (2013) SOD1 integrates signals from oxygen and glucose to repress respiration. *Cell* **152**, 224-235
68. Broxton, C. N., He, B., Bruno, V. M., and Culotta, V. C. (2018) A role for Candida albicans superoxide dismutase enzymes in glucose signaling. *Biochem Biophys Res Commun* **495**, 814-820
69. Bedard, K., Lardy, B., and Krause, K. H. (2007) NOX family NADPH oxidases: not just in mammals. *Biochimie* **89**, 1107-1112
70. Takemoto, D., Tanaka, A., and Scott, B. (2007) NADPH oxidases in fungi: diverse roles of reactive oxygen species in fungal cellular differentiation. *Fungal Genet Biol* **44**, 1065-1076
71. Bedard, K., and Krause, K. H. (2007) The NOX family of ROS-generating NADPH oxidases: physiology and pathophysiology. *Physiol Rev* **87**, 245-313
72. Abreu, I. A., and Cabelli, D. E. (2010) Superoxide dismutases-a review of the metal-associated mechanistic variations. *Biochim Biophys Acta* **1804**, 263-274
73. St-Pierre, J., Buckingham, J. A., Roebuck, S. J., and Brand, M. D. (2002) Topology of superoxide production from different sites in the mitochondrial electron transport chain. *J Biol Chem* **277**, 44784-44790
74. Han, D., Canali, R., Rettori, D., and Kaplowitz, N. (2003) Effect of glutathione depletion on sites and topology of superoxide and hydrogen peroxide production in mitochondria. *Mol Pharmacol* **64**, 1136-1144
75. Liu, Y., Fiskum, G., and Schubert, D. (2002) Generation of reactive oxygen species by the mitochondrial electron transport chain. *J Neurochem* **80**, 780-787
76. Liu, Z., Thornton, J., Spirek, M., and Butow, R. A. (2008) Activation of the SPS amino acid-sensing pathway in Saccharomyces cerevisiae correlates with the phosphorylation state of a sensor component, Ptr3. *Mol Cell Biol* **28**, 551-563
77. Wood, L. K., and Thiele, D. J. (2009) Transcriptional activation in yeast in response to copper deficiency involves copper-zinc superoxide dismutase. *J Biol Chem* **284**, 404-413
78. Geier, B. M., Schagger, H., Ortwein, C., Link, T. A., Hagen, W. R., Brandt, U., and Von Jagow, G. (1995) Kinetic properties and ligand binding of the eleven-subunit cytochrome-c oxidase from Saccharomyces cerevisiae isolated with a novel large-scale purification method. *Eur J Biochem* **227**, 296-302
79. Rich, P. R., and Marechal, A. (2010) The mitochondrial respiratory chain. *Essays Biochem* **47**, 1-23
80. Aoki, S., Ito-Kuwa, S., Nakamura, Y., and Masuhara, T. (1990) Comparative pathogenicity of a wild-type strain and respiratory mutants of Candida albicans in mice. *Zentralbl Bakteriol* **273**, 332-343

81. Grahl, N., Dinamarco, T. M., Willger, S. D., Goldman, G. H., and Cramer, R. A. (2012) Aspergillus fumigatus mitochondrial electron transport chain mediates oxidative stress homeostasis, hypoxia responses and fungal pathogenesis. *Mol Microbiol* **84**, 383-399
82. Dancis, A., Klausner, R. D., Hinnebusch, A. G., and Barriocanal, J. G. (1990) Genetic evidence that ferric reductase is required for iron uptake in Saccharomyces cerevisiae. *Mol Cell Biol* **10**, 2294-2301
83. De Luca, N. G., and Wood, P. M. (2000) Iron uptake by fungi: contrasted mechanisms with internal or external reduction. *Adv Microb Physiol* **43**, 39-74
84. Kosman, D. J. (2003) Molecular mechanisms of iron uptake in fungi. *Mol Microbiol* **47**, 1185-1197
85. Almeida, R. S., Wilson, D., and Hube, B. (2009) Candida albicans iron acquisition within the host. *FEMS Yeast Res* **9**, 1000-1012
86. Kosman, D. J. (2018) The teleos of metallo-reduction and metallo-oxidation in eukaryotic iron and copper trafficking. *Metallomics* **10**, 370-377
87. Dancis, A. (1998) Genetic analysis of iron uptake in the yeast Saccharomyces cerevisiae. *J Pediatr* **132**, S24-29
88. Keller, G., Bird, A., and Winge, D. R. (2005) Independent metalloregulation of Ace1 and Mac1 in Saccharomyces cerevisiae. *Eukaryot Cell* **4**, 1863-1871
89. Thiele, D. J. (1988) ACE1 regulates expression of the Saccharomyces cerevisiae metallothionein gene. *Mol Cell Biol* **8**, 2745-2752
90. Furst, P., and Hamer, D. (1989) Cooperative activation of a eukaryotic transcription factor: interaction between Cu(I) and yeast ACE1 protein. *Proc Natl Acad Sci U S A* **86**, 5267-5271
91. Jungmann, J., Reins, H. A., Lee, J., Romeo, A., Hassett, R., Kosman, D., and Jentsch, S. (1993) MAC1, a nuclear regulatory protein related to Cu-dependent transcription factors is involved in Cu/Fe utilization and stress resistance in yeast. *EMBO J* **12**, 5051-5056
92. Jensen, L. T., Posewitz, M. C., Srinivasan, C., and Winge, D. R. (1998) Mapping of the DNA binding domain of the copper-responsive transcription factor Mac1 from Saccharomyces cerevisiae. *J Biol Chem* **273**, 23805-23811
93. Jensen, L. T., and Winge, D. R. (1998) Identification of a copper-induced intramolecular interaction in the transcription factor Mac1 from Saccharomyces cerevisiae. *EMBO J* **17**, 5400-5408
94. Graden, J. A., and Winge, D. R. (1997) Copper-mediated repression of the activation domain in the yeast Mac1p transcription factor. *Proc Natl Acad Sci U S A* **94**, 5550-5555
95. Labbe, S., Zhu, Z., and Thiele, D. J. (1997) Copper-specific transcriptional repression of yeast genes encoding critical components in the copper transport pathway. *J Biol Chem* **272**, 15951-15958
96. van Bakel, H., Strengman, E., Wijmenga, C., and Holstege, F. C. (2005) Gene expression profiling and phenotype analyses of S. cerevisiae in response to changing copper reveals six genes with new roles in copper and iron metabolism. *Physiol Genomics* **22**, 356-367
97. Rajasingham, R., Smith, R. M., Park, B. J., Jarvis, J. N., Govender, N. P., Chiller, T. M., Denning, D. W., Loyse, A., and Boulware, D. R. (2017) Global burden of disease of HIV-associated cryptococcal meningitis: an updated analysis. *Lancet Infect Dis* **17**, 873-881
98. Sabiiti, W., and May, R. C. (2012) Mechanisms of infection by the human fungal pathogen Cryptococcus neoformans. *Future Microbiol* **7**, 1297-1313
99. Chuck, S. L., and Sande, M. A. (1989) Infections with Cryptococcus neoformans in the acquired immunodeficiency syndrome. *N Engl J Med* **321**, 794-799

100. Kovacs, J. A., Kovacs, A. A., Polis, M., Wright, W. C., Gill, V. J., Tuazon, C. U., Gelmann, E. P., Lane, H. C., Longfield, R., Overturf, G., and et al. (1985) Cryptococcosis in the acquired immunodeficiency syndrome. *Ann Intern Med* **103**, 533-538
101. Zhu, X., and Williamson, P. R. (2004) Role of laccase in the biology and virulence of Cryptococcus neoformans. *FEMS Yeast Res* **5**, 1-10
102. McClelland, E. E., Bernhardt, P., and Casadevall, A. (2006) Estimating the relative contributions of virulence factors for pathogenic microbes. *Infect Immun* **74**, 1500-1504
103. Torres-Guererro, H., and Edman, J. C. (1994) Melanin-deficient mutants of Cryptococcus neoformans. *J Med Vet Mycol* **32**, 303-313
104. Ding, C., Yin, J., Tovar, E. M., Fitzpatrick, D. A., Higgins, D. G., and Thiele, D. J. (2011) The copper regulon of the human fungal pathogen Cryptococcus neoformans H99. *Mol Microbiol* **81**, 1560-1576
105. Garcia-Santamarina, S., Festa, R. A., Smith, A. D., Yu, C. H., Probst, C., Ding, C., Homer, C. M., Yin, J., Noonan, J. P., Madhani, H., Perfect, J. R., and Thiele, D. J. (2018) Genome-wide analysis of the regulation of Cu metabolism in Cryptococcus neoformans. *Mol Microbiol* **108**, 473-494
106. Ding, C., Festa, R. A., Chen, Y. L., Espart, A., Palacios, O., Espin, J., Capdevila, M., Atrian, S., Heitman, J., and Thiele, D. J. (2013) Cryptococcus neoformans copper detoxification machinery is critical for fungal virulence. *Cell Host Microbe* **13**, 265-276
107. Liu, T. B., Perlin, D. S., and Xue, C. (2012) Molecular mechanisms of cryptococcal meningitis. *Virulence* **3**, 173-181
108. Benedict, K., Jackson, B. R., Chiller, T., and Beer, K. D. (2019) Estimation of Direct Healthcare Costs of Fungal Diseases in the United States. *Clin Infect Dis* **68**, 1791-1797
109. Latge, J. P., and Chamilos, G. (2019) Aspergillus fumigatus and Aspergillosis in 2019. *Clin Microbiol Rev* **33**
110. Kusuya, Y., Hagiwara, D., Sakai, K., Yaguchi, T., Gonoi, T., and Takahashi, H. (2017) Transcription factor Afmac1 controls copper import machinery in Aspergillus fumigatus. *Curr Genet* **63**, 777-789
111. Cai, Z., Du, W., Zeng, Q., Long, N., Dai, C., and Lu, L. (2017) Cu-sensing transcription factor Mac1 coordinates with the Ctr transporter family to regulate Cu acquisition and virulence in Aspergillus fumigatus. *Fungal Genet Biol* **107**, 31-43
112. Wiemann, P., Perevitsky, A., Lim, F. Y., Shadkchan, Y., Knox, B. P., Landero Figueora, J. A., Choera, T., Niu, M., Steinberger, A. J., Wuthrich, M., Idol, R. A., Klein, B. S., Dinauer, M. C., Huttenlocher, A., Osherov, N., and Keller, N. P. (2017) Aspergillus fumigatus Copper Export Machinery and Reactive Oxygen Intermediate Defense Counter Host Copper-Mediated Oxidative Antimicrobial Offense. *Cell Rep* **19**, 2174-2176
113. Park, Y. S., Kang, S., Seo, H., and Yun, C. W. (2018) A copper transcription factor, AfMac1, regulates both iron and copper homeostasis in the opportunistic fungal pathogen Aspergillus fumigatus. *Biochem J* **475**, 2831-2845
114. Lewis, R. E., Cahyame-Zuniga, L., Leventakos, K., Chamilos, G., Ben-Ami, R., Tamboli, P., Tarrand, J., Bodey, G. P., Luna, M., and Kontoyiannis, D. P. (2013) Epidemiology and sites of involvement of invasive fungal infections in patients with haematological malignancies: a 20-year autopsy study. *Mycoses* **56**, 638-645
115. Wachtler, B., Citiulo, F., Jablonowski, N., Forster, S., Dalle, F., Schaller, M., Wilson, D., and Hube, B. (2012) Candida albicans-epithelial interactions: dissecting the roles of active penetration, induced endocytosis and host factors on the infection process. *PLoS One* **7**, e36952

116. Tsay, S. V., Mu, Y., Williams, S., Epson, E., Nadle, J., Bamberg, W. M., Barter, D. M., Johnston, H. L., Farley, M. M., Harb, S., Thomas, S., Bonner, L. A., Harrison, L. H., Hollick, R., Marceaux, K., Mody, R. K., Pattee, B., Shrum Davis, S., Phipps, E. C., Tesini, B. L., Gellert, A. B., Zhang, A. Y., Schaffner, W., Hillis, S., Ndi, D., Graber, C. R., Jackson, B. R., Chiller, T., Magill, S., and Vallabhaneni, S. (2020) Burden of Candidemia in the United States, 2017. *Clin Infect Dis*
117. Cleveland, A. A., Harrison, L. H., Farley, M. M., Hollick, R., Stein, B., Chiller, T. M., Lockhart, S. R., and Park, B. J. (2015) Declining incidence of candidemia and the shifting epidemiology of Candida resistance in two US metropolitan areas, 2008-2013: results from population-based surveillance. *PLoS One* **10**, e0120452
118. Lockhart, S. R., Iqbal, N., Cleveland, A. A., Farley, M. M., Harrison, L. H., Bolden, C. B., Baughman, W., Stein, B., Hollick, R., Park, B. J., and Chiller, T. (2012) Species identification and antifungal susceptibility testing of Candida bloodstream isolates from population-based surveillance studies in two U.S. cities from 2008 to 2011. *J Clin Microbiol* **50**, 3435-3442
119. Morgan, J., Meltzer, M. I., Plikaytis, B. D., Sofair, A. N., Huie-White, S., Wilcox, S., Harrison, L. H., Seaberg, E. C., Hajjeh, R. A., and Teutsch, S. M. (2005) Excess mortality, hospital stay, and cost due to candidemia: a case-control study using data from population-based candidemia surveillance. *Infect Control Hosp Epidemiol* **26**, 540-547
120. Marvin, M. E., Mason, R. P., and Cashmore, A. M. (2004) The CaCTR1 gene is required for high-affinity iron uptake and is transcriptionally controlled by a copper-sensing transactivator encoded by CaMAC1. *Microbiology* **150**, 2197-2208
121. Woodacre, A., Mason, R. P., Jeeves, R. E., and Cashmore, A. M. (2008) Copper-dependent transcriptional regulation by Candida albicans Mac1p. *Microbiology* **154**, 1502-1512
122. Helmerhorst, E. J., Murphy, M. P., Troxler, R. F., and Oppenheim, F. G. (2002) Characterization of the mitochondrial respiratory pathways in Candida albicans. *Biochim Biophys Acta* **1556**, 73-80
123. Broxton, C. N., and Culotta, V. C. (2016) An Adaptation to Low Copper in Candida albicans Involving SOD Enzymes and the Alternative Oxidase. *PLoS One* **11**, e0168400
124. Hwang, C. S., Rhie, G., Kim, S. T., Kim, Y. R., Huh, W. K., Baek, Y. U., and Kang, S. O. (1999) Copper- and zinc-containing superoxide dismutase and its gene from Candida albicans. *Biochim Biophys Acta* **1427**, 245-255
125. Weisiger, R. A., and Fridovich, I. (1973) Mitochondrial superoxide simutase. Site of synthesis and intramitochondrial localization. *J Biol Chem* **248**, 4793-4796
126. Lamarre, C., LeMay, J. D., Deslauriers, N., and Bourbonnais, Y. (2001) Candida albicans expresses an unusual cytoplasmic manganese-containing superoxide dismutase (SOD3 gene product) upon the entry and during the stationary phase. *J Biol Chem* **276**, 43784-43791
127. Culbertson, E. M., Khan, A. A., Muchenditsi, A., Lutsenko, S., Sullivan, D. J., Petris, M. J., Cormack, B. P., and Culotta, V. C. (2020) Changes in mammalian copper homeostasis during microbial infection. *Metallomics* **12**, 416-426
128. Drakesmith, H., Nemeth, E., and Ganz, T. (2015) Ironing out Ferroportin. *Cell Metab* **22**, 777-787
129. Williams, D. M., Lee, G. R., and Cartwright, G. E. (1974) Ferroxidase activity of rat ceruloplasmin. *Am J Physiol* **227**, 1094-1097
130. Eid, C., Hemadi, M., Ha-Duong, N. T., and El Hage Chahine, J. M. (2014) Iron uptake and transfer from ceruloplasmin to transferrin. *Biochim Biophys Acta* **1840**, 1771-1781

131. Hood, M. I., and Skaar, E. P. (2012) Nutritional immunity: transition metals at the pathogen-host interface. *Nat Rev Microbiol* **10**, 525-537
132. Vogl, T., Leukert, N., Barczyk, K., Strupat, K., and Roth, J. (2006) Biophysical characterization of S100A8 and S100A9 in the absence and presence of bivalent cations. *Biochim Biophys Acta* **1763**, 1298-1306
133. Strupat, K., Rogniaux, H., Van Dorsselaer, A., Roth, J., and Vogl, T. (2000) Calcium-induced noncovalently linked tetramers of MRP8 and MRP14 are confirmed by electrospray ionization-mass analysis. *J Am Soc Mass Spectrom* **11**, 780-788
134. Vogl, T., Roth, J., Sorg, C., Hillenkamp, F., and Strupat, K. (1999) Calcium-induced noncovalently linked tetramers of MRP8 and MRP14 detected by ultraviolet matrix-assisted laser desorption/ionization mass spectrometry. *J Am Soc Mass Spectrom* **10**, 1124-1130
135. Stephan, J. R., and Nolan, E. M. (2016) Calcium-induced Tetramerization and Zinc Chelation Shield Human Calprotectin from Degradation by Host and Bacterial Extracellular Proteases. *Chem Sci* **7**, 1962-1975
136. Gilston, B. A., Skaar, E. P., and Chazin, W. J. (2016) Binding of transition metals to S100 proteins. *Sci China Life Sci* **59**, 792-801
137. Cunden, L. S., and Nolan, E. M. (2018) Bioinorganic Explorations of Zn(II) Sequestration by Human S100 Host-Defense Proteins. *Biochemistry* **57**, 1673-1680
138. Kehl-Fie, T. E., Chitayat, S., Hood, M. I., Damo, S., Restrepo, N., Garcia, C., Munro, K. A., Chazin, W. J., and Skaar, E. P. (2011) Nutrient metal sequestration by calprotectin inhibits bacterial superoxide defense, enhancing neutrophil killing of Staphylococcus aureus. *Cell Host Microbe* **10**, 158-164
139. Damo, S. M., Kehl-Fie, T. E., Sugitani, N., Holt, M. E., Rathi, S., Murphy, W. J., Zhang, Y., Betz, C., Hench, L., Fritz, G., Skaar, E. P., and Chazin, W. J. (2013) Molecular basis for manganese sequestration by calprotectin and roles in the innate immune response to invading bacterial pathogens. *Proc Natl Acad Sci U S A* **110**, 3841-3846
140. Nakashige, T. G., Stephan, J. R., Cunden, L. S., Brophy, M. B., Wommack, A. J., Keegan, B. C., Shearer, J. M., and Nolan, E. M. (2016) The Hexahistidine Motif of Host-Defense Protein Human Calprotectin Contributes to Zinc Withholding and Its Functional Versatility. *J Am Chem Soc* **138**, 12243-12251
141. Hayden, J. A., Brophy, M. B., Cunden, L. S., and Nolan, E. M. (2013) High-affinity manganese coordination by human calprotectin is calcium-dependent and requires the histidine-rich site formed at the dimer interface. *J Am Chem Soc* **135**, 775-787
142. Hadley, R. C., Gagnon, D. M., Brophy, M. B., Gu, Y., Nakashige, T. G., Britt, R. D., and Nolan, E. M. (2018) Biochemical and Spectroscopic Observation of Mn(II) Sequestration from Bacterial Mn(II) Transport Machinery by Calprotectin. *J Am Chem Soc* **140**, 110-113
143. Nakashige, T. G., Zhang, B., Krebs, C., and Nolan, E. M. (2015) Human calprotectin is an iron-sequestering host-defense protein. *Nat Chem Biol* **11**, 765-771
144. Nakashige, T. G., Zygiel, E. M., Drennan, C. L., and Nolan, E. M. (2017) Nickel Sequestration by the Host-Defense Protein Human Calprotectin. *J Am Chem Soc* **139**, 8828-8836
145. Clohessy, P. A., and Golden, B. E. (1995) Calprotectin-mediated zinc chelation as a biostatic mechanism in host defence. *Scand J Immunol* **42**, 551-556
146. Lusitani, D., Malawista, S. E., and Montgomery, R. R. (2003) Calprotectin, an abundant cytosolic protein from human polymorphonuclear leukocytes, inhibits the growth of Borrelia burgdorferi. *Infect Immun* **71**, 4711-4716

147. Gaddy, J. A., Radin, J. N., Loh, J. T., Piazuelo, M. B., Kehl-Fie, T. E., Delgado, A. G., Ilca, F. T., Peek, R. M., Cover, T. L., Chazin, W. J., Skaar, E. P., and Scott Algood, H. M. (2014) The host protein calprotectin modulates the Helicobacter pylori cag type IV secretion system via zinc sequestration. *PLoS Pathog* **10**, e1004450
148. Miyasaki, K. T., Bodeau, A. L., Murthy, A. R., and Lehrer, R. I. (1993) In vitro antimicrobial activity of the human neutrophil cytosolic S-100 protein complex, calprotectin, against Capnocytophaga sputigena. *J Dent Res* **72**, 517-523
149. Akerstrom, B., and Bjorck, L. (2009) Bacterial surface protein L binds and inactivates neutrophil proteins S100A8/A9. *J Immunol* **183**, 4583-4592
150. Nisapakultorn, K., Ross, K. F., and Herzberg, M. C. (2001) Calprotectin expression inhibits bacterial binding to mucosal epithelial cells. *Infect Immun* **69**, 3692-3696
151. Kehl-Fie, T. E., Zhang, Y., Moore, J. L., Farrand, A. J., Hood, M. I., Rathi, S., Chazin, W. J., Caprioli, R. M., and Skaar, E. P. (2013) MntABC and MntH contribute to systemic Staphylococcus aureus infection by competing with calprotectin for nutrient manganese. *Infect Immun* **81**, 3395-3405
152. Garcia, Y. M., Barwinska-Sendra, A., Tarrant, E., Skaar, E. P., Waldron, K. J., and Kehl-Fie, T. E. (2017) A Superoxide Dismutase Capable of Functioning with Iron or Manganese Promotes the Resistance of Staphylococcus aureus to Calprotectin and Nutritional Immunity. *PLoS Pathog* **13**, e1006125
153. Gaddy, J. A., Radin, J. N., Cullen, T. W., Chazin, W. J., Skaar, E. P., Trent, M. S., and Algood, H. M. (2015) Helicobacter pylori Resists the Antimicrobial Activity of Calprotectin via Lipid A Modification and Associated Biofilm Formation. *mBio* **6**, e01349-01315
154. Juttukonda, L. J., Chazin, W. J., and Skaar, E. P. (2016) Acinetobacter baumannii Coordinates Urea Metabolism with Metal Import To Resist Host-Mediated Metal Limitation. *mBio* **7**
155. Makthal, N., Nguyen, K., Do, H., Gavagan, M., Chandrangsu, P., Helmann, J. D., Olsen, R. J., and Kumaraswami, M. (2017) A Critical Role of Zinc Importer AdcABC in Group A Streptococcus-Host Interactions During Infection and Its Implications for Vaccine Development. *EBioMedicine* **21**, 131-141
156. Montgomery, R. R., Schreck, K., Wang, X., and Malawista, S. E. (2006) Human neutrophil calprotectin reduces the susceptibility of Borrelia burgdorferi to penicillin. *Infect Immun* **74**, 2468-2472
157. Posey, J. E., and Gherardini, F. C. (2000) Lack of a role for iron in the Lyme disease pathogen. *Science* **288**, 1651-1653
158. Aguirre, J. D., Clark, H. M., McIlvin, M., Vazquez, C., Palmere, S. L., Grab, D. J., Seshu, J., Hart, P. J., Saito, M., and Culotta, V. C. (2013) A manganese-rich environment supports superoxide dismutase activity in a Lyme disease pathogen, Borrelia burgdorferi. *J Biol Chem* **288**, 8468-8478
159. Wang, P., Lutton, A., Olesik, J., Vali, H., and Li, X. (2012) A novel iron- and copper-binding protein in the Lyme disease spirochaete. *Mol Microbiol* **86**, 1441-1451
160. Ramsey, M. E., Hyde, J. A., Medina-Perez, D. N., Lin, T., Gao, L., Lundt, M. E., Li, X., Norris, S. J., Skare, J. T., and Hu, L. T. (2017) A high-throughput genetic screen identifies previously uncharacterized Borrelia burgdorferi genes important for resistance against reactive oxygen and nitrogen species. *PLoS Pathog* **13**, e1006225
161. Ouyang, Z., He, M., Oman, T., Yang, X. F., and Norgard, M. V. (2009) A manganese transporter, BB0219 (BmtA), is required for virulence by the Lyme disease spirochete, Borrelia burgdorferi. *Proc Natl Acad Sci U S A* **106**, 3449-3454

162. Troxell, B., Xu, H., and Yang, X. F. (2012) Borrelia burgdorferi, a pathogen that lacks iron, encodes manganese-dependent superoxide dismutase essential for resistance to streptonigrin. *J Biol Chem* **287**, 19284-19293
163. Whitehouse, C. A., Williams, L. R., and Austin, F. E. (1997) Identification of superoxide dismutase activity in Borrelia burgdorferi. *Infect Immun* **65**, 4865-4868
164. Esteve-Gassent, M. D., Elliott, N. L., and Seshu, J. (2009) sodA is essential for virulence of Borrelia burgdorferi in the murine model of Lyme disease. *Mol Microbiol* **71**, 594-612
165. Bourret, T. J., Boylan, J. A., Lawrence, K. A., and Gherardini, F. C. (2011) Nitrosative damage to free and zinc-bound cysteine thiols underlies nitric oxide toxicity in wild-type Borrelia burgdorferi. *Mol Microbiol* **81**, 259-273
166. Bertin, P. B., Lozzi, S. P., Howell, J. K., Restrepo-Cadavid, G., Neves, D., Teixeira, A. R., de Sousa, M. V., Norris, S. J., and Santana, J. M. (2005) The thermophilic, homohexameric aminopeptidase of Borrelia burgdorferi is a member of the M29 family of metallopeptidases. *Infect Immun* **73**, 2253-2261
167. Nguyen, K. T., Wu, J. C., Boylan, J. A., Gherardini, F. C., and Pei, D. (2007) Zinc is the metal cofactor of Borrelia burgdorferi peptide deformylase. *Arch Biochem Biophys* **468**, 217-225
168. Troxell, B., and Yang, X. F. (2013) Metal-dependent gene regulation in the causative agent of Lyme disease. *Front Cell Infect Microbiol* **3**, 79
169. Troxell, B., Ye, M., Yang, Y., Carrasco, S. E., Lou, Y., and Yang, X. F. (2013) Manganese and zinc regulate virulence determinants in Borrelia burgdorferi. *Infect Immun* **81**, 2743-2752
170. Vasudevan, B., and Chatterjee, M. (2013) Lyme borreliosis and skin. *Indian J Dermatol* **58**, 167-174
171. Neubert, U., Krampitz, H. E., and Engl, H. (1986) Microbiological findings in erythema (chronicum) migrans and related disorders. *Zentralbl Bakteriol Mikrobiol Hyg A* **263**, 237-252
172. Marques, A., Schwartz, I., Wormser, G. P., Wang, Y., Hornung, R. L., Demirkale, C. Y., Munson, P. J., Turk, S. P., Williams, C., Lee, C. R., Yang, J., and Petzke, M. M. (2017) Transcriptome Assessment of Erythema Migrans Skin Lesions in Patients With Early Lyme Disease Reveals Predominant Interferon Signaling. *J Infect Dis* **217**, 158-167
173. Iotzova-Weiss, G., Dziunycz, P. J., Freiberger, S. N., Lauchli, S., Hafner, J., Vogl, T., French, L. E., and Hofbauer, G. F. (2015) S100A8/A9 stimulates keratinocyte proliferation in the development of squamous cell carcinoma of the skin via the receptor for advanced glycation-end products. *PLoS One* **10**, e0120971
174. Nukui, T., Ehama, R., Sakaguchi, M., Sonegawa, H., Katagiri, C., Hibino, T., and Huh, N. H. (2008) S100A8/A9, a key mediator for positive feedback growth stimulation of normal human keratinocytes. *J Cell Biochem* **104**, 453-464
175. Thorey, I. S., Roth, J., Regenbogen, J., Halle, J. P., Bittner, M., Vogl, T., Kaesler, S., Bugnon, P., Reitmaier, B., Durka, S., Graf, A., Wockner, M., Rieger, N., Konstantinow, A., Wolf, E., Goppelt, A., and Werner, S. (2001) The Ca2+-binding proteins S100A8 and S100A9 are encoded by novel injury-regulated genes. *J Biol Chem* **276**, 35818-35825
176. Lessard, J. C., Pina-Paz, S., Rotty, J. D., Hickerson, R. P., Kaspar, R. L., Balmain, A., and Coulombe, P. A. (2013) Keratin 16 regulates innate immunity in response to epidermal barrier breach. *Proc Natl Acad Sci U S A* **110**, 19537-19542
177. Lesniak, W., and Graczyk-Jarzynka, A. (2015) The S100 proteins in epidermis: Topology and function. *Biochim Biophys Acta* **1850**, 2563-2572

178. Wilkinson, M. M., Busuttil, A., Hayward, C., Brock, D. J., Dorin, J. R., and Van Heyningen, V. (1988) Expression pattern of two related cystic fibrosis-associated calcium-binding proteins in normal and abnormal tissues. *J Cell Sci* **91 (Pt 2)**, 221-230
179. Diaz-Ochoa, V. E., Lam, D., Lee, C. S., Klaus, S., Behnsen, J., Liu, J. Z., Chim, N., Nuccio, S. P., Rathi, S. G., Mastroianni, J. R., Edwards, R. A., Jacobo, C. M., Cerasi, M., Battistoni, A., Ouellette, A. J., Goulding, C. W., Chazin, W. J., Skaar, E. P., and Raffatellu, M. (2016) Salmonella Mitigates Oxidative Stress and Thrives in the Inflamed Gut by Evading Calprotectin-Mediated Manganese Sequestration. *Cell Host Microbe* **19**, 814-825
180. de Koning, J. (1993) Histopathologic patterns of erythema migrans and borrelial lymphocytoma. *Clin Dermatol* **11**, 377-383
181. de Carvalho, G. C., Domingues, R., de Sousa Nogueira, M. A., Calvielli Castelo Branco, A. C., Gomes Manfrere, K. C., Pereira, N. V., Aoki, V., Sotto, M. N., Da Silva Duarte, A. J., and Sato, M. N. (2016) Up-regulation of Proinflammatory Genes and Cytokines Induced by S100A8 in CD8+ T Cells in Lichen Planus. *Acta Derm Venereol* **96**, 485-489
182. Eming, S. A., Koch, M., Krieger, A., Brachvogel, B., Kreft, S., Bruckner-Tuderman, L., Krieg, T., Shannon, J. D., and Fox, J. W. (2010) Differential proteomic analysis distinguishes tissue repair biomarker signatures in wound exudates obtained from normal healing and chronic wounds. *J Proteome Res* **9**, 4758-4766
183. Grimbaldeston, M. A., Geczy, C. L., Tedla, N., Finlay-Jones, J. J., and Hart, P. H. (2003) S100A8 induction in keratinocytes by ultraviolet A irradiation is dependent on reactive oxygen intermediates. *J Invest Dermatol* **121**, 1168-1174
184. J., M., R., E., and F., P. (2010) *Rook's Textbook of Dermatology*, Blackwell Science LtD, Malden, MA
185. Hsu, K., Champaiboon, C., Guenther, B. D., Sorenson, B. S., Khammanivong, A., Ross, K. F., Geczy, C. L., and Herzberg, M. C. (2009) Anti-Infective Protective Properties of S100 Calgranulins. *Antiinflamm Antiallergy Agents Med Chem* **8**, 290-305
186. Xu, Q., Seemanapalli, S. V., Reif, K. E., Brown, C. R., and Liang, F. T. (2007) Increasing the recruitment of neutrophils to the site of infection dramatically attenuates Borrelia burgdorferi infectivity. *J Immunol* **178**, 5109-5115
187. Duray, P. H. (1989) Histopathology of clinical phases of human Lyme disease. *Rheum Dis Clin North Am* **15**, 691-710
188. Vogl, T., Eisenblatter, M., Voller, T., Zenker, S., Hermann, S., van Lent, P., Faust, A., Geyer, C., Petersen, B., Roebrock, K., Schafers, M., Bremer, C., and Roth, J. (2014) Alarmin S100A8/S100A9 as a biomarker for molecular imaging of local inflammatory activity. *Nat Commun* **5**, 4593
189. Frosch, M., Strey, A., Vogl, T., Wulffraat, N. M., Kuis, W., Sunderkotter, C., Harms, E., Sorg, C., and Roth, J. (2000) Myeloid-related proteins 8 and 14 are specifically secreted during interaction of phagocytes and activated endothelium and are useful markers for monitoring disease activity in pauciarticular-onset juvenile rheumatoid arthritis. *Arthritis Rheum* **43**, 628-637
190. Wang, Y., Zhang, Z., Zhang, L., Li, X., Lu, R., Xu, P., Zhang, X., Dai, M., Dai, X., Qu, J., Lu, F., and Chi, Z. (2016) S100A8 promotes migration and infiltration of inflammatory cells in acute anterior uveitis. *Sci Rep* **6**, 36140
191. Costa, M., Cruz, E., Oliveira, S., Benes, V., Ivacevic, T., Silva, M. J., Vieira, I., Dias, F., Fonseca, S., Goncalves, M., Lima, M., Leitao, C., Muckenthaler, M. U., Pinto, J., and Porto, G. (2015) Lymphocyte gene expression signatures from patients and mouse models of hereditary hemochromatosis reveal a function of HFE as a negative regulator of CD8+ T-lymphocyte activation and differentiation in vivo. *PLoS One* **10**, e0124246

192. Pollack, R. J., Telford, S. R., 3rd, and Spielman, A. (1993) Standardization of medium for culturing Lyme disease spirochetes. *J Clin Microbiol* **31**, 1251-1255
193. Barbour, A. G. (1984) Isolation and cultivation of Lyme disease spirochetes. *Yale J Biol Med* **57**, 521-525
194. Sohnle, P. G., Hunter, M. J., Hahn, B., and Chazin, W. J. (2000) Zinc-reversible antimicrobial activity of recombinant calprotectin (migration inhibitory factor-related proteins 8 and 14). *J Infect Dis* **182**, 1272-1275
195. Linder, M. C. (2016) Ceruloplasmin and other copper binding components of blood plasma and their functions: an update. *Metallomics*, 887-905

196. Masuoka, J., Hegenauer, J., Van Dyke, B. R., and Saltman, P. (1993) Intrinsic stoichiometric equilibrium constants for the binding of zinc(II) and copper(II) to the high affinity site of serum albumin. *J Biol Chem* **268**, 21533-21537
197. Waldvogel-Abramowski, S., Waeber, G., Gassner, C., Buser, A., Frey, B. M., Favrat, B., and Tissot, J. D. (2014) Physiology of iron metabolism. *Transfus Med Hemother* **41**, 213-221
198. Sohnle, P. G., Hahn, B. L., and Santhanagopalan, V. (1996) Inhibition of Candida albicans growth by calprotectin in the absence of direct contact with the organisms. *J Infect Dis* **174**, 1369-1372
199. Stork, M., Grijpstra, J., Bos, M. P., Manas Torres, C., Devos, N., Poolman, J. T., Chazin, W. J., and Tommassen, J. (2013) Zinc piracy as a mechanism of Neisseria meningitidis for evasion of nutritional immunity. *PLoS Pathog* **9**, e1003733
200. Jean, S., Juneau, R. A., Criss, A. K., and Cornelissen, C. N. (2016) Neisseria gonorrhoeae Evades Calprotectin-Mediated Nutritional Immunity and Survives Neutrophil Extracellular Traps by Production of TdfH. *Infect Immun* **84**, 2982-2994
201. Nowakowski, A. B., and Petering, D. H. (2011) Reactions of the fluorescent sensor, Zinquin, with the zinc-proteome: adduct formation and ligand substitution. *Inorg Chem* **50**, 10124-10133
202. Ollig, J., Kloubert, V., Wessels, I., Hasse, H., and Rink, L. (2016) Parameters Influencing Zinc in Experimental Systems *in vivo* and *in vitro*. *Metals* **6**
203. Outten, F. W., Huffman, D. L., Hale, J. A., and O'Halloran, T. V. (2001) The independent cue and cus systems confer copper tolerance during aerobic and anaerobic growth in Escherichia coli. *J Biol Chem* **276**, 30670-30677
204. Kersten, A., Poitschek, C., Rauch, S., and Aberer, E. (1995) Effects of penicillin, ceftriaxone, and doxycycline on morphology of Borrelia burgdorferi. *Antimicrob Agents Chemother* **39**, 1127-1133
205. Alban, P. S., Johnson, P. W., and Nelson, D. R. (2000) Serum-starvation-induced changes in protein synthesis and morphology of Borrelia burgdorferi. *Microbiology* **146 (Pt 1)**, 119-127
206. Lantos, P. M., Auwaerter, P. G., and Wormser, G. P. (2014) A systematic review of Borrelia burgdorferi morphologic variants does not support a role in chronic Lyme disease. *Clin Infect Dis* **58**, 663-671
207. Merilainen, L., Herranen, A., Schwarzbach, A., and Gilbert, L. (2015) Morphological and biochemical features of Borrelia burgdorferi pleomorphic forms. *Microbiology* **161**, 516-527

208. Edgeworth, J. D., Abiose, A., and Jones, B. R. (1993) An immunohistochemical analysis of onchocercal nodules: evidence for an interaction between macrophage MRP8/MRP14 and adult Onchocerca volvulus. *Clin Exp Immunol* **92**, 84-92
209. Basika, T., Munoz, N., Casaravilla, C., Irigoin, F., Batthyany, C., Bonilla, M., Salinas, G., Pacheco, J. P., Roth, J., Duran, R., and Diaz, A. (2012) Phagocyte-specific S100 proteins in the local response to the Echinococcus granulosus larva. *Parasitology* **139**, 271-283
210. Marti, T., Erttmann, K. D., and Gallin, M. Y. (1996) Host-parasite interaction in human onchocerciasis: identification and sequence analysis of a novel human calgranulin. *Biochem Biophys Res Commun* **221**, 454-458
211. Gottsch, J. D., Eisinger, S. W., Liu, S. H., and Scott, A. L. (1999) Calgranulin C has filariacidal and filariastatic activity. *Infect Immun* **67**, 6631-6636
212. Akpek, E. K., Liu, S. H., Thompson, R., and Gottsch, J. D. (2002) Identification of paramyosin as a binding protein for calgranulin C in experimental helminthic keratitis. *Invest Ophthalmol Vis Sci* **43**, 2677-2684
213. Broome, A. M., Ryan, D., and Eckert, R. L. (2003) S100 protein subcellular localization during epidermal differentiation and psoriasis. *J Histochem Cytochem* **51**, 675-685
214. Hughes, C. A., Kodner, C. B., and Johnson, R. C. (1992) DNA analysis of Borrelia burgdorferi NCH-1, the first northcentral U.S. human Lyme disease isolate. *J Clin Microbiol* **30**, 698-703
215. Zuckert, W. R. (2007) Laboratory maintenance of Borrelia burgdorferi. *Curr Protoc Microbiol* **Chapter 12**, Unit 12C 11
216. Hopkin, K. A., Papazian, M. A., and Steinman, H. M. (1992) Functional differences between manganese and iron superoxide dismutases in Escherichia coli K-12. *J Biol Chem* **267**, 24253-24258
217. Turski, M. L., and Thiele, D. J. (2009) New roles for copper metabolism in cell proliferation, signaling, and disease. *J Biol Chem* **284**, 717-721
218. Festa, R. A., and Thiele, D. J. (2011) Copper: an essential metal in biology. *Curr Biol* **21**, R877-883
219. Liochev, S. I., and Fridovich, I. (2002) The Haber-Weiss cycle -- 70 years later: an alternative view. *Redox Rep* **7**, 55-57; author reply 59-60
220. Foster, A. W., Osman, D., and Robinson, N. J. (2014) Metal preferences and metallation. *J Biol Chem* **289**, 28095-28103
221. Tan, G., Cheng, Z., Pang, Y., Landry, A. P., Li, J., Lu, J., and Ding, H. (2014) Copper binding in IscA inhibits iron-sulphur cluster assembly in Escherichia coli. *Mol Microbiol* **93**, 629-644
222. Chillappagari, S., Seubert, A., Trip, H., Kuipers, O. P., Marahiel, M. A., and Miethke, M. (2010) Copper stress affects iron homeostasis by destabilizing iron-sulfur cluster formation in Bacillus subtilis. *J Bacteriol* **192**, 2512-2524
223. Besold, A. N., Culbertson, E. M., and Culotta, V. C. (2016) The Yin and Yang of copper during infection. *J Biol Inorg Chem* **21**, 137-144
224. Ladomersky, E., and Petris, M. J. (2015) Copper tolerance and virulence in bacteria. *Metallomics* **7**, 957-964
225. Sheldon, J. R., and Skaar, E. P. (2019) Metals as phagocyte antimicrobial effectors. *Curr Opin Immunol* **60**, 1-9
226. Fu, Y., Chang, F. M., and Giedroc, D. P. (2014) Copper transport and trafficking at the host-bacterial pathogen interface. *Acc Chem Res* **47**, 3605-3613
227. Dupre-Crochet, S., Erard, M., and Nubetae, O. (2013) ROS production in phagocytes: why, when, and where? *J Leukoc Biol* **94**, 657-670

228. Wink, D. A., Hines, H. B., Cheng, R. Y., Switzer, C. H., Flores-Santana, W., Vitek, M. P., Ridnour, L. A., and Colton, C. A. (2011) Nitric oxide and redox mechanisms in the immune response. *J Leukoc Biol* **89**, 873-891
229. Schatzman, S. S., and Culotta, V. C. (2018) Chemical Warfare at the Microorganismal Level: A Closer Look at the Superoxide Dismutase Enzymes of Pathogens. *ACS Infect Dis* **4**, 893-903
230. Samanovic, M. I., Ding, C., Thiele, D. J., and Darwin, K. H. (2012) Copper in microbial pathogenesis: meddling with the metal. *Cell Host Microbe* **11**, 106-115
231. Djoko, K. Y., Franiek, J. A., Edwards, J. L., Falsetta, M. L., Kidd, S. P., Potter, A. J., Chen, N. H., Apicella, M. A., Jennings, M. P., and McEwan, A. G. (2012) Phenotypic characterization of a copA mutant of Neisseria gonorrhoeae identifies a link between copper and nitrosative stress. *Infect Immun* **80**, 1065-1071
232. Schwan, W. R., Warrener, P., Keunz, E., Stover, C. K., and Folger, K. R. (2005) Mutations in the cueA gene encoding a copper homeostasis P-type ATPase reduce the pathogenicity of Pseudomonas aeruginosa in mice. *Int J Med Microbiol* **295**, 237-242
233. Garcia-Santamarina, S., and Thiele, D. J. (2015) Copper at the Fungal Pathogen-Host Axis. *J Biol Chem* **290**, 18945-18953
234. Brechting, P. J., and Rappleye, C. A. (2019) Histoplasma Responses to Nutritional Immunity Imposed by Macrophage Activation. *J Fungi (Basel)* **5**
235. Yapar, N. (2014) Epidemiology and risk factors for invasive candidiasis. *Ther Clin Risk Manag* **10**, 95-105
236. Zaoutis, T. E., Argon, J., Chu, J., Berlin, J. A., Walsh, T. J., and Feudtner, C. (2005) The epidemiology and attributable outcomes of candidemia in adults and children hospitalized in the United States: a propensity analysis. *Clin Infect Dis* **41**, 1232-1239
237. MacCallum, D. M., and Odds, F. C. (2005) Temporal events in the intravenous challenge model for experimental Candida albicans infections in female mice. *Mycoses* **48**, 151-161
238. Nose, Y., Kim, B. E., and Thiele, D. J. (2006) Ctr1 drives intestinal copper absorption and is essential for growth, iron metabolism, and neonatal cardiac function. *Cell Metab* **4**, 235-244
239. Prohaska, J. R. (1983) Changes in tissue growth, concentrations of copper, iron, cytochrome oxidase and superoxide dismutase subsequent to dietary or genetic copper deficiency in mice. *J Nutr* **113**, 2048-2058
240. Allen, K. J., Buck, N. E., Cheah, D. M., Gazeas, S., Bhathal, P., and Mercer, J. F. (2006) Chronological changes in tissue copper, zinc and iron in the toxic milk mouse and effects of copper loading. *Biometals* **19**, 555-564
241. Buiakova, O. I., Xu, J., Lutsenko, S., Zeitlin, S., Das, K., Das, S., Ross, B. M., Mekios, C., Scheinberg, I. H., and Gilliam, T. C. (1999) Null mutation of the murine ATP7B (Wilson disease) gene results in intracellular copper accumulation and late-onset hepatic nodular transformation. *Hum Mol Genet* **8**, 1665-1671
242. Sato, M., and Gitlin, J. D. (1991) Mechanisms of copper incorporation during the biosynthesis of human ceruloplasmin. *J Biol Chem* **266**, 5128-5134
243. Schosinsky, K. H., Lehmann, H. P., and Beeler, M. F. (1974) Measurement of ceruloplasmin from its oxidase activity in serum by use of o-dianisidine dihydrochloride. *Clin Chem* **20**, 1556-1563
244. Stepien, K. M., and Guy, M. (2018) Caeruloplasmin oxidase activity: measurement in serum by use of o-dianisidine dihydrochloride on a microplate reader. *Ann Clin Biochem* **55**, 149-157

245. Vashchenko, G., Bleackley, M. R., Griffiths, T. A., and MacGillivray, R. T. (2011) Oxidation of organic and biogenic amines by recombinant human hephaestin expressed in Pichia pastoris. *Arch Biochem Biophys* **514**, 50-56
246. Marques, L., Auriac, A., Willemetz, A., Banha, J., Silva, B., Canonne-Hergaux, F., and Costa, L. (2012) Immune cells and hepatocytes express glycosylphosphatidylinositol-anchored ceruloplasmin at their cell surface. *Blood Cells Mol Dis* **48**, 110-120
247. Cerveza, P. J., Mehrbod, F., Cotton, S. J., Lomeli, N., Linder, M. C., Fonda, E. G., and Wickler, S. J. (2000) Milk ceruloplasmin and its expression by mammary gland and liver in pigs. *Arch Biochem Biophys* **373**, 451-461
248. Banha, J., Marques, L., Oliveira, R., Martins Mde, F., Paixao, E., Pereira, D., Malho, R., Penque, D., and Costa, L. (2008) Ceruloplasmin expression by human peripheral blood lymphocytes: a new link between immunity and iron metabolism. *Free Radic Biol Med* **44**, 483-492
249. Mostad, E. J., and Prohaska, J. R. (2011) Glycosylphosphatidylinositol-linked ceruloplasmin is expressed in multiple rodent organs and is lower following dietary copper deficiency. *Exp Biol Med (Maywood)* **236**, 298-308
250. Wiggins, J. E., Goyal, M., Wharram, B. L., and Wiggins, R. C. (2006) Antioxidant ceruloplasmin is expressed by glomerular parietal epithelial cells and secreted into urine in association with glomerular aging and high-calorie diet. *J Am Soc Nephrol* **17**, 1382-1387
251. Muchenditsi, A., Yang, H., Hamilton, J. P., Koganti, L., Housseau, F., Aronov, L., Fan, H., Pierson, H., Bhattacharjee, A., Murphy, R., Sears, C., Potter, J., Wooton-Kee, C. R., and Lutsenko, S. (2017) Targeted inactivation of copper transporter Atp7b in hepatocytes causes liver steatosis and obesity in mice. *Am J Physiol Gastrointest Liver Physiol* **313**, G39-G49
252. Armitage, A. E., Eddowes, L. A., Gileadi, U., Cole, S., Spottiswoode, N., Selvakumar, T. A., Ho, L. P., Townsend, A. R., and Drakesmith, H. (2011) Hepcidin regulation by innate immune and infectious stimuli. *Blood* **118**, 4129-4139
253. Ganz, T. (2003) Hepcidin, a key regulator of iron metabolism and mediator of anemia of inflammation. *Blood* **102**, 783-788
254. Cherukuri, S., Tripoulas, N. A., Nurko, S., and Fox, P. L. (2004) Anemia and impaired stress-induced erythropoiesis in aceruloplasminemic mice. *Blood Cells Mol Dis* **33**, 346-355
255. Goldstein, I. M., Kaplan, H. B., Edelson, H. S., and Weissmann, G. (1982) Ceruloplasmin: an acute phase reactant that scavenges oxygen-derived free radicals. *Ann N Y Acad Sci* **389**, 368-379
256. Gutteridge, J. M., Winyard, P. G., Blake, D. R., Lunec, J., Brailsford, S., and Halliwell, B. (1985) The behaviour of caeruloplasmin in stored human extracellular fluids in relation to ferroxidase II activity, lipid peroxidation and phenanthroline-detectable copper. *Biochem J* **230**, 517-523
257. Gutteridge, J. M. (1986) Antioxidant properties of the proteins caeruloplasmin, albumin and transferrin. A study of their activity in serum and synovial fluid from patients with rheumatoid arthritis. *Biochim Biophys Acta* **869**, 119-127
258. Richards, D. A. (1983) Use of high-performance liquid chromatography to study the caeruloplasmin-catalysed oxidation of biogenic amines. I. Single substrate systems. *J Chromatogr* **256**, 71-79

259. Shiva, S., Wang, X., Ringwood, L. A., Xu, X., Yuditskaya, S., Annavajjhala, V., Miyajima, H., Hogg, N., Harris, Z. L., and Gladwin, M. T. (2006) Ceruloplasmin is a NO oxidase and nitrite synthase that determines endocrine NO homeostasis. *Nat Chem Biol* **2**, 486-493
260. Vrancken, K., Schroeder, H. J., Longo, L. D., Power, G. G., and Blood, A. B. (2013) Role of ceruloplasmin in nitric oxide metabolism in plasma of humans and sheep: a comparison of adults and fetuses. *Am J Physiol Regul Integr Comp Physiol* **305**, R1401-1410
261. Kim, B. E., Turski, M. L., Nose, Y., Casad, M., Rockman, H. A., and Thiele, D. J. (2010) Cardiac copper deficiency activates a systemic signaling mechanism that communicates with the copper acquisition and storage organs. *Cell Metab* **11**, 353-363
262. Chun, H., Catterton, T., Kim, H., Lee, J., and Kim, B. E. (2017) Organ-specific regulation of ATP7A abundance is coordinated with systemic copper homeostasis. *Sci Rep* **7**, 12001
263. Ohrvik, H., and Thiele, D. J. (2015) The role of Ctr1 and Ctr2 in mammalian copper homeostasis and platinum-based chemotherapy. *J Trace Elem Med Biol* **31**, 178-182
264. Kaplan, J. H., and Lutsenko, S. (2009) Copper transport in mammalian cells: special care for a metal with special needs. *J Biol Chem* **284**, 25461-25465
265. Kuo, Y. M., Zhou, B., Cosco, D., and Gitschier, J. (2001) The copper transporter CTR1 provides an essential function in mammalian embryonic development. *Proc Natl Acad Sci U S A* **98**, 6836-6841
266. Wang, Y., Zhu, S., Weisman, G. A., Gitlin, J. D., and Petris, M. J. (2012) Conditional knockout of the Menkes disease copper transporter demonstrates its critical role in embryogenesis. *PLoS One* **7**, e43039
267. Cromer, D., Evans, K. J., Schofield, L., and Davenport, M. P. (2006) Preferential invasion of reticulocytes during late-stage Plasmodium berghei infection accounts for reduced circulating reticulocyte levels. *Int J Parasitol* **36**, 1389-1397
268. Basir, R., Rahiman, S. F., Hasballah, K., Chong, W., Talib, H., Yam, M., Jabbarzare, M., Tie, T., Othman, F., Moklas, M., Abdullah, W., and Ahmad, Z. (2012) Plasmodium berghei ANKA Infection in ICR Mice as a Model of Cerebral Malaria. *Iran J Parasitol* **7**, 62-74
269. Kuo, Y. M., Gybina, A. A., Pyatskowit, J. W., Gitschier, J., and Prohaska, J. R. (2006) Copper transport protein (Ctr1) levels in mice are tissue specific and dependent on copper status. *J Nutr* **136**, 21-26
270. Poti, K. E., Balaban, A. E., Pal, P., Kobayashi, T., Goldberg, D. E., Sinnis, P., and Sullivan, D. J. (2019) In vivo compartmental kinetics of Plasmodium falciparum histidine-rich protein II in the blood of humans and in BALB/c mice infected with a transgenic Plasmodium berghei parasite expressing histidine-rich protein II. *Malar J* **18**, 78
271. Culotta, V. C., Howard, W. R., and Liu, X. F. (1994) CRS5 encodes a metallothionein-like protein in Saccharomyces cerevisiae. *J Biol Chem* **269**, 25295-25302
272. Gross, C., Kelleher, M., Iyer, V. R., Brown, P. O., and Winge, D. R. (2000) Identification of the copper regulon in Saccharomyces cerevisiae by DNA microarrays. *J Biol Chem* **275**, 32310-32316
273. Sheng, Y., Abreu, I. A., Cabelli, D. E., Maroney, M. J., Miller, A. F., Teixeira, M., and Valentine, J. S. (2014) Superoxide dismutases and superoxide reductases. *Chem Rev* **114**, 3854-3918
274. Weisiger, R. A., and Fridovich, I. (1973) Mitochondrial superoxide dismutase site of synthesis and intramitochondrial localization. *J Biol Chem* **248**, 4793-4796
275. Jaarsma, D., Rognoni, F., van Duijn, W., Verspaget, H. W., Haasdijk, E. D., and Holstege, J. C. (2001) CuZn superoxide dismutase (SOD1) accumulates in vacuolated mitochondria in transgenic mice expressing amyotrophic lateral sclerosis-linked SOD1 mutations. *Acta Neuropathol* **102**, 293-305

276. Okado-Matsumoto, A., and Fridovich, I. (2001) Subcellular distribution of superoxide dismutases (SOD) in rat liver Cu,Zn-SOD in mitochondria. *j Biol Chem* **276**, 38388-38393
277. Montllor-Albalate, C., Colin, A. E., Chandrasekharan, B., Bolaji, N., Andersen, J. L., Wayne Outten, F., and Reddi, A. R. (2019) Extra-mitochondrial Cu/Zn superoxide dismutase (Sod1) is dispensable for protection against oxidative stress but mediates peroxide signaling in Saccharomyces cerevisiae. *Redox Biol* **21**, 101064
278. Juarez, J. C., Manuia, M., Burnett, M. E., Betancourt, O., Boivin, B., Shaw, D. E., Tonks, N. K., Mazar, A. P., and Donate, F. (2008) Superoxide dismutase 1 (SOD1) is essential for H2O2-mediated oxidation and inactivation of phosphatases in growth factor signaling. *Proc Natl Acad Sci U S A* **105**, 7147-7152
279. Reuss, O., Vik, A., Kolter, R., and Morschhauser, J. (2004) The SAT1 flipper, an optimized tool for gene disruption in Candida albicans. *Gene* **341**, 119-127
280. Khemiri, I., Tebbji, F., and Sellam, A. (2020) Transcriptome Analysis Uncovers a Link Between Copper Metabolism, and Both Fungal Fitness and Antifungal Sensitivity in the Opportunistic Yeast Candida albicans. *Front Microbiol* **11**, 935
281. Bambach, A., Fernandes, M. P., Ghosh, A., Kruppa, M., Alex, D., Li, D., Fonzi, W. A., Chauhan, N., Sun, N., Agrellos, O. A., Vercesi, A. E., Rolfes, R. J., and Calderone, R. (2009) Goa1p of Candida albicans localizes to the mitochondria during stress and is required for mitochondrial function and virulence. *Eukaryot Cell* **8**, 1706-1720
282. Becker, J. M., Kauffman, S. J., Hauser, M., Huang, L., Lin, M., Sillaots, S., Jiang, B., Xu, D., and Roemer, T. (2010) Pathway analysis of Candida albicans survival and virulence determinants in a murine infection model. *Proc Natl Acad Sci U S A* **107**, 22044-22049
283. Rae, T. D., Schmidt, P. J., Pufahl, R. A., Culotta, V. C., and O'Halloran, T. V. (1999) Undetectable intracellular free copper: the requirement of a copper chaperone for superoxide dismutase. *Science* **284**, 805-808
284. Nguyen, N., Quail, M. M. F., and Hernday, A. D. (2017) An Efficient, Rapid, and Recyclable System for CRISPR-Mediated Genome Editing in Candida albicans. *mSphere* **2**
285. Kropat, J., Gallaher, S. D., Urzica, E. I., Nakamoto, S. S., Strenkert, D., Tottey, S., Mason, A. Z., and Merchant, S. S. (2015) Copper economy in Chlamydomonas: prioritized allocation and reallocation of copper to respiration vs. photosynthesis. *Proc Natl Acad Sci U S A* **112**, 2644-2651
286. Merchant, S., Hill, K., and Howe, G. (1991) Dynamic interplay between two copper-titrating components in the transcriptional regulation of cyt c6. *EMBO J* **10**, 1383-1389
287. Merchant, S., and Bogorad, L. (1986) Regulation by copper of the expression of plastocyanin and cytochrome c552 in Chlamydomonas reinhardi. *Mol Cell Biol* **6**, 462-469
288. Hippmann, A. A., Schuback, N., Moon, K. M., McCrow, J. P., Allen, A. E., Foster, L. J., Green, B. R., and Maldonado, M. T. (2017) Contrasting effects of copper limitation on the photosynthetic apparatus in two strains of the open ocean diatom Thalassiosira oceanica. *PLoS One* **12**, e0181753
289. Uhl, M. A., Biery, M., Craig, N., and Johnson, A. D. (2003) Haploinsufficiency-based large-scale forward genetic analysis of filamentous growth in the diploid human fungal pathogen C.albicans. *EMBO J* **22**, 2668-2678
290. Garcia-Sanchez, S., Mavor, A. L., Russell, C. L., Argimon, S., Dennison, P., Enjalbert, B., and Brown, A. J. (2005) Global roles of Ssn6 in Tup1- and Nrg1-dependent gene regulation in the fungal pathogen, Candida albicans. *Mol Biol Cell* **16**, 2913-2925

291. Huang, G. H., Nie, X. Y., and Chen, J. Y. (2006) CaMac1, a Candida albicans copper ion-sensing transcription factor, promotes filamentous and invasive growth in Saccharomyces cerevisiae. *Acta Biochim Biophys Sin (Shanghai)* **38**, 213-217
292. Singh, R. P., Prasad, H. K., Sinha, I., Agarwal, N., and Natarajan, K. (2011) Cap2-HAP complex is a critical transcriptional regulator that has dual but contrasting roles in regulation of iron homeostasis in Candida albicans. *J Biol Chem* **286**, 25154-25170
293. Chen, C., Pande, K., French, S. D., Tuch, B. B., and Noble, S. M. (2011) An iron homeostasis regulatory circuit with reciprocal roles in Candida albicans commensalism and pathogenesis. *Cell Host Microbe* **10**, 118-135
294. Ziegler, L., Terzulli, A., Gaur, R., McCarthy, R., and Kosman, D. J. (2011) Functional characterization of the ferroxidase, permease high-affinity iron transport complex from Candida albicans. *Mol Microbiol* **81**, 473-485
295. Mamouei, Z., Zeng, G., Wang, Y. M., and Wang, Y. (2017) Candida albicans possess a highly versatile and dynamic high-affinity iron transport system important for its commensal-pathogenic lifestyle. *Mol Microbiol* **106**, 986-998
296. Paul, B. T., Manz, D. H., Torti, F. M., and Torti, S. V. (2017) Mitochondria and Iron: current questions. *Expert Rev Hematol* **10**, 65-79
297. Kim, H. J., Khalimonchuk, O., Smith, P. M., and Winge, D. R. (2012) Structure, function, and assembly of heme centers in mitochondrial respiratory complexes. *Biochim Biophys Acta* **1823**, 1604-1616
298. Schatzman, S. S., Peterson, R. L., Teka, M., He, B., Cabelli, D. E., Cormack, B. P., and Culotta, V. C. (2020) Copper-only superoxide dismutase enzymes and iron starvation stress in Candida fungal pathogens. *J Biol Chem* **295**, 570-583
299. Sorgo, A. G., Brul, S., de Koster, C. G., de Koning, L. J., and Klis, F. M. (2013) Iron restriction-induced adaptations in the wall proteome of Candida albicans. *Microbiology* **159**, 1673-1682
300. Muzzey, D., Schwartz, K., Weissman, J. S., and Sherlock, G. (2013) Assembly of a phased diploid Candida albicans genome facilitates allele-specific measurements and provides a simple model for repeat and indel structure. *Genome Biol* **14**, R97
301. Jiang, N., Liu, X., Yang, J., Li, Z., Pan, J., and Zhu, X. (2011) Regulation of copper homeostasis by Cuf1 associates with its subcellular localization in the pathogenic yeast Cryptococcus neoformans H99. *FEMS Yeast Res* **11**, 440-448
302. Conti, H. R., Huppler, A. R., Whibley, N., and Gaffen, S. L. (2014) Animal models for candidiasis. *Curr Protoc Immunol* **105**, 19 16 11-19 16 17
303. Tamarit, J., Irazusta, V., Moreno-Cermeno, A., and Ros, J. (2006) Colorimetric assay for the quantitation of iron in yeast. *Anal Biochem* **351**, 149-151
304. Li, D., Chen, H., Florentino, A., Alex, D., Sikorski, P., Fonzi, W. A., and Calderone, R. (2011) Enzymatic dysfunction of mitochondrial complex I of the Candida albicans goa1 mutant is associated with increased reactive oxidants and cell death. *Eukaryot Cell* **10**, 672-682
305. Gleason, J. E., Li, C. X., Odeh, H. M., and Culotta, V. C. (2014) Species-specific activation of Cu/Zn SOD by its CCS copper chaperone in the pathogenic yeast Candida albicans. *J Biol Inorg Chem* **19**, 595-603
306. Jensen, L. T., and Culotta, V. C. (2005) Activation of CuZn superoxide dismutases from Caenorhabditis elegans does not require the copper chaperone CCS. *J Biol Chem* **280**, 41373-41379
307. Collart, M. A., and Oliviero, S. (2001) Preparation of yeast RNA. *Curr Protoc Mol Biol* **Chapter 13**, Unit13 12

308. Kim, D., Pertea, G., Trapnell, C., Pimentel, H., Kelley, R., and Salzberg, S. L. (2013) TopHat2: accurate alignment of transcriptomes in the presence of insertions, deletions and gene fusions. *Genome Biol* **14**, R36
309. Anders, S., and Huber, W. (2010) Differential expression analysis for sequence count data. *Genome Biol* **11**, R106
310. Cai, Z., Du, W., Liu, L., Pan, D., and Lu, L. (2019) Molecular Characteristics of the Conserved Aspergillus nidulans Transcription Factor Mac1 and Its Functions in Response to Copper Starvation. *mSphere* **4**
311. Moran, G. P. (2012) Transcript profiling reveals rewiring of iron assimilation gene expression in Candida albicans and C. dubliniensis. *FEMS Yeast Res* **12**, 918-923
312. Colin, J., Candelli, T., Porrua, O., Boulay, J., Zhu, C., Lacroute, F., Steinmetz, L. M., and Libri, D. (2014) Roadblock termination by reb1p restricts cryptic and readthrough transcription. *Mol Cell* **56**, 667-680

Curriculum Vitae

Edward M. Culbertson

Eculber3@jhu.edu
615 North Wolfe Street W8704 • Baltimore, MD 21205 • (814) 758-3202

Education

Johns Hopkins University Bloomberg School of Public Health — Baltimore, MD
Ph.D. Biochemistry and Molecular Biology — August 2020

Edinboro University of Pennsylvania — Edinboro, PA
B.S. *magna cum laude* Industrial Biochemistry — May, 2014

Research Experience

Graduate student
Johns Hopkins Bloomberg School of Public Health — Baltimore, MD
Department of Biochemistry and Molecular Biology — 2014-present
PI: Dr. Valeria Culotta

- Found a new virulence factor in the pathogenic yeast *Candida albicans.*
- Discovered that downregulation of an important Cu enzyme during Cu starvation frees up Cu for respiration.
- Characterized the effect of infection upon Fe and Cu homeostasis in a murine model.
- Identified immune cells present in Lyme disease patients at the site of tick bite or erythema migrans (bull's-eye rash).

Summer Intern
University of Auburn
Auburn, AL
Department of Polymer and Fiber Engineering
Summer 2013
PI: Dr. Maria L. Auad

- Generated and characterized polymeric fibers made of chitosan and alginate
- Loaded fibers with Sulfathiazole and studied the kinetics of their release with UV-Vis spectroscopy

Undergraduate researcher
Edinboro University of Pennsylvania — Edinboro, PA
Department of Chemistry — 2012-2014
PI: Dr. Qun Gu

- Demonstrated with the fluorophore anthracene that the absorbance spectra of certain fluorophores can be calculated by two emission spectra with different geometric parameters.

Publications

[1] **Culbertson, E. M**., Cormack, B. P., and Culotta, V. C. (2020) Expanded role of Cu-binding transcription factor *MAC1* in *Candida albicans*. *Mol Microbiology.* 10.1111/mmi.14591.

[2] **Culbertson, E. M**., Khan, A. A., Muchenditsi, A., Lutsenko, S., Sullivan, D. J., Petris, M. J., Cormack, B. P., and Culotta, V. C. (2020) Changes in mammalian copper homeostasis during microbial infection. *Metallomics* 12, 416-426

[3] Robinett, N. G., **Culbertson, E. M**., Peterson, R. L., Sanchez, H., Andes, D. R., Nett, J. E., and Culotta, V. C. (2019) Exploiting the vulnerable active site of a copper-only superoxide dismutase to disrupt fungal pathogenesis. *J Biol Chem* 294, 2700-2713

[4] Besold, A. N*., **Culbertson, E. M***., Nam, L., Hobbs, R. P., Boyko, A., Maxwell, C. N., Chazin, W. J., Marques, A. R., and Culotta, V. C. (2018) Antimicrobial action of calprotectin that does not involve metal withholding. *Metallomics* 10, 1728-1742
*co-first authors

[5] Besold, A. N., Gilston, B. A., Radin, J. N., Ramsoomair, C., **Culbertson, E. M**., Li, C. X., Cormack, B. P., Chazin, W. J., Kehl-Fie, T. E., and Culotta, V. C. (2018) Role of Calprotectin in Withholding Zinc and Copper from Candida albicans. *Infect Immun* 86, e00779-17

[6] Rossi, D. C. P., Gleason, J. E., Sanchez, H., Schatzman, S. S., **Culbertson, E. M**., Johnson, C. J., McNees, C. A., Coelho, C., Nett, J. E., Andes, D. R., Cormack, B. P., and Culotta, V. C. (2017) Candida albicans FRE8 encodes a member of the NADPH oxidase family that produces a burst of ROS during fungal morphogenesis. *PLoS Pathog* 13, e1006763

[7] Besold, A. N., **Culbertson, E. M**., and Culotta, V. C. (2016) The Yin and Yang of copper during infection. *J Biol Inorg Chem* 21, 137-144

[8] Sibaja, B., **Culbertson, E.**, Marshall, P., Boy, R., Broughton, R. M., Solano, A. A., Esquivel, M., Parker, J., De La Fuente, L., and Auad, M. L. (2015) Preparation of alginate-chitosan fibers with potential biomedical applications. *Carbohydr Polym* 134, 598-608

Honors and Awards

Best Poster 2018
Copper 2018 Conference: Sorrento, Italy

Best Poster 2017
Gordon Research Conference Cell Biology of Metals: Mount Snow, VT

Ruth L. Kirschstein National Research Service Award (NRSA) Individual Predoctoral Fellowship
National Institute of Diabetes and Digestive and Kidney Diseases (F31DK111114) 2016

Outstanding Departmental Senior for the College of Science and Health Professions
Edinboro University Chemistry Department 2014

College Chemistry Award 2014
Society for Analytical Chemists of Pittsburgh

Best Poster 2014
Edinboro University Celebration of Scholarship

Research Experience for Undergraduates Fellowship 2013
National Science Foundation – Auburn University

POLYED Undergraduate Award for Achievement in Organic Chemistry 2012
Edinboro University

Board of Governors Math/Science Scholarship 2010
Edinboro University

Oral Presentations

Baltimore Fungal Biology Club 2019
Baltimore, MD
Cu economy for respiration in *Candida albicans*
Edward Culbertson

Biochemistry and Molecular Biology Annual Retreat 2019
Baltimore, MD
Role of *Candida albicans* Mac1 during Cu starvation
Edward Culbertson

Biochemistry and Molecular Biology Annual Retreat 2017
Gettysburg, PA
Iron and ceruloplasmin during fungal infection
Edward Culbertson

Gordon Research Seminar – Cell Biology of Metals 2017
Mount Snow, VT
The importance of Cu during fungal infection
Edward Culbertson

Poster Presentations at International Meetings

Copper 2018 2018
Sorrento, Italy
The importance of Cu during fungal infection
Edward Culbertson, Cissy Li, Chynna Broxton, Brendan Cormack and Valeria Culotta

American Society of Microbiologists: Conference on *Candida* and Candidiasis 2018
Providence, RI
The importance of Cu during fungal infection
Edward Culbertson, Cissy Li, Chynna Broxton, Brendan Cormack, and Valeria Culotta

Gordon Research Conference: Cell Biology of Metals 2017
Mount Snow, VT
The importance of Cu during infection
Edward Culbertson, Cissy Li, Aslam Khan, Michael Petris, Brendan Cormack and Valeria Culotta

FASEB SRC on Trace Elements in Biology and Medicine 2016
Big Sky, MT
Copper, iron, and ceruloplasmin during fungal infection
Edward Culbertson, Cissy Li, Brendan Cormack, Lydia Finney, and Valeria Culotta

Leadership Experience

Diversity and Inclusion Committee Member 2019-20

- Served on Biochemistry and Molecular Biology's Diversity and Inclusion Committee. Assisted with planning fall and spring events as well as contributed to a monthly Diversity and Inclusion Newsletter.

Biochemistry and Molecular Biology Retreat Planning Committee Member 2018-19

- Assisted with the planning, organization and execution of the 2018 and 2019 Biochemistry and Molecular Biology Annual Retreat. Managed faculty, post-docs, and PhD student judges to determine the best verbal and poster presentation.

Co-Chair of the Events Planning Committee 2015

- Served as an organizer for Department of Biochemistry and Molecular Biology's Social and networking events

Vice President of the R.W. Bunsen Society 2012

- Organized, delegated, and assisted with R.W. Bunsen Society functions including: Chemistry Department tutoring schedule, senior gifts, and trips to see Chemistry Department alumni's workplaces.

Skills and Techniques

Gel electrophoresis
Western Blotting
Quantitative Real Time PCR
Cloning and molecular biology
CRISPR – Cas9 gene editing
Immunohistochemistry
Atomic Absorbance Spectroscopy
Mouse Dissection
Mouse Infection
Cellular respiration

Relevant Coursework

Johns Hopkins Bloomberg School of Public Health
Genome Integrity and Cancer

Johns Hopkins University, School of Medicine
Cell Structure and Dynamics
Pathways and Regulation
Macromolecular Structure and Analysis
Biochemical and Biophysical Principles
Fundamentals of Genetics
Molecular Biology and Genomics
Organic Mechanisms in Biology
Computational Biology and Bioinformatics

Mentoring / Teaching / Volunteer Experience

Research Mentoring 2016, 2017, 2018

- Mentored one Ph.D. rotation student and two Master's students.

Johns Hopkins University, Bloomberg School of Public Health
Teaching Assistant
Cellular Stress in Physiology and Disease 2017, 2018, 2019

- Master's level class focusing on how cells respond to stress and how disease states arise when proper cellular response is perturbed. Organized class materials, recorded and uploaded lectures, held review sessions before exams, and graded exams.

Johns Hopkins Project Bridge: Science at the Market
2019
Baltimore, MD

- Educated children and adults in fundamental science principles through hands-on demonstrations at Baltimore's 32nd Street market.